UNIVERSITY OF OKLAHOMA

GRADUATE COLLEGE

THREE-DIMENSIONAL BONE TISSUE ENGINEERING STRATEGIES USING POLYMERIC SCAFFOLDS

A DISSERTATION

SUBMITTED TO THE GRADUATE FACULTY

in partial fulfillment of the requirements for the

Degree of

DOCTOR OF PHILOSOPHY

By

SAMUEL B. VANGORDON
Norman, Oklahoma
2013

THREE-DIMENSIONAL BONE TISSUE ENGINEERING STRATEGIES USING POLYMERIC SCAFFOLDS

A DISSERTATION APPROVED FOR THE
DEPARTMENT OF BIOENGINEERING

BY

Dr. Vassilios Sikavitsas, Chair

Dr. Dimitrios Papavassiliou, Co-Chair

Dr. Matthias Nollert

Dr. Binil Starly

Dr. John Fagan

Acknowledgments

I would first and foremost like to thank my main advisor Dr. Vassilios I. Sikavitsas for taking a chance on me. I know he saw more in me then I knew from the start. His guidance helped me achieve a goal most said was impossible for me and would never happen. I will miss the spur of the moment visits to the lab that ran into wildly entertaining old stories about when he was in college. Another special thanks is extended to my co-advisor Dr. Dimitrios Papavassiliou, who's almost endless well of knowledge continued to push my research. His encouragement and support always allowed me to go just a little bit farther when I thought I couldn't. A sincere thank you is extended to Drs. Matthias Nollert, Binil Starly, and John Fagan for always getting together on short notice to help me achieve my goal.

I am eternally indebted to Dr. Roman Voronov for all of his hard work and cooperation. His dedication to our research effort allowed our intertwined projects to succeed. I would also like to thank Josè Alvarez-Barreto for teaching me the skills that set the seed for the research I produce. Thanks go to Mark Curtis for helping me obtain images from the beast of a μCT machine. I would also like to thank all my other lab mates that helped me along the way: Bonnie Landy, Taren Blue, Rita Issa, Brandon Engebretson, Warren Yates, Thomas Whittaker, Kevin Buettner, Maude Glause, Kyle Burke, Jenny Keller, Valerie Rivera, Laura Place, Hope Baumgarner, and Michael Kubala. Thank you to the staff in the School of Chemical, Biological, and Materials Engineering, who kept the wheels of the machine working and smiling the entire time.

For my father, Roderick VanGordon, there is no appreciation great enough for me to give. I don't know if I could have done it without him because never doubted me

when I decided to start and he never feared that I would never finish. I would like to thank my mother, Lois VanGordon, coming around with encouragement once she knew I was serious. To my brother, Phillip VanGordon, for asking me to do things and understanding when I couldn't make it. Lastly, I would like to thank my grandfather Maurice VanGordon, for reminding me this is what I should do and sticking around till I finished.

Table of Contents

List of Tables

Table of Figures

Abstract

Bone tissue engineering has emerged due to a lack in effective and convenient bone graft alternatives to treat skeletal defects. This has lead to research into materials and methods with the goal of producing viable bone tissue grafts. These methods of research combine the major components of tissue engineering: cells, scaffolds, and stimuli from chemical and mechanical means. Polymer materials have provided many options in the way of scaffold design and function. In this manuscript, 4 various studies examine the use of polymer scaffolds employed in bone tissue engineering applications.

New porous polyetheretherketone(PEEK) foams were investigated as new biomaterial scaffolding for medical bone tissue applications. When the porous PEEK material was cultured with mesenchymal stem cells (MSC) statically using osteogenic media (α-minimal essential media (αMEM) supplemented with dexamethasone, ascorbic acid and beta-glycerophosphate) it was discovered that this new form of PEEK had the same osteocondutive properties to that of conventional PEEK. The architecture of the new PEEK lacked an interconnected pore network desirable for bone neotissue formation and was only 50% porous. The generated porosity also reduced the mechanical properties of the material. It was found that this new porous PEEK would be useful as an implant in areas that require reduced modulus or tissue ingrowth at the surface.

Preosteoblastic MSCs seeded onto poly(lactic acid) (PLA) scaffolds have been found to be able to differentiate along the osteoblatic lineage when cultured in flow perfusion bioreactors. A study was performed to investigate the influence of polymeric scaffold architectures on the development of MSCs cultured in perfusion bioreactors. It was found that non-woven PLA fiber mesh scaffolds had accelerated tissue formation

and ostoblastic differentiation over porous PLA foams within 4 days. These effects were diminished by 8 days of culture.

While perfusion bioreactors have been shown to encourage cellular proliferation, osteogenic differentiation, and tissue formation, accelerated flow rates can detach cells from the surface of PLA scaffolds. Porous foam PLA scaffolds were seeded with MSCs by static and oscillatory dynamic seeding. Cell seeding was performed with either basic α-minimal essential media or osteogenic media. Seeded scaffolds were then subjected to a 1 mL/min/scaffold unidirectional flow in order to detach cells from the surface of the scaffold. It was found that seeding efficiencies differed due to seeding method and what media was used. During detaching flow experiments, scaffolds seeded dynamically using osteogenic media were able to withstand fluid shear up to 48 hours from elevated unidirectional flow. While, scaffolds seeded dynamically with αMEM had 78.4±7.5% of its originally attached cells detached after 48 hours of fluid flow.

Lastly, in order to seek a method to be able to nondestructively assess constructs generated for bone tissue engineering, conventional high resolution microcomputed tomography (μCT) was coupled with computer image processing techniques to produce a method of virtual histology. The computational techniques were able to segment and identify MSCs seeded dynamically upon a PLA non-woven fiber meshes. To further test the virtual histology technique, a construct composed of PLA non-woven fiber scaffold, cells, soft tissue and mineralized tissue was imaged using μCT and the components of the construct were sectioned apart without destroying the construct.

Chapter 1: Introduction

Bone defects are broad, varied, and debilitating ailments. Symptoms of mild skeletal disorders can be limited to sporadic aches and pains, while more severe cases carry chances of inhibited mobility and fragile bones. Prolonged neglect can result in severe pain, chronic breakage, or potentially life-threatening consequences. Treatments of skeletal deficiencies are apparently necessary but currently available supplemental remedies for skeletal defects are flawed. Autografts, healthy tissue taken from the patient and considered the "gold standard" in bone replacement therapies, are plagued with the problems of viable material availability and donor site morbidity. The two next best alternatives, allografts (pieces of tissue taken from the same species) and xenografts (pieces of tissue taken from a different but compatible species), remove these problems but are linked with infection, disease transmission and host rejection(1-3). Non-cellular artificial materials used in bone replacements that have been used often result in pain and discomfort for the patient. The obstacles associated with these supplements keep them from being the optimum bone replacement. These shortcomings create opportunities for the field of tissue engineering to create improved bone supplement alternatives through the employment of engineering principles within biological systems(4).

Tissue engineering has emerged from an anticipated need to improve the replacement or regeneration of damaged, diseased, or otherwise failing organs and tissues of the body. A way this need is fulfilled is by combining cells with a carrier on which cell expansion and tissue growth can arise. The inclusion of mechanical and chemical stimuli to cell/carrier constructs help to promote and control functional tissue development(5). These new tissue constructs are developed so they may be implanted and integrated into targeted sites of injury. This presents the major components for tissue engineering strategies as cells, scaffolds, and stimuli from mechanical and chemical means. Scaffolds provide a base structure for the attachment, migration, and proliferation of cells and the formation of tissue(4). Ideal scaffolds for bone tissue engineering are porous matrices that provide proper mechanical support while allowing for cellular ingrowth(6-7). The material that scaffolds are constructed of should elicit a minimal immune response. Scaffolds for bone tissue engineering have been constructed out of various natural (e.g., collagen) and synthetic (e.g., poly(ethylene glycol)) materials(8). Many different types of cells have been used in bone tissue engineering. The selected cell type should be able to proliferate and deposit tissue-specific extracellular matrix (ECM). Stem cells (SC) or in the case of bone tissue engineering mesenchymal stem cells (MSC) have been favored for their high proliferation rates and their ability to differentiate into osteoblasts(9-13). As a way of mimicry, various stimuli that would be present in the natural environment an engineered tissue would encounter *in vivo* are used in tissue engineering. Some chemical stimuli that have been used are growth and differentiation factors. These chemical factors can be peptides, hormones, proteins, or other biomolecules that trigger chemical responses. Chemical factors are often placed in culture media or contained within or on the surface of scaffolds and are known to influence ECM synthesis, cell proliferation, and cell differentiation. Bioreactors constitute a major component in tissue engineering strategies. They have been designed to apply mechanical forces to tissue constructs by compression, stretching, and/or fluid shear(14-15). Mechanical factors have shown similar influences to those of chemical factors. The combination of biomaterials, cells, and stimulatory factors allow for the development of improved engineered bone tissue constructs.

Over the life of tissue engineering, many methods of analysis have been employed to gauge the ways bone like tissue is developed. These methods of analysis which look at engineered constructs are crucial to the understanding of tissue engineering. Forms of analysis can be broken down into chemical, mechanical, and visual methods. Assays and genetic analysis are common examples of chemical analysis. Assays have been developed to quantify osteopontin, osteocalcin, and alkaline phosphatase activity; which are well known chemical markers of osteogenic differentiation(15-17). Tissue and cellular expression of RUN-X, Osterix, and Collagen I can be found by genetic analysis using polymerase chain reaction (PCR). Physical testing of compression modulus, flexural modulus or failure can tell if a material or tissue construct has characteristics that are suitable for any applications within the body. Imaging of cells and constructs can allow for the detection of cell morphologies, cellular proliferation, ECM deposition, and ECM mineralization. Creation and development of improved methods of analysis steers the field of tissue engineering closer and closer to the goal of functional tissue replacements.

The major components of tissue engineering (i.e. cells, scaffold, and stimuli) have been explored and many different combinations have been proposed in the pursuit of developing functional tissues. An example of the plethora of proposed concepts explored involves the multitude of material options available to create scaffolds for bone tissue engineering (e.g. titanium, polycaprolactone, collagen, etc.) Such components are constantly being developed, refined, and combined. The various constructs or samples that result from these changes must be analyzed. Analysis of these constructs serves as a feedback control that fuels the development of future constructs. This makes analysis of developed constructs very important. This brings about the need for a wide array of methods needed to evaluate each new technique, material, and stimuli used to develop bone-like tissues. These methods of evaluation in turn continue to be developed and tweaked in order to better understand what component changes and combinations help develop better tissue engineered constructs. Thus a system for the development of improved engineered constructs is implemented.

This manuscript puts forward investigations into scaffold design, stimuli effects, and cellular construct analysis for bone tissue engineering. To start out, chapter 2 will give a general overview of bone, bone tissue engineering, and methods of analysis used on bone tissue constructs. Chapter 3 will discuss an alternative 3D form of polyetheretherketone (PEEK) that has a porous nature built into it during the manufacturing process that could allow bone tissue ingrowth along the external architecture leading to better bonding of implants to surrounding bone tissue. How the influence of scaffold architecture can cause different 3-dimensional tissue development when under similar growth conditions within a flow perfusion bioreactor, will be shown in chapter 4. Entering into chapter 5, a glance at the influences of chemical and mechanical stimuli on the seeding of cells onto 3D polymer scaffolds will be presented. Chapter 6 will discuss the development of a method to evaluate 3D engineered constructs using conventional high resolution micro-computed tomography (μCT.) Finally, chapter 7 will provide some general conclusions to the presented investigations and some potential future avenues of research development. Through this research the ability to design potential bone substitutes is improved.

Chapter 2: *In Vitro* Bone Tissue Engineering

2.1 Introduction

Defects of the musculoskeletal are difficult to treat and there are major problems associated with therapies that require supplemental material in order for bones to heal. Lack of effective materials that will help the body regenerate lost or damaged tissue has given rise to increased interest in bone tissue engineering. Bone tissue engineering (BTE) seeks to find solutions that will encourage and form new tissue at targeted bone defect sites. The newly formed tissue should have all the mechanical and biological functions of healthy bone tissue.

The components that BTE makes use of are cells, a carrier on which cells can expand and tissue can generate, and stimuli from chemical and mechanical means. Complex bioreactor systems have arisen making use of all of the components in order to generate engineered bone-like tissues. This chapter will describe the structure and formation of bone, the components that come together in BTE, and methods of analyzing constructs that are generated.

2.2 Bone

Bone is a hard mineralized connective tissue responsible for providing structure and allowing motion of the body. Bone also generates blood cells and retains reserves of calcium and other important ions(18). While bones are semi-rigid structures they have a porous architecture. Structures of bone can differ based upon their location and their function but all forms are comprised of cells, organic extracellular matrix, and mineralization(15, 19).

2.2.1 Bone Structure

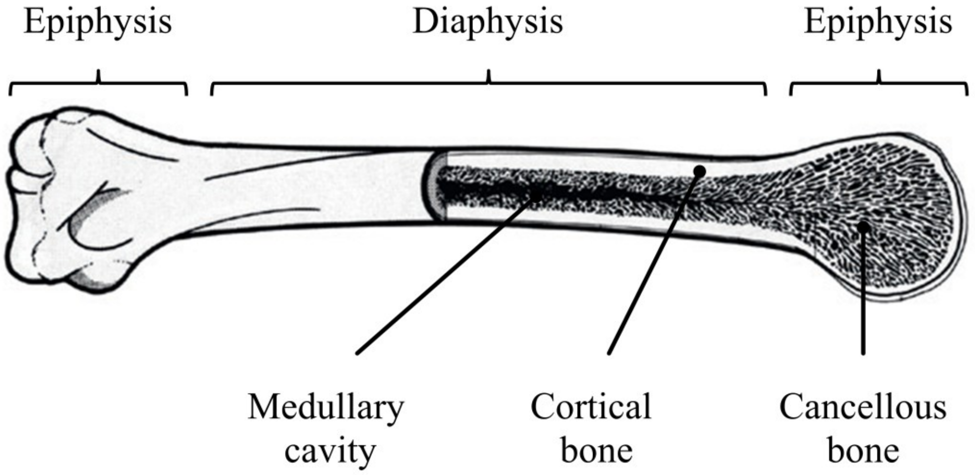

Figure 2.1: Image representation of long bone bisection. Long bones are composed of a shaft (diaphysis) and two heads (epiphyses.) The shaft of the bone contains a cavity (medullary) that contains the marrow. Cancellous (trabecular or spongy) bone lines the cavity and fills the ends of the bone. The body of the bone is enveloped in cortical(compact) bone. (image modified from Stocum(20).)

There are over 200 bones in the human body. These bones are generated by either intramembraneous or endochondral ossification. These processes form cortical (a.k.a compact) and cancellous (a.k.a. trabecular or spongy) bone tissues. While cortical bone tissue makes up the hard surface for which bone is known for, cancellous bone tissue has a spongy web-like appearance and is found inside the metaphyses and epiphyses of long bones. While differing in macrostructure both tissues are porous with compact bone being almost solid at 10% porosity and cancellous bone being between 50 to 90% porous(15) (Figure 2.1). Balances in these macroforms of bone change the elastic and rigid mechanical properties of bones(18). An example of this is how the metaphysic(center) of long bones have thicker amounts of cortical bone on its circumference to allow it to withstand torsional forces while the epiphysis(the end) have thinner amounts of cortical bone and contain cancellous packing allowing them to withstand heavier compression loads(18-20).

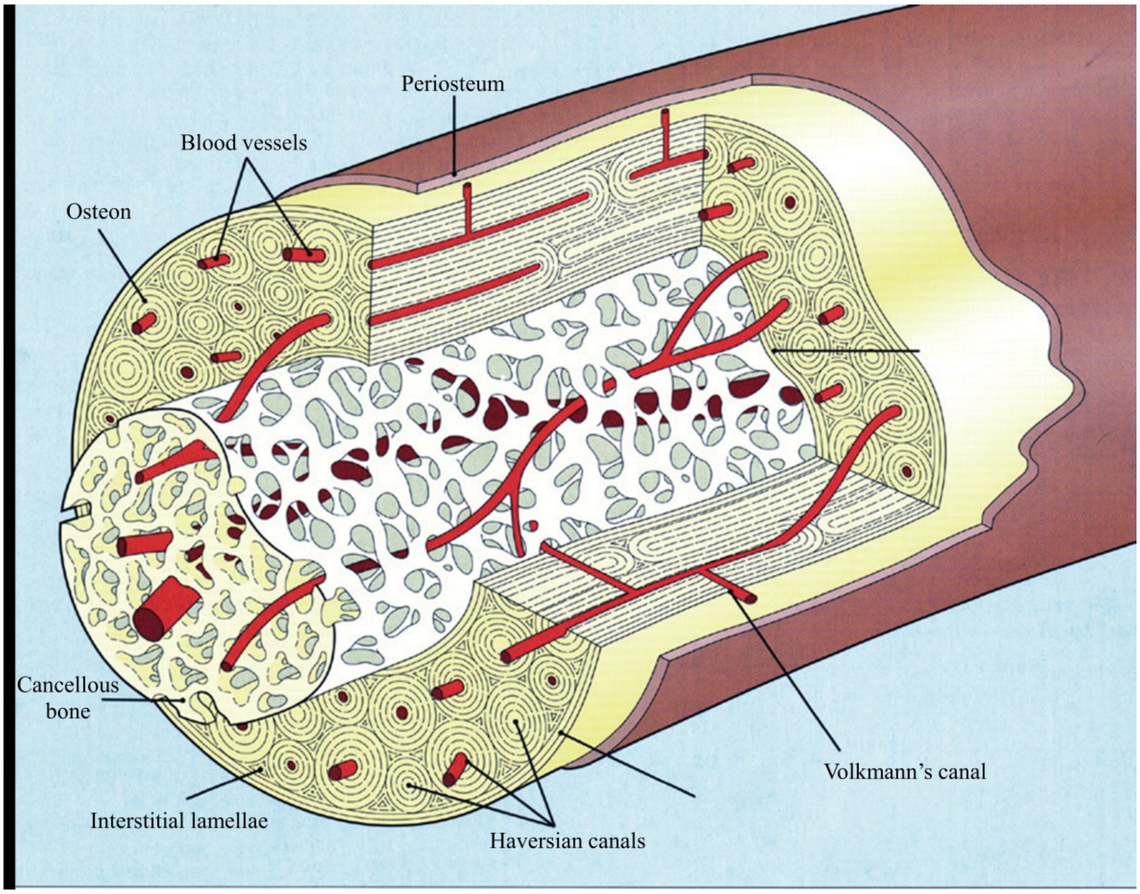

Figure 2.2: Image of the internal structure of long bone diaphysis. Cortical bone is composed of a series of oteons that run longitudinal to the length of the bone. The osteons are made of rings of lacunae around a blood vessel(Haversian canal). Volkman's canals connect the Haversian canals with the internal marrow and the highly vascularized periosteum which lines the bone. Interstitial lamellae from previous osteon formations line the space between osteons. (image modified from Stocum(20)).

Cortical bone is mainly comprised of a series of blood vessel surrounded by osteons. The spaces in between osteons consist of interstitial bone left over from prior osteons. Osteons are cylindrical structures that are layers of lacunae embedded with osteocytes. The blood vessels contained in the center of the osteons are called Harvesian canals(19). These canals are intertwined with Volkmann's canals that while connecting them to one another connect the marrow and to vessels in the periosteum lining the outside the bone(15, 20) (Figure 2.2).

The scaffolding architecture of bone can be of a woven or lamellar form. Woven bone is laid down in a random pattern that is rapidly generated. This form of bone is generated during injuries to the bone and endochondral ossification. Calcified woven bone that is remodeled is usually formed into laemellar bone. Laemellar bone has larger collagen fibrils and the layers the osteon formed are of organized structure providing it with superior mechanical strength(15, 18-19).

2.2.2 Bone Cells

Bones contain many different kinds of cells that are responsible for the upkeep of bone health. Osteoblasts, osteocytes, and osteoclasts are cells that are most closely associated most with bone formation and remodeling(19). Osteoblasts are considered responsible for the synthesis and mineralization of bone matrix(21). Osteoblasts differentiate from mesenchymal stem cells (MSC) and reside with bone lining cells along the surface of bone when they are not forming bone matrix(22). As bone matrix is formed osteoblasts are incorporated into the matrix becoming osteocytes. Osteocytes contained in the bone matrix communicate with other osteocytes and cells lining the bone surface though gap-junction-processes contained in channels (canaliculi). Osteocytes of theorized to be the sensory cells responsible for bone remodeling because the way they are situated within bone matrix would allow them to perceive mechanical queues and they have the ability to communicate with other cells throughout bone matrix(15, 18). Remodeling consists of processes of bone formation and bone resorption.

Bone resorption is the business of multinucleated osteoclasts. Coming from a hematopoietic origin, osteoclasts are formed by the fusion of pre-osteoclasts that are derived from colony-forming unit macrophages. Osteoclasts are responsible for the secretion of enzymes that allow the matrix of bone to be broken down(15, 23).

2.2.3 Organic Component

The organic scaffolding (extracellular matrix) that helps hold the structure of bone together is essentially comprised of collagen, type I (~90%) with minor amounts of types III, V, and VI(15, 21). The way that the collagen fibrils crosslink and align help control the structural strength of the bone(18-19). The remainder of material contained in the extracelluar matrix is composed of over 200 other proteins. Many of these proteins are adsorbed from serum and surrounding tissue while only about 50 are involved in the creation and upkeep of the bone. Many non-collagenous proteins are either growth factors (e.g. bone morphogenetic proteins (BMP) and transforming growth factor beta (TGF-β)) or structural proteins (osteocalcin, osteopontin, glycosaminoglycans and bone sialoprotein) that are entrapped in the matrix during formation(15, 21).

2.2.4 Mineral Phase

The feature of bone that makes it distinctive from other tissues is its calcium and phosphate rich mineralized structure. The main component of the mineral phase are mineral crystals similar to hydroxyapatite [$Ca_{10}(PO_4)_3(OH)$]. Though pure hydroxyapatite is highly insouluable small impurities (i.e. carbonate, sodium, potassium, citrate and trace elements such as strontium, lead, etc) are built into forming crystals. This is theorized to be done to help in the resorption of bone during remodeling(21). The formed mineral crystals align with the collagenous matrix fibrils(19).

The degree of mineralization has been associated with mechanical function of the bone contributing to brittleness and rigidity(18).

2.3 Mechanisms of Bone Formation

Bones are known to form by two processes intramembranous ossification and endochondral ossification. During intramembranous ossification, mesenchymal precursor cells first form condensations that become invaded by vasculature. This invasion of vasculature then causes the precursor cells to differentiate into osteoblasts. The mature osteoblasts go on to form osteoids that will become the bone. As the mineralized matrix builds up, osteoblasts become entrapped in the matrix becoming osteocytes. The bones that are formed in this manner are mainly flat bones (e.g. mandible and cranial vault(19, 24).)

Unlike intramembranous ossification, endochondral ossification must first pass though a cartilaginous phase. The first step in endochondral ossification is the condensing of MSCs forming a cartilaginous template. The MSCs differentiate into chondrocytes which go into a state of hypertrophic growth. The neocartilage is then invaded by osteoblasts that lay down a bone collar that will later become cortical bone. The template then becomes vascularized. The vascularized neocartilage is then invaded by osteoclasts, and various precursor cells. The cartilaginous structure is then remodeled by the osteoclasts and osteoblasts. The remaining chondrocytes die off except at the ends of the bone where they form organized structures Like the long bones, much of the body's skeletal structure is formed by the endochondral ossification process(24-26).

Bones that are initially formed by either intramembranous or endochondrial ossification are healed in a similar fashion. Bones are in a constant state of flux being modeled and remodeled throughout life(15, 19, 23, 27-28). Remodeling reforms bones to adjust the mechanical needs of the skeleton preventing weaknesses or defects(5, 15, 18). The remodeling process starts out by osteoclasts forming on the surface of the bone after hormonal and physical triggers(29). Once the osteoclasts are attached to the surface, the cells tear down the bone matrix, both mineral and organic. This forms a cone like cavity in the bone. Once the cavity reaches a predetermined depth the osteoclasts cease their resorption process(20, 29). The cavity then begins to fill with MSCs. The MSCs differentiate into osteoblasts which begin to form new osteon. The osteoblasts start layering organic collagen rich matrix into the cavity and entrapping some osteoblasts causing them to become osteocytes. After a point the matrix begins to mineralize. The osteoblasts lay the organic matrix to the surface of the bone and later it becomes fully mineralized. Once completed the surface of the bone become dormant until there is a defect or the next round of remodeling(15, 19-20, 23, 27).

2.4 Bone Tissue Engineering

At a cost of costing $850 billion a year (7.7% of the US-GDP) musculoskeletal disorders remain a major concern in the United States(30). With more than 500,000 procedures US and 2.2 million worldwide per year, bone is the second most common transplanted tissue after blood(31). Damaged bone that requires supplemental material for treatments currently involves the use of autografts, allografts, or xenografts(32). Autografts are by far the most used because of its osteoinductive ability(33). Autografts are pieces of tissue which are removed from a healthy tissue site within the same patient and placed in the site of damage. Allografts are pieces of tissue that are removed from an individual of the same species. These grafts are sometimes removed from cadavers whenever larger pieces are required(33). When autograft and allografts are not available xenografts are used. Xenografts are pieces of tissue that is removed from an individual of a different yet compatible species. All of these choices are plagued with such problems as availability of material, donor site morbidity, graft rejection from immune response, and infection(31, 33-34). In order to try and alleviate these problems associated with the current choices in bone supplements, bone tissue engineering has arisen.

The goal of BTE is to create new supplemental alternatives to fill nonunion fractures and allow and encourage natural healing and remodeling of bone tissue. The tissue engineering motif in constructing supplements in to combine cells, a carrier, and stimuli(4). A common method in producing supplements first entails the extraction of healthy cells. The cells are then expanded and placed or seeded upon a carrier or 3D scaffold. The seeded scaffold is placed into a bioreactor where it is subjected to chemical and mechanical stimuli(35). The cell/scaffold construct is cultured under controlled conditions allowing the cells to proliferate and tissue to form(16-17). The formed construct could then be potentially implanted into a defect.

2.4.1 Cells in BTE

The type of cells that are chosen for the creation of a functional tissue is crucially important. It is preferred that the cells have a high capacity to proliferate and also contain the ability to create tissue matrix. Cells that have been considered for BTE are preosteoblastic MSCs, primary osteoblasts, and osteocytes. These cells are known for their roles in bone formation and remodeling(36). Because the goal of BTE is the formation of bone tissue, osteoclasts, who play an integral role in bone remodeling by breaking down bone tissue, are not ideal. MSC have an edge over osteoblasts and osteocytes when considering cells for bone tissue generation because of their higher proliferation rate. They also hold the capacity to differentiate into osteoblasts *in vitro*(37) and have been found to be osteoinductive when transplanted into a bone injury site(38). When exposed to mechanical stimulation, especially fluid shear, MSCs have demonstrated accelerated osteoblastic differentiation(39-40). MSCs are often obtained from healthy bone marrow which has been previously used *in vivo*(41-42). Several studies have shown MSC potential for bone regeneration(7, 43-44).

2.4.2 Scaffolds in BTE

The carriers in BTE, scaffolds, must meet certain criteria in order to be useful in creating a bone supplement. Scaffolds must provide proper a mechanical foundation which allows cellular attachment, cellular proliferation, ECM production and ECM attachment. When trying to create a neotissue from MSCs the scaffold must also allow or encourage osteogenic differentiation. Materials that are commonly used in the creation of scaffolds for BTE are natural polymers(8, 45-46), synthetic polymers(8), ceramics(47), and metals like titanium(48). Many scaffolds have been fabricated from natural polymers such as fibrin and collagen which are commonly found in many ECMs of the body. Though natural materials present better interaction with cells they commonly lack structural support that is desirable for bone grafts that may be implanted in load bearing bone. Some of the many synthetic polymers that have been applied to scaffold constuction are polyanhydrides, poly(butylenes terephthalate) poly(ethylene oxide), polycarbonates, polyfumarates, and polyphosphazene(8). Scaffolds that are composed of synthetic polymers have shown to have greater structural rigidity but lack the increased cell interaction that is common with natural materials. Poly(lactic acid) (PLA), poly(glycolic acid) (PGA), and their copolymers, poly(lactic-co-glycolic acid) (PLGA) are popular for their biodegradability and Food and Drug Administration approval(8). A certain amount of biodegradability of a scaffold is usually desired. If a biodegradable scaffold is properly designed it will allow proper fusion and tissue genesis after implantation into a defect. As the tissue is rebuilt the biodegradable scaffold will get replaced with natural modeling materials while maintaining mechanical stability until it is completely gone from the implantation site(1, 49-50).

The majority of BTE scaffolds that have been investigated are either of injectable or preconstructed forms(33, 51). The allure of injectables is in there more noninvasive form of delivery and their potential to be placed in difficultly shaped defects(52). Some the drawbacks of injectables are poor mechanical properties, minimal porosity to allow for nutrient delivery, and defect size limitations. Many preconstructed scaffolds in BTE are highly porous (~70-90%) to allow for proper oxygen and nutrient transport and are constructed as porous foams, fiber meshes, and organized structures from rapid prototyping(50). Some scaffolds have been constructed with and incorporated nanostructure which has been found to promote osteogenesis(53-54). Some of the common preconstructed scaffold fabrication techniques consist of solvent casting, particulate leaching, melt blowing, electrospinning, fiber bonding, melt molding, and membrane lamination(51, 55-59). While preconstructed scaffolds can be made to have higher mechanical strength, implantation of the produced construct is potentially more invasive.

2.4.3 Chemical Stimuli

Often chemicals or growth factors are placed in culture media to encourage oteoblastic differentiation, the deposition of ECM, and the later mineralization of the ECM(37, 60). When promoting osteogenic differentiation from culture media dexamethasone and BMP-2 are most commonly used supplemental additives. Dexamethasone is a corticosteroid that has been shown to promote osteoblast differentiation in several cell culture systems. Through SOX9 expression enhancement, dexamethasone has also been involved in chondrocytic differentiation(61) and the induction of alkaline phosphatae (ALP) secretion of mature chondrocytes. These observations suggest it important role in calcification of cartilage tissue(15). The as a part of the transforming growth factor β (TGFβ) superfamily, BMP-2 stimulates proliferation, differentiation, and ECM production of both chondrocytes and osteoblasts. BMP-2 is commonly used in BTE because it is an effective differentiation facilitator of MSC differentiation into osteoblasts(15, 62). Because of their implications in osteoblastic differentiation, other members of the TGFβ superfamily like BMP-4, BMP-6, and BMP-7 and different TGFβ isoforms are also made use of during BTE(63). Phosphate rich salts and ascorbic acids are added to media's to provide nutrient sources for mineralization(15, 37).

The incorporation of differentiating growth factors or peptides into scaffolds by physical or chemical means is a common tissue engineering strategy that results in enhanced osteoinductivity(48, 55, 64). This is done to improve the cell scaffold interaction by trying to mimic the body's natural tissues because some scaffolding materials are not extensively "cell friendly"(65). Two popular materials that are used in the modification of material surfaces are arginine-glycine-aspartic acid (RGD) and collagen(66-68).

2.4.4 Mechanical Stimuli

The formation and remodeling of bone are sensitive to mechanic forces exerted on bone tissue(15, 18, 36, 69). When bones are loaded and unloaded parts of the bone are compressed and tensed. This causes deformation in the bone tissue leading to pressure changes of the interstitial fluid bringing about flow. This flow is manifested by fluid movements through the canaliculi and lacunae of bone(70-73). The mechanical loading causes stresses and strains to be translated to major bone cells (i.e. osteoblasts and osteocytes) as deformations of the cell bodies(74-75). The full picture of how mechanical stimuli are converted into biochemical responses is not yet clear. Current hypothesis involve cilia(76-80), focal adhesions(81-85), intracellular junctions(86-90) and membrane ion channels(81, 91-94). Mechanical stimuli is observed to regulate the function, proliferation, and differentiation of osteoblasts and their procurer cells MSCs(18, 95-97). Interstitial flow within bone is crucial for homeostasis and enhances *in vitro* osteogenesis(98-100). An adequately perfused bone graft can lead to increased nutrient transport, cells stimulation, and bone regeneration(98).

2.5 Bioreactors in BTE

A bioreactor is a device that is designed to culture cells and tissue on 3D scaffolds within a sterile environment in a controlled fashion(101). Bioreactors can use stimuli from both chemical and mechanical means. Mechanical stimuli in bone tissue generating bioreactors try to mimic those found in normal bone behavior. Popular bioreactors in BTE use of dynamic fluid flow as mechanical stimuli. Spinner flasks, rotating wall bioreactors and perfusion systems have been some of the most explored systems(102). Ideal bioreactor designs deliver oxygen and nutrients throughout a 3D scaffold while removing cell waste allowing for cell migration, cell proliferation, and tissue generation. Figure 2.3 contains some representations of common bioreactor designs.

It has been observed that mechanical loading of cellularized constructs modulates cell proliferation(103-104), ECM production, ECM calcification(103, 105), and osteogenic gene expression(103, 106). Bioreactor systems that operate with mechanical loading are based on cell culture compressions or cell-seeded membrane deformation. Many of these systems operate only on 2D cultures while many bone tissue supplements need to be 3D. While this is true it does give insight into influences direct mechanical stimulation of cells.

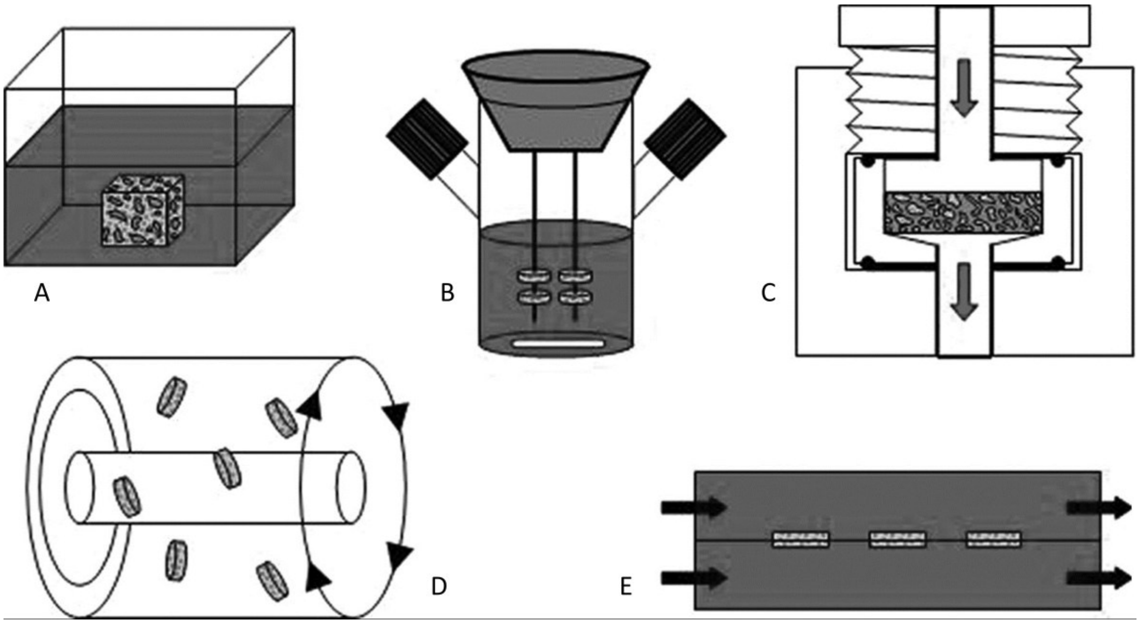

Figure 2.3: Bioreactor systems used in the generation artificial bone grafts *in vitro*. (A) static culture, (B)spinner flask, (C)scaffold perfusion (D) rotating wall vessel (E) perfused column.(image modified from VanGordon et al.(35))

2.5.1 Spinner Flask

One of the simplest bioreactor designs is the spinner flask. Scaffolds are suspended in culture media inside a closed cylindrical vessel. The convective flow in the media is generated either by a magnetic stir bar or an overhead drive. The convective flow is used to encourage uniform nutrient and oxygen distribution and renewal over scaffolds(107-108). The stirring action also creates a turbulent fluid environment creating eddies near the surface of contained scaffolds. Spinner flask cultures have shown improved cell seeding(109), proliferation(100, 110) , and osteoblastic differentiation over static cultures(39, 107)

A major problem with conventional spinner flask designs is nonhomogenous shear stresses. This exposes cells and tissue to a wide range of stresses. Another downfall of the spinner flask is the inability of media to penetrate into the internal architecture. This forces the internal porous networks to rely on diffusion from concentration gradients(99, 111). When Shea et al. cultured MC3T3-E1, a preosteoblastic-like cell line derived form the craniums of embryonic mice, on highly porous PLA scaffolds. The cells could not penetrate more than 200 μm from the surface of the construct after 12 weeks. Although the simple design of the spinner flask makes it desirable, flow perfusion systems have show much more improved cellular proliferation, tissue formation, and osteogenesis(14, 98, 102).

2.5.2 Rotating Wall Vessel

A rotating-wall vessel is composed of two concentric cylinders in which the annular space between the cylinders serves as a culture chamber(102). This bioreactor was designed for the study of cell cultures in a microgravity environment by the National Aeronautics and Space Administration(112-113). During operation the outer cylinder rotates axially around a stationary gas permeable inner cylinder. This motion creates a dynamic laminar flow in the space between the cylinders. At certain rotationally speeds a pseudo microgravity environment is created that can suspend scaffolds in culture media(114).

The fluid flows created in a rotating-wall vessel are moderate creating a narrow range of shear force on the cells and later generated tissue resided along the exterior of scaffolds. Due to a stagnation zone at the upstream edge, shear stresses decrease as you move along the axial direction of flow. This causes shear forces to be similar from scaffold to scaffold(115). While nutrient and oxygen delivery in rotating wall vessels is improved over static cultures allowing for increased soft tissue deposition, they lack the increased osteogenesis ability of spinner flasks. Spinner flask cultures have higher ALP activity, osteocalcin secretion, and mineral deposition from MSCs seed on 3D porous 75:25 PLGA biodegradable scaffolds(112). Although stimuli from rotating wall reactors are not ideal for bone tissue osteogenesis they are more suited for transitional osteochondrial tissue growth(116) and widely used in 3D cartilage development(117-118).

2.5.3 Perfusion Systems

Perfusion systems were designed in order to improve nutrient delivery into a 3D construct by driving fluid flow through the scaffold's interior. It has been found that shear forces generated by fluid flow have stimulatory effects on bone cells(107, 119-120). Because of their porous infiltrating design, perfusion systems also improve cell seeding, provide uniform cell distributions, and improve ECM production and maturity(66, 102, 107, 110, 120-123). Holtorf et al. even found that when bone marrow stromal cells were cultured on titanium fiber meshes under flow perfusion without the chemical stimulant dexamethasone in the culture media, the cultures had greater scaffold cellularity, ALP activity, osteopontin secretion, and mineral deposition when compared to MSCs cultured statically in the presence or absence of dexamethasone(40). These findings exhibited the ability of perfusion culturing alone to enhance osteogenic differentiation in adult SCs from the bone marrow. Most perfusion systems fall into 2 catagories, perfusion columns and scaffold perfusion.

Perfusion columns are designed with a sealed culture chamber where scaffolds are placed in the fluid flow path. This encourages media to pass through the interconnected pores of a scaffolds interior(110, 124-126). Even though there is increased transport of nutrients and oxygen through scaffolds, media flow can pass around the scaffolds and remain in the flow chamber. The freedom of flow limits control of convective flow through developing constructs(127).

Unlike perfusion columns, scaffold perfusion systems pass culture media directly through the scaffold isolating flow inside of a scaffolds internal porous network(102, 127-129). This method of perfusion creates better control of fluid shear forces that cells experience in the scaffold. This isolation of media through the scaffold also creates better nutrient and oxygen delivery and waste removal because media can be constantly moving over the surface of the cells and tissue(122, 130).

2.6 Graft Genesis in Flow Perfusion Bioreactor Systems

Later on this manuscript will be discussed some studies that make use of flow perfusion bioreactors. These types of bioreactors are known to produce uniform distributions of cells and encourage even ECM growth on scaffolds seeded with MSCs(66, 100). Even though it has been found that sometimes cell cultures that are grown statically have comparable cellular proliferation and ALP activity, perfused cultures show an increase in deposited ECM mineralization. Goldstein et al . statically seeded PLGA scaffolds with osteoblastic cells and cultured them statically and in both spinner flask and perfusion bioreactors(99). The cell seeded scaffolds that were cultured in the perfusion bioreactor exhibited increased ALP activity and had a more even distribution of cells throughout the scaffolds porous architecture. A similar study was performed by Meinel et al. where collagen scaffolds were seeded with human MSCs and cultured in both spinner flasks and perfusion bioreactors(128). Meinel et al. found that the scaffolds cultured under flow perfusion exhibited a more uniform distribution of mineralized tissue compared to the constructs cultured in the spinner flasks. Meinel et al. also found that the spinner flask cultured scaffolds had more mineralization than the scaffolds cultured in the flow perfusion systems. Because of the soft nature of the collagen, the scaffolds used in the perfusion system degraded which could account for the less mineralization found. This also shows the destructive force of fluid shear forced in perfusion systems.

Although shear forces within a perfusion bioreactor can be destructive they also can be osteoinductive. Bancroft et al. wanted to examine the osteoinductive potential of fluid shear so they seeded some rat MSCs onto titanium fiber meshes and cultured them under different flow rates in a perfusion bioreactor(119). As flow rates increased generating higher shear forces, increased distributions of deposited ECM and mineral were observed. Although increased fluid flow rates though porous scaffolds come with increased shear forces it also comes with higher nutrient delivery into the scaffold. To isolate the phenomena from one another Sikavitsas et al. cultured MSCs on similar titanium mesh scaffolds and instead of increasing the flow rate they changed the viscosity of the media(107). Increasing viscosity of a fluid proportionately increases the shear forces at the surface of the scaffold while maintaining the same flow rate. His group found that with a constant flow rate, amounts of mineralization and ECM deposition increased as the viscosity of the media increased. These findings couple increased fluid shear forces with increased osteogenesis and a valuable mechanical stimulus when generating bone graft substitutes.

A common observation systems that use fluid shear is an increase cell proliferation(17, 102, 122). Cartmell et al found that this is not always dose dependent(120). When his group seed human trabecular bones with MC3T3-E1 cells and cultured them statically and in perfusion bioreactors with varied amount of fluid flow, they found that scaffolds cultured under 0.01 mL/min flow rates had higher cellular proliferation over static cultured scaffolds and scaffolds cultured under higher flow rates of 0.2-1.0 mL/min. While the higher flow rates had less cellular proliferation they did have upreagulation osteoblastic linked differentiation factor Runx2, osteocalcin, and ALP that was higher than the lower flow rate and static cultures.

2.7 Cell Seeding in Bioreactors

When culturing tissue constructs *in vitro*, the crucial first step is the cellularization of a engineered scaffold(131). A proper amount of cells must attach to a scaffold or the cells will not properly proliferate and deposit ECM. In order to encourage homogeneous growth through a construct cells must be evenly distributed throughout the scaffold. The first thing to consider before seeding is the scaffold material. While some materials such as collagen and decelluarized bone easily enduce cellular attachment(33), materials such as synthetic polymers(8) are sometime hydrophobic and lack may sites for cellular attachment. Modifications to the surface of these materials by chemical or physical means can greatly improve cellular attachment(66, 132).

Methods of seeding cells determine the amount and location of cellular attachment. The method chosen will ultimately decide cellular migration, proliferation, and tissue fate(133). Static seeding is the most basic form of seeding where a cell suspension is deposited over the top of a scaffold. This places the majority of cells at the top of scaffolds leading to a larger build up of ECM at one side of the scaffold. Cells seeded using spinner increase the distribution along the peripheral surface of the scaffold without infiltration of cells into the interior. Seeding using perfusion bioreactors has showed greater success with distributing cells throughout a porous scaffold's architecture(109-110, 121, 123). Seeding using a perfusion bioreactor system can yield a 20% increase in cellularity(102). These techniques usually involve the oscillation of flow to pass cells through the scaffolds many times increasing the opportunity for cells to attach at many different points throughout the porous network. Lower flow rates are considered better during seeding in perfusion systems but due to differences in scaffolds and bioreactor designs this magnitude varies. Another unknown with the use of perfusion systems for seeding are the effects of mechanical stimuli during the seeding process. This is discussed later in chapter 5.

2.8 Methods of Analysis

When tissues are generated using tissue engineering methods they must be evaluated. Developed constructs are commonly evaluated by chemical, mechanical, and/or imaging means. The mechanical properties of scaffolds can change when cells intrude upon a scaffold, proliferate, and produce tissue and a mineralized extra cellular matrix. This can turn a scaffold that before did not have the mechanical properties required into a viable bone supplement alternative. The influence of cell and tissue growth can also reduce the mechanical stiffness of a material and remove it as a viable bone supplement option. Mechanical evaluation is usually performed by subjecting scaffolds to different kinds of stress, strain, and compressive forces. In BTE, constructs and materials are tested to see where and if they can perform in the areas of the skeleton. Many materials must have high compressive strength to be placed as supplements in load bearing areas such as hips and long bones. Many mechanical testing methods have been standardized (e.g. ISO 178, ISO 180, & ISO 527) so materials are all tested in the same fashion.

Chemical testing of BTE constructs is used to evaluate such things as cell number, matrix deposition, matrix composition, mineralization, cellular expressions, and cellular differentiation. A common method of chemical testing is the use of microplate assays. Microplate assays are used to find such things as cell number through DNA quantification (e.g. PicoGreen®), ALP activity, matrix mineralization through calcium quantification, and biomolecules expressed during MSC differentiation and matrix deposition (e.g. collagen I, osteopontin, osteocalcin, osteonectin, and bone sialoproteins)(102). Increased understanding of chemical pathways and cellular differentiation has started to push towards heavier evaluation of constructs by RT-PCR and reverse transcription. Pathway markers like cyclooxygenases (Cox-1, Cox-2), SMAD-1, SMAD-5, Runx2, Sp7 transcription factor (Osx), and extracellular-signal regulated protein kinases (ERK-1, ERK-2) are compared against "housekeeping" genes (e.g., glyceraldehyde 3-phosphate dehydrogenase) to evaluate differentiation and matrix maturity.

Imaging techniques are used to evaluate scaffold structure and cell and tissue morphologies, growth, distribution, expression, and composition. Imaging of constructs gives a visual analysis of engineered constructs. Light microscopy and scanning electron microscopy (SEM) are commonly used to look at tissue and cell morphologies. SEM is used to evaluate scaffold structures(8, 53-54). Energy dispersive X-ray spectroscopy (EDS) has been used in conjunction SEM in order to analyze surface elements of scaffolds determining tissue mineralization. Light and fluorescent microscopy is currently the main technique for evaluating 3D constructs. In order for the 3D scaffolds to be fully evaluated by light or fluorescent microscopy it first must be processed by histology. Histological processing of 3D scaffolds involves fixing the tissue to the scaffold, embedding the scaffold in paraffin wax and cutting it into thin pieces and mounting the pieces onto slides. The pieces then can be stained to look for mineralization, cell distribution tissue formation and with the help of immunohistochemistry some cellular and tissue expressions can be evaluated. Like histological processing for light and fluorescent microscopy tissue constructs must be processed for SEM. Because these processing techniques only allow for destructive endpoint evaluation of 3D scaffolds, alternative imaging methods like micro-computed tomography are being developed for use in tissue engineering. More detail on this is explained further in chapter 7.

Chapter 3: Investigation of Porous PEEK Foams for Orthopedic Device Implants

3.1 Introduction

Investigations into polyetheretherketone (PEEK) materials for implantation were first explored by Williams et al. in 1987(134). Since its first looks at biocompatibility, implantable grade versions of the material have been created (i.e. PEEK-OPTIMA®, Invibio). The materials have been found in routine use in spinal fusion cages and intervertebral spacers. A degree of this increase in the material's use is due to its radiolucency which allows for easy imaging of bone fusion. PEEK also has a reduced mechanical modulus which allows for a reduction in material deformation and decomposition of bone near the implant site. Since PEEK is light weight, durable, and an electrical insulator it has use in orthopaedic and craniomaxillofacial implantations.

PEEK is a thermoplastic that can be processed by industrial processing techniques. Other materials can be incorporated into PEEK (e.g. carbon fiber and ceramic beads) to adjust the materials properties. Incorporation of carbon-fibers into PEEK has shown increased mechanical strength and stiffness of the material(135-138). These modifications with carbon-fibers have resulted in its tensile strength being raised from 100 to 230 MPa and the mechanical modulus being increased from 3.5 to 18 GPa. These improvements could allow PEEK to be used in load bearing applications. Despite this ability to be augmented, investigations into PEEK constructs that could mimic cancellous bone have been limited. A potential solution for this is the incorporation of pores into PEEK materials. This could result in reduced modulus that could allow for force dampening expanding the use of PEEK in medical applications. The addition of pores could also improve tissue fixation to implants by allowing for cellular and tissue ingrowth(136) allowing the tissue to interlace with the material.

Production scale methods of fabricating porous PEEK are limited in their translation into uses for implantable medical material production. MuCell®, a gas assisted injection moulding method that introduces supercritical gas during screw-recovery extrusion shows some potential. The method creates a closed cell porosity with pore diameters up to 100μm(139). Although this does not create a porous network compatible with osteoconductivity, variations on the technology have been investigated using PLA which combine salt-leaching with the supercritical process(140). The combination of the two techniques has created materials with interconnected porous networks. Methods of creating scaffolds using compression molding and salt leaching have also been described for polyaryletherketones including PEEK(141-143). However challenges remain with the high temperatures required to process PEEK (400 ºC) and when additives or fillers are incorporated during processing the material viscosity is affected.

In this study a new porous PEEK foam material fabricated by twin screw compounding and porogen extraction is evaluated for biocompatibility in bone applications. Biological interaction and mechanical characteristics were investigated. When a long bone orthopedic device is implanted it comes in contact with bone and marrow cells. To test the cell material interaction, pieces of the porous PEEK foam were cultured *in vitro* using preosteoblastic MSC for 21 days. The responses of the cells were measured using cell number, alkaline phosphatase activity, calcium content, and EDS surface particle analysis. Interactions of the cells with the material surface were imaged using SEM. Cultured and uncultured scaffolds were tested for tensile, flexural and compressive properties. Porous foam PEEK material was also mechanically tested for potential orthopedic medical device applications.

3.2 Materials and Methods

3.2.1 Cell Culture

Mesenchymal stem cells were isolated by previously outlined methods(144). from 8-week old male Wistar rats. Briefly, rats were humanely euthanized using CO_2, after which the tibiae and femora were removed. The proximal epiphysis of the femur and the distal epiphysis of the tibia were cut off using bone shears. A syringe containing culture media(α-modified minimum essential media, α-MEM, Atlanta Biologicals), supplemented with 10% fetal bovine serum (FBS) (Atlanta Biologicals) and 1% antibiotics (Invitrogen) was inserted through the opposing epiphysis of that which was removed. The marrow was flushed from the bone and suspended. The suspension was distributed to tissue culture treated polystyrene 75cm^2 flasks supplemented with additional culture media and incubated at 37 °C and 5% CO_2. Flasks were rinsed with phosphate buffered saline (PBS) and media was replaced after 2 days of culture to discard non-adherent cells. Culture media was replaced with fresh α-MEM media every 2 days. When cultures reached ~70% confluency, they were rinsed with PBS, detached with 0.25% Trypsin (Invitrogen), centrifuged at 400g for 5 minutes, resuspended in fresh culture media and distributed into new culture flasks. Cell cultures were maintained until the third passage, at which the cells were detached and resuspened in fresh culture media for seeding.

3.2.2 PEEK Scaffold Preparation and Seeding

Medical grade porous PEEK foams were fabricated by Invibio Ltd (Lancashire, UK). The PEEK foams were fabricated by twin screw compounding of PEEK with a porogen. Once extruded the porogen was extracted using water at supercritical temperature (up to 200ºC) and pressure (up to 15bar). The resulting foams had an the average porosity of ~50% with a mean pore diameter of 100µm. Scaffolds where cut from the porous PEEK foams(13.5x 7.25x 4.25mm, LxWxH) for cell culturing. The cut scaffolds underwent ethylene oxide sterilization in an Anproline AN74i(Andersen Sterilizers).

To prepare the scaffold for culturing, sterile scaffolds had to be wetted with cell culture media. While in culture media, vacuum was applied to the scaffolds to remove air from the internal porosity. The wet scaffolds were then placed in a 6-well low-attachment culture plate (Corning Incorporated). Cell suspensions of $5x10^5$ cells in 0.1mL of culture media were statically seeded upon scaffolds by pipetting the suspension upon the tops of each scaffold (7.25x 13.5mm surface). The 6-well plates were then placed in an incubator (37 °C and 5% CO_2) and the cells were allowed to attach for 4 hours. After the attachment period, 5mL of osteogenic media (culture media supplemented with 10 nM dexamethasone and 0.01 M β-glycerophosphate sodium salt and 50 mg/L ascorbic acid, all from Sigma-Aldrich Corp., St. Louis MO) was added to each well containing a scaffold. The scaffolds were then placed in an incubator (37 °C and 5% CO_2) and cultured for 1, 7, 14, or 21 days. Media was replaced every 3 days during the culture periods. PEEK scaffolds were taken from the same manufacturing batch and sample sets consisted of 4 to 6 structures (n=4-6).

3.2.3 SEM Preparation and Imaging

In order to prepare for SEM imaging samples that had cell/tissue cutures were first briefly rinsed two times with PBS. Samples were then fixed with 2% glutaraldehyde in 0.1 M sodium cacodylate buffer overnight at 4°C. At the end of the fixation period, samples were washed twice with 0.1 sodium cacodylate buffer and then passed through serial dehydration with ethanol-water solutions. Dehydrated samples were then critical point dried, mounted to metal stubs and gold-palladium sputter coated using a Hummer VI Triode Sputter Coater (Anatech Ltd.). Plain PEEK scaffolds with no cell/tissue cultures on them were not rinsed and dehydrated but were mounted on metal stubs and gold-palladium sputter coated. SEM images were produced using a Zeiss 960 scanning electron microscope (SEM, Carl Zeiss SMT Inc) at 15kV. Digital images were captured using EDS 2006 and EDS 2008 digital imaging software (IXRF Systems). Energy dispersive x-ray spectroscopy (EDS) surface element analysis was performed on an Oxford 6533 Link Pentatet X-ray analyzer (Oxford Instruments).

3.2.4 Assays

At the end of the assigned culture periods (1, 7, 14, or 21 days), samples needed to be prepared for assay analysis. First, samples were removed from the culture plates and rinsed briefly with PBS. The cellular constructs were then cut into small ~1x1 mm pieces using a scalpel. The small pieces were then placed in vials with of 3 mL deionized water (DIH_2O). After which they were subjected to three freeze and thaw cycles to lyse the cells. To ensure the release of cellular materials from the samples, samples were first processed for 1 minute using a Tekmar Tissumizer SDT1810 (Tekmar, Cincinnati OH) and then sonicated for 1 minute with a Sonicator Ultrasonic Processor W385 (Heat Systems-*Ultrasonic* Inc.).

3.2.5 DNA Assay

Scaffold cellularity was determined using a fluorometric PicoGreen® dsDNA quantification assay (Invitrogen). Known concentration solutions of λDNA were used to create a standard curve. Following procedures indicated by the manufacturer, sample and standard aliquots of 43 μL were placed in individual wells of a 96-well plate along with 107 μL of reaction buffer (20 x 10^{-3} M Tris-HCl, 1 x 10^{-3} M EDTA, pH 7.5) and 150 μL of PicoGreen® dye. Solutions were allowed to incubate in the dark at room temperature for at least 5 min after which using a Synergy™ HT Multi-Mode Microplate Reader fluorescence was measured (490 nm excitation and 520 nm emission). Scaffold cellularity was calculated using total amount of DNA detected in the sample divided by the amount of DNA contained in one cell. (3 pg/cell.)

3.2.6 Alkaline Phosphatase Assay

ALP activity in the samples was determined using a linear kinetic assay where a catalytic dephosphorylation reaction converts p-nitrophenyl phosphate (p-NPP) to p-nitrophenol (pNP) in the presence of a base. Alkaline phosphatase is an enzyme whose increased expression by preosteoblastic cells indicates that the cells are committing towards an osteoblastic differentiation pathway(145-148). Within a 96-well plate, 80 μL of sample or standard solution were added to each well, along with 20 μL of basic buffer (Sigma-Aldrich). Then the substrate, 4-Nitrophenyl phosphate disodium salt hexahydrate (Sigma-Aldrich) in DIH_2O, was added to each well (100 μL). The reaction was allowed to proceed for 30 minutes and then it was stopped using 100 μL of 0.1 N sodium hydroxide. A Synergy™ HT Multi-Mode Microplate Reader was then used to read the absorbances of the samples at 405 nm. The samples were compared to standards in the plate with known concentrations of product, pNP, resulting in activities in picomoles (pmol) of product formed per hour. To represent activity of enzyme on a per cell basis, activity was divided by the total number of cells, as determined with the PicoGreen® assay.

3.2.7 Osteopontin Assay

A rat osteopontin sandwich ELISA assay kit (Assay Designs, Ann Arbor MI) was used to determine the concentration of osteopontin in media samples. Media samples were taken from all constructs before each media change. Equal sample volumes drawn from culture media were combined to make two representative samples per time point. The final media samples were comprised of equally combined media from between 3 and 16 cultured constructs. Earlier culture time points had more samples to draw upon over later culture time points. Briefly, samples and standards made from recombinant rat osteopontin were incubated in a precoated transparent 96-well plate allowing the osteopontin within the solutions to attach to the wells. Sample and standard solutions were removed and the wells were washed. A rabbit polyclonal antibody to rat osteopontin labeled with horseradish peroxidase was added to each well and incubated. The antibody solution was removed and the wells were washed again. A horseradish peroxidase reactive substrate was then added and allowed to incubate. After the set incubation period the reaction was stopped and the absorbance was read at 450 nm using a Synergy™ HT Multi-Mode Microplate Reader. The osteopontin concentrations were converted to per day production units based on the number of days between each feeding.

3.2.8 Calcium Assay

Calcium content of the cultured scaffolds was measured using an ortho-cresolphthalein compound colorimetric method (Kit 587-M, Sigma-Aldrich). Calcium is a major component of mineralized extracellular matrix and measureable presence is an indication of a maturing osteoblastic culture(15, 149). First in order to free up calcium ions from the hydroxyapatite-like mineralized matrix, samples previously used in DNA and

ALP activity assays were incubated in 0.5 M acetic acid. The samples were placed on a shaker under gentle agitation and allowed to incubate for 1 hour. After the incubation period 10 μL of samples and standards were added to each well of a transparent 96-well plate. An equal amount of calcium binding solution (0.024% ortho-cresolphtalein complexone and 0.25% 8-hydroxyquinoline) and the buffer solution (500 mmol/L 2-amino-2-methyl-1,3 propanediol and other nonreactive stabilizers) were combined. 200 μL of the combined solution was added to each well containing a sample or standard. Standards were composed of serial dilutions of concentrations of calcium chloride ($CaCl_2$) to produce a standard curve. The plate was allowed to incubate at room temperature for 10 min after which the absorbance was read at 575 nm.

3.2.9 Statistical Analysis

Four to six samples were used (n = 4-6) for all experiments. Values were reported as the average of all samples within an experimental group with error reported as the standard error of the mean. Statistical analysis was performed using ANOVA and multiple pair-wise comparisons were conducted using the Tukey method with a confidence level of 95%.

3.2.10 Mechanical Testing

ISO test procedures were used to measure the mechanical properties of samples. Solid PEEK controls compared to samples using evaluations of tensile strength and strain at break (ISO 527), impact strength (ISO 180), and flexural strength and modulus (ISO 178). Sample cell/tissue constructs after 21 days of *in vitro* culture were subjected to quasi-static compressive testing using an Instron 1122 test rig (Instron) with a compressive load of 250 N at 0.02 mm/sec or 2.55 N/mm^2 of sample surface area. An uncultured porous PEEK sample was prepared like those for culture by placing under vacuum to remove air and wet the scaffold. Then the uncultured sample was soaked in osteogenic media for 21 days before analysis. For device application specific testing 13 x 15 x 4 mm "cervical" squares = 195 mm^2 of the plain uncultured porous PEEK were used. The "cervical" square samples underwent ASTM D695/ISO604 and Dynamic fatigue test ASTM *F2077-03-Test method for intervertebral body fusion devices* in order to screen the material in a medical device context where typical nonporous PEEK is used. Parameters for the testing were: 10 Hz, Fmax: 2.0 kN, corresponding to 10 N/mm^2, Fmin: 0.2 kN, giving a load ratio of 10.

3.3 Results

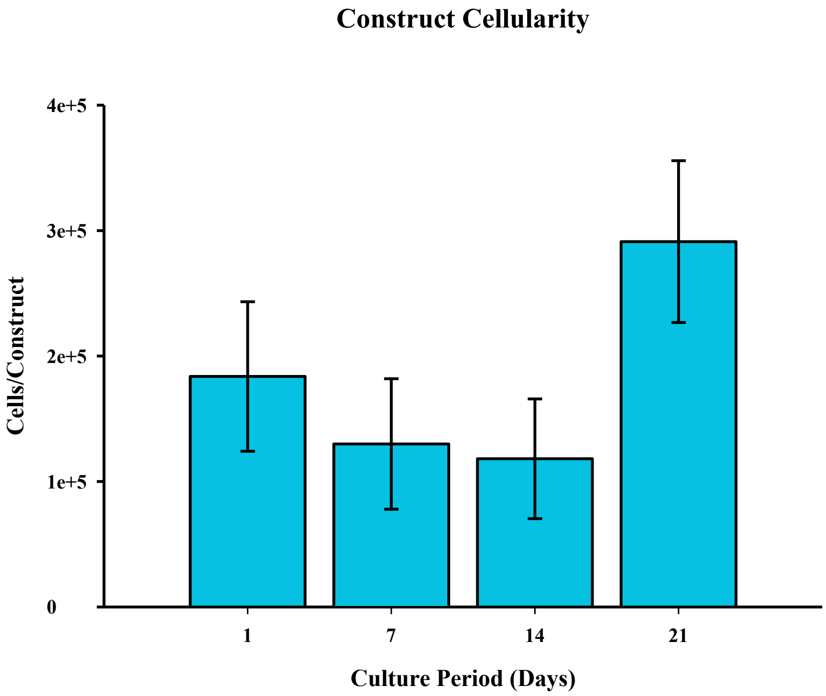

Figure 3.1: Graph depicting construct cellularity of mesenchymal stem cells *in vitro* cultured on porous PEEK. It is observed that there is no statistical significance in the difference in cellular content over the course of culture periods.

3.3.1 Cell-Scaffold Interactions

Porous PEEK scaffolds were seeded statically with $5\text{x}10^5$ MSCs and cultured for periods of 1, 7, 14, and 21 days. The cellular attachment after 1 day of culture was 37±13% of that of seeding. Scaffold cellularity did not statistically change over the course of scaffold culturing as seen in Figure 3.1. The highest cellular content was observed in the 21 day cultures with $2.9\text{x}10^5 \pm 0.64\text{x}10^5$ cells. Alkaline phophatase activity was measured in 7, 14, and 21-day cultures (Figure 3.2) The enzyme activity rose from 7 to 14 day cultures followed by a significant drop from 14 to 21 day cultures ($p<0.05$). Calcium content of scaffolds was measured in 7, 14 and 21 day cultures to evaluate mineralization of ECM (Figure 3.3). The calcium levels rose significantly from 7 to 21 day cultures. The protein content levels of extracellular glycoprotein osteopontin were measured at the 7, 10, 14, and 21 day culture times. Secreted levels of osteopontin remained constant though the culturing periods with the lowest, 43.6±17.6 pg/mL/day, at 10 days and the highest, 70.3±3.7 pg/mL/day, at 14 days.

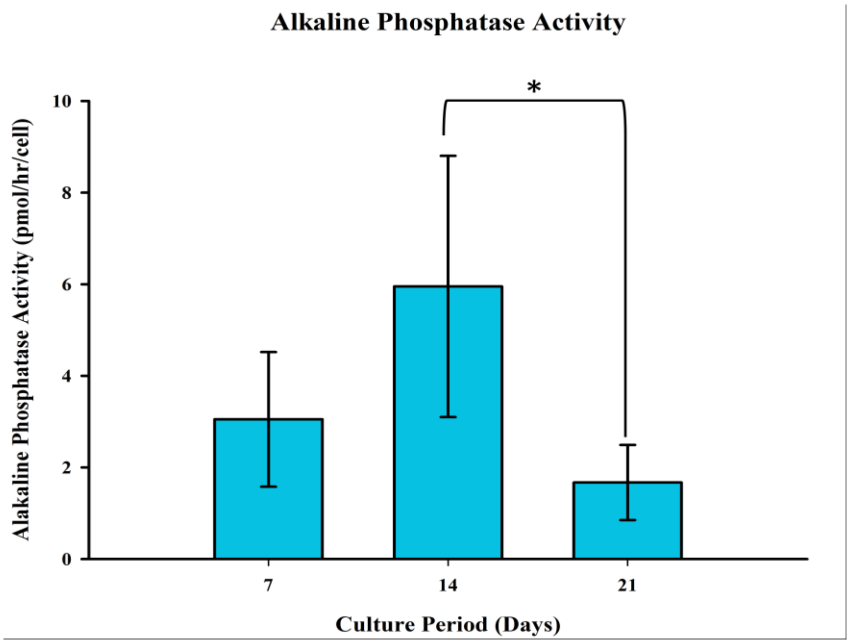

Figure 3.2: Alkaline phosphatase activity for PEEK scaffolds cultured for 7, 14, and 21 days. A drop (* indicates significance p<0.05) in ALP activity was seen between 14 and 21 days of culture.

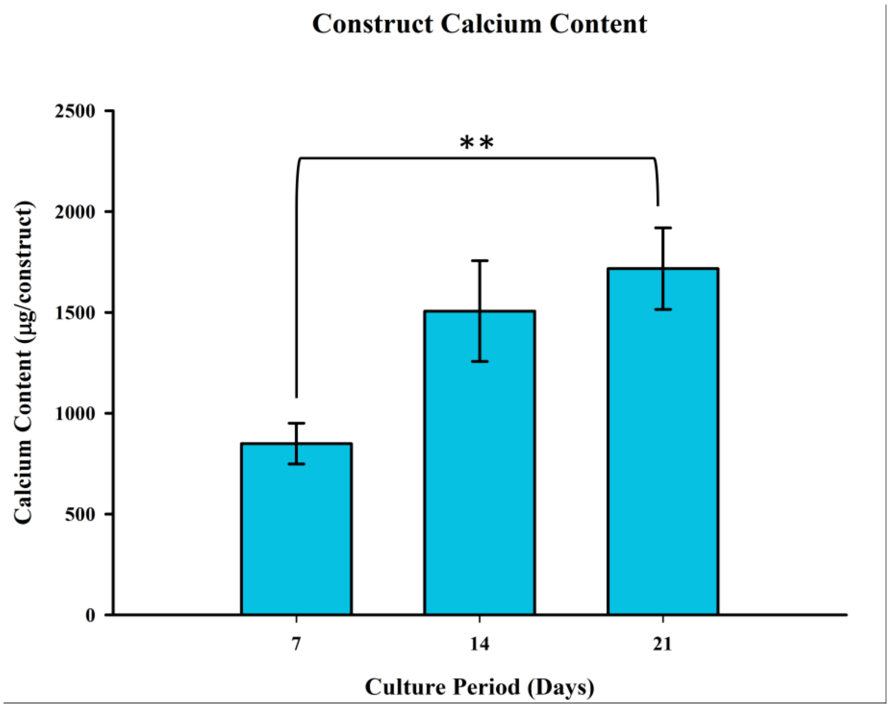

Figure 3.3: Calcium content from mineralized matrix formation on PEEK constructs after 7, 14, and 21 days of culturing. A significant increase in calcium content (** indicates significance p<0.01) is seen between 7 to 21 day cultures.

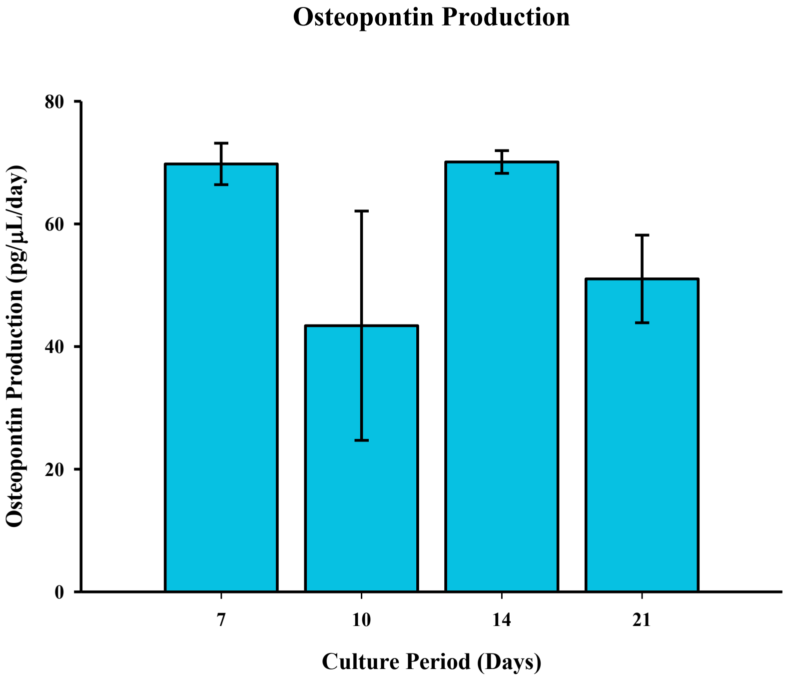

Figure 3.4: Concentrations of osteopontin in culture media as determined through ELISA for samples taken 7, 10, 14, and 21 days during culturing. An almost constant production of the secreted protein is observed throughout culturing.

3.3.2 Cell Morphology and Imaging

Scanning electron microscopy (SEM) was performed on dry, uncultured samples of the porous PEEK biomaterial (Figure 3.5). Through μCT scans (figure not shown) pore sizes in material range from 50 to 500 microns in relative diameter, a porosity of ~50%, and limited pore interconnectivity near the surface. Based on this pore size, cell migration into the limited interconnected pores existing near the surface would be feasible.

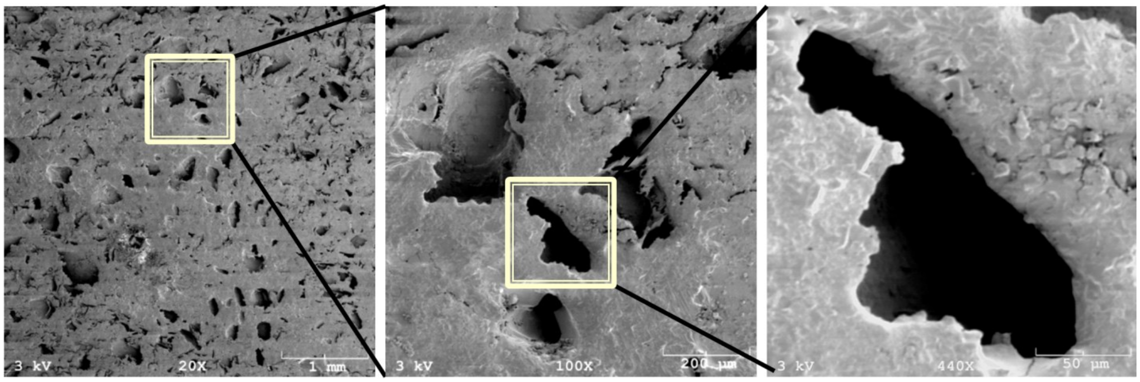

Figure 3.5: Scanning electron microscopy (SEM) images of the nonseeded PEEK constructs. The images show a network of pores of various sizes at the surface of the material. Magnifications from left to right: 20x, 100x, and 440x.

Cell and tissue morphology of 3, 7, 14 and 21 day *in vitro* cultured constructs was observed using SEM imaging (Figure 3.6). At day 3, cells had rounded spherical appearances with minimal attachment to the biomaterial. As seen from Figure 3.6, cells were found on the interior of scaffold pores. Cells started to lie down upon the surface and create a continuous network by day 7. At 14 days of culture, the cells are in contact with one another along the surface of the biomaterial with some extracellular matrix being observed. This is carried on to 21 days with increased amounts of matrix laid along the surface with some mineralized matrix present.

Surface elemental analysis was performed using EDS in order to map for major components of mineralized matrix. The three elements that were searched for were carbon, calcium, and phosphorus. Analysis was performed on 7, 14, and 21 day cultured samples. Mapped analyses of selected samples are shown in Figure 3.7 (7 day), Figure 3.8 (14 day) and Figure 3.9 (21 day). Carbon, represented by green, shows background signal provided PEEK's carbon rich structure. Calcium, represented in blue, and phosphorous, represented in red, are major components of mineralized matrix. In 7 day EDS maps, the surface of the PEEK scaffold is not fully covered and much carbon is observed. The 7 day calcium and phosphorus signals were observed corresponding with the cells that were flat slightly polygonal shape, similar to osteoblastic morphology, in SEM imaging.

Elemental scans of 14 day cultured constructs showed strong signals for calcium and phosphorus. The strongest signals are observed from the cells which display the signs of good attachment and osteoblastic differentiation. Strong signals for phosphorus and calcium suggest mineralized matrix formation in the area of cells. Increased amplitude in the elemental spectra confirms the presence of the elements. When 21 day cultures are analyzed, regions with cells displayed calcium and phosphorus signals, suggesting osteoblastic differentiation. The mapped areas with the highest calcium signal appeared to be engulfed in matrix.

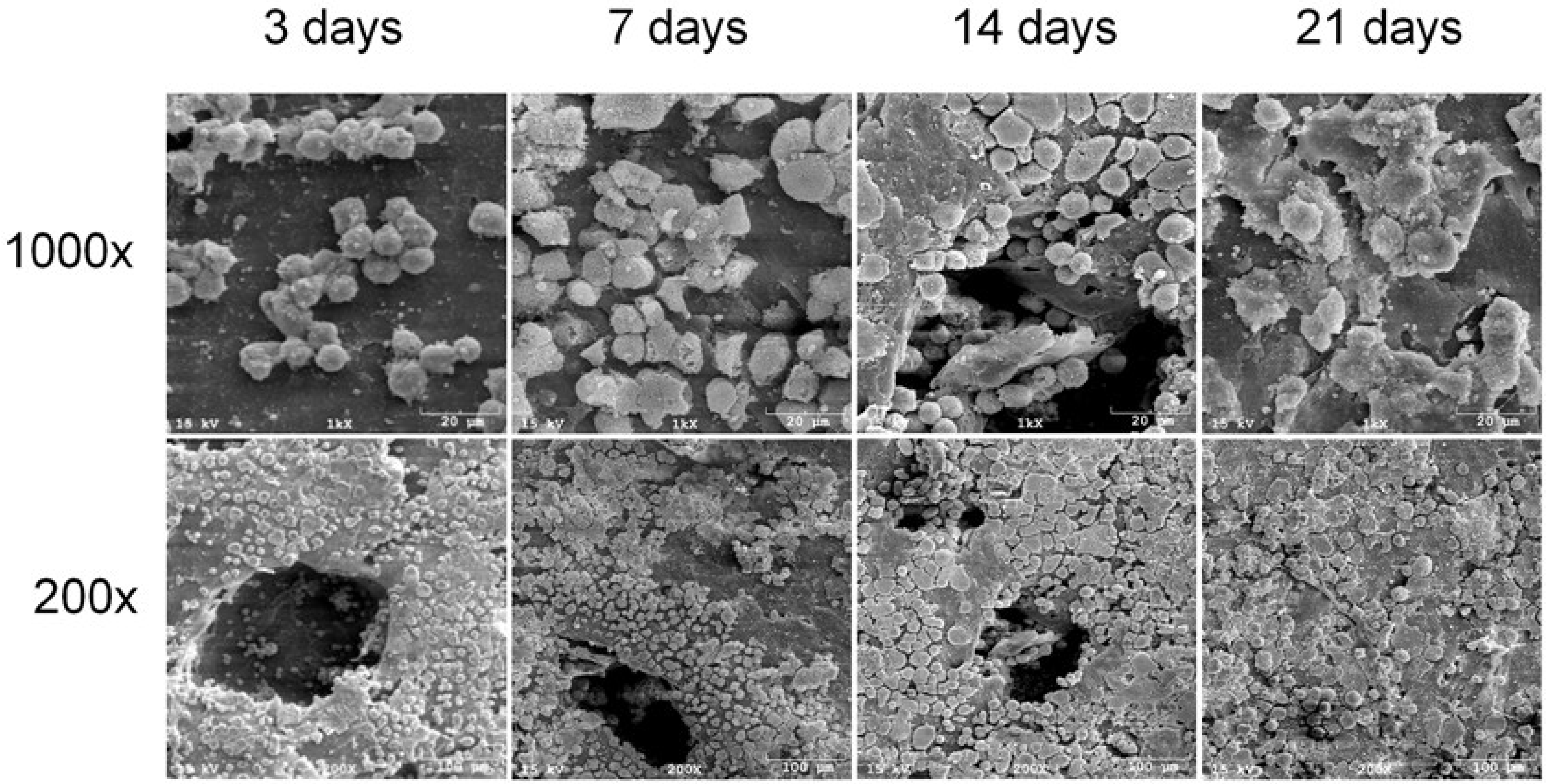

Figure 3.6: SEM images of MSC's cultured *in vitro* on the surface of porous PEEK scaffolds. As culture time progress cells can be observed lying down upon the surface, depositing tissue and invading pore spaces. (Magnification: top images 1000x and bottom images 200x)

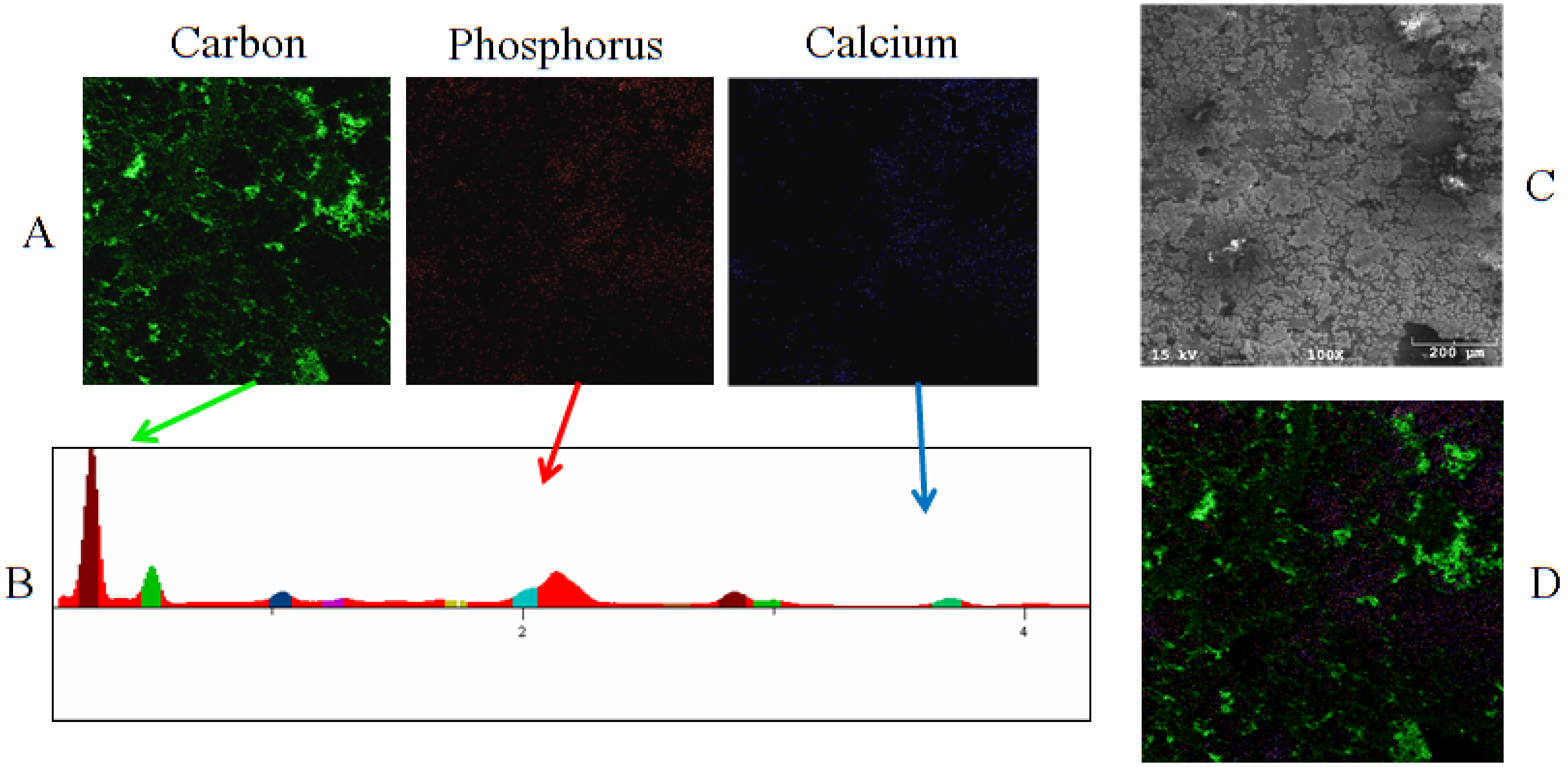

Figure 3.7: EDS images of 7 day *in vitro* cultured PEEK construct. (A) Image maps of carbon (green), phosphorus (red), and calcium (calcium). (B) Elemental spectrum of the sample, with arrows pointing out the peaks of carbon, phosphorus, and calcium. (C) SEM image of mapped area at 100x magnification. (D) SEM image overlaid with colored elemental maps. It can be observed from the maps that much of the surface is still not covered with cells.

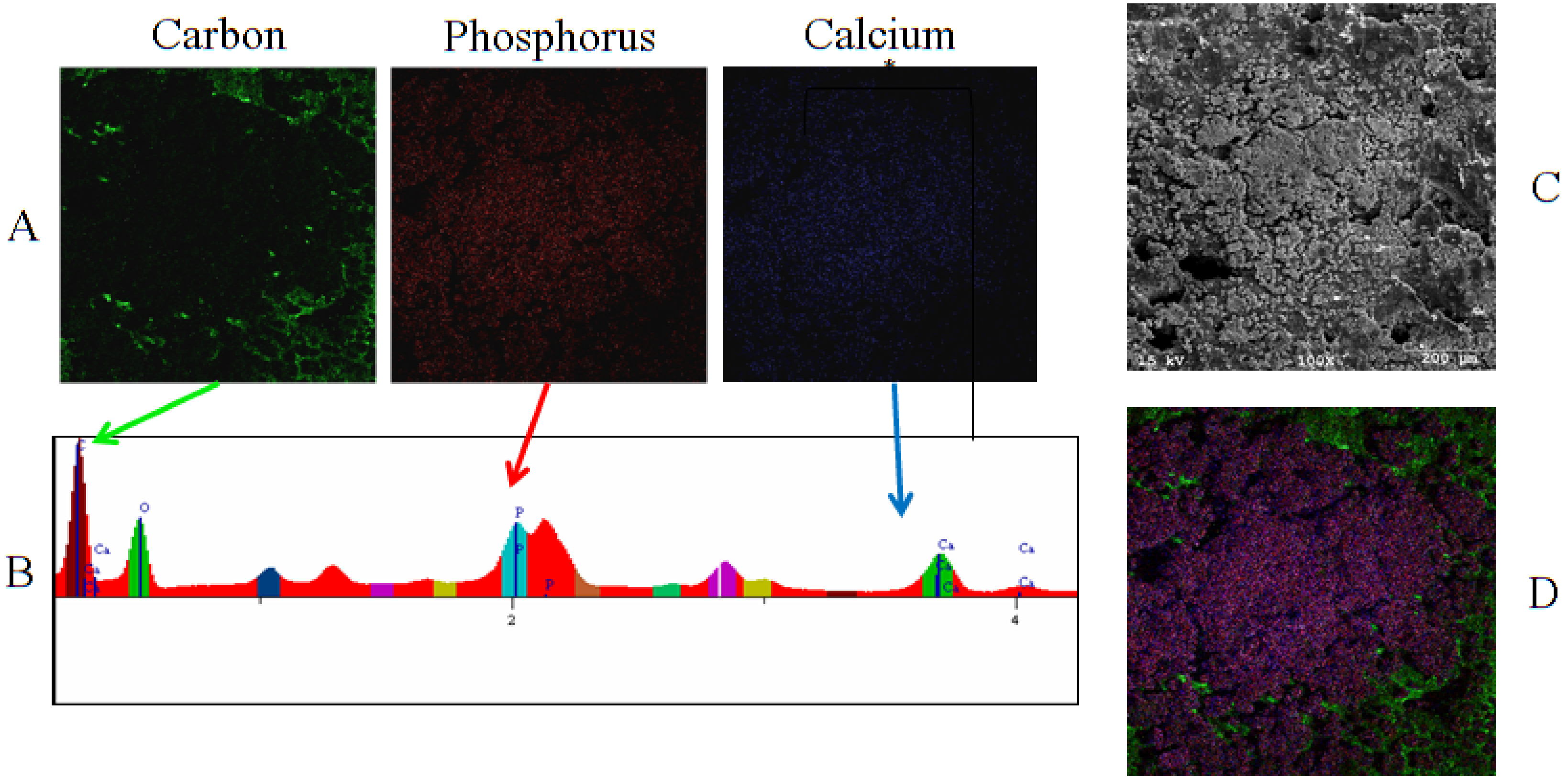

Figure 3.8: EDS images of 14 day *in vitro* cultured PEEK construct. (A) Image maps of carbon (green), phosphorus (red), and calcium (calcium). (B) Elemental spectrum of the sample, with arrows pointing out the peaks of carbon, phosphorus, and calcium. (C) SEM image of mapped area at 100x magnification. (D) SEM image overlaid with colored elemental maps. Stronger signals of carbon and phosphorus by flat polygonal cells denote maturing culture.

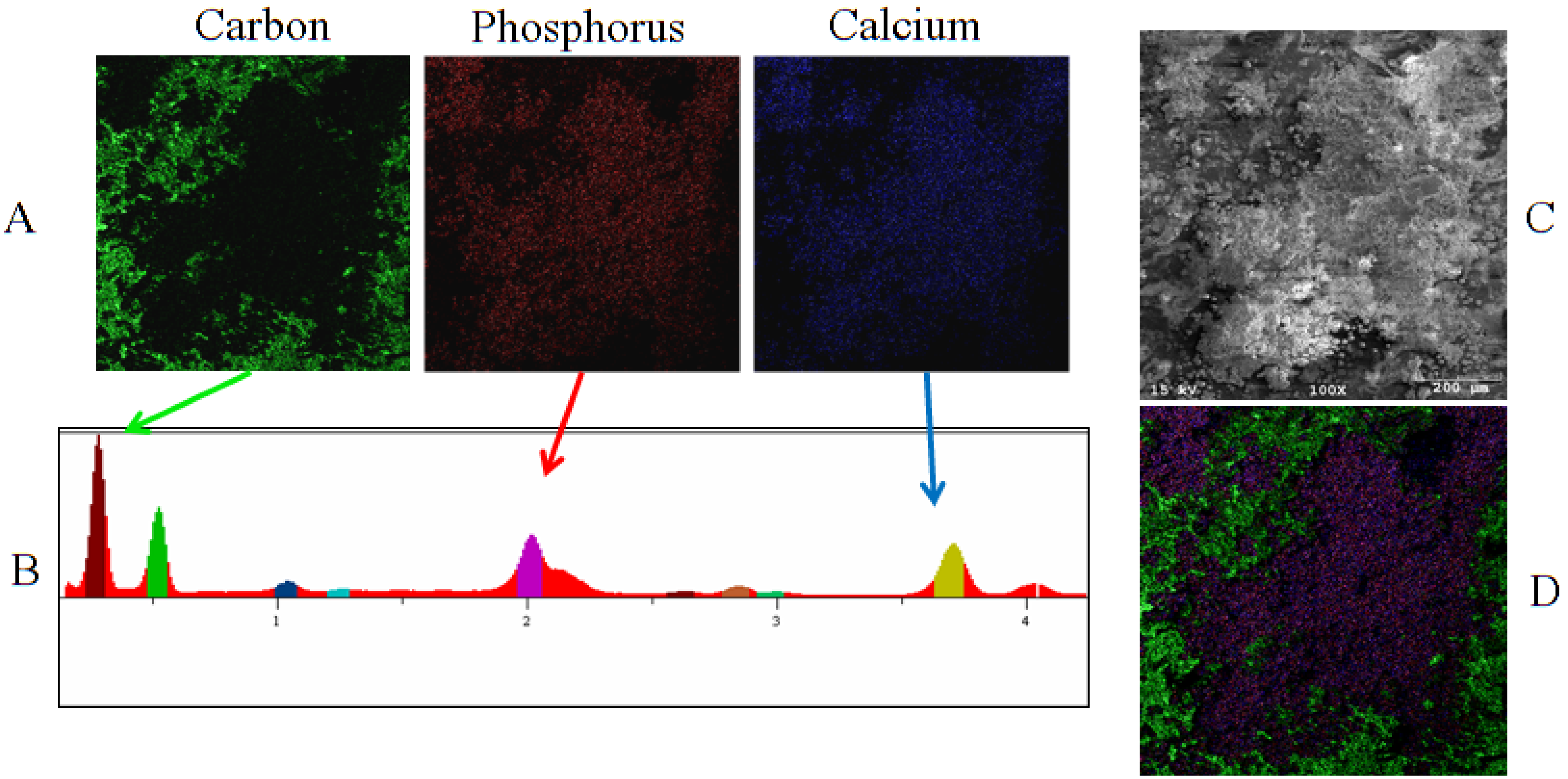

Figure 3.9: EDS images of 21 day *in vitro* cultured PEEK construct. (A) Image maps of carbon (green), phosphorus (red), and calcium (calcium). (B) Elemental spectrum of the sample, with arrows pointing out the peaks of carbon, phosphorus, and calcium. (C) SEM image of mapped area at 100x magnification. (D) SEM image overlaid with colored elemental maps. Intense mapped signals for calcium and phosphorus over areas of matrix deposition denote mature mineralized tissue culture.

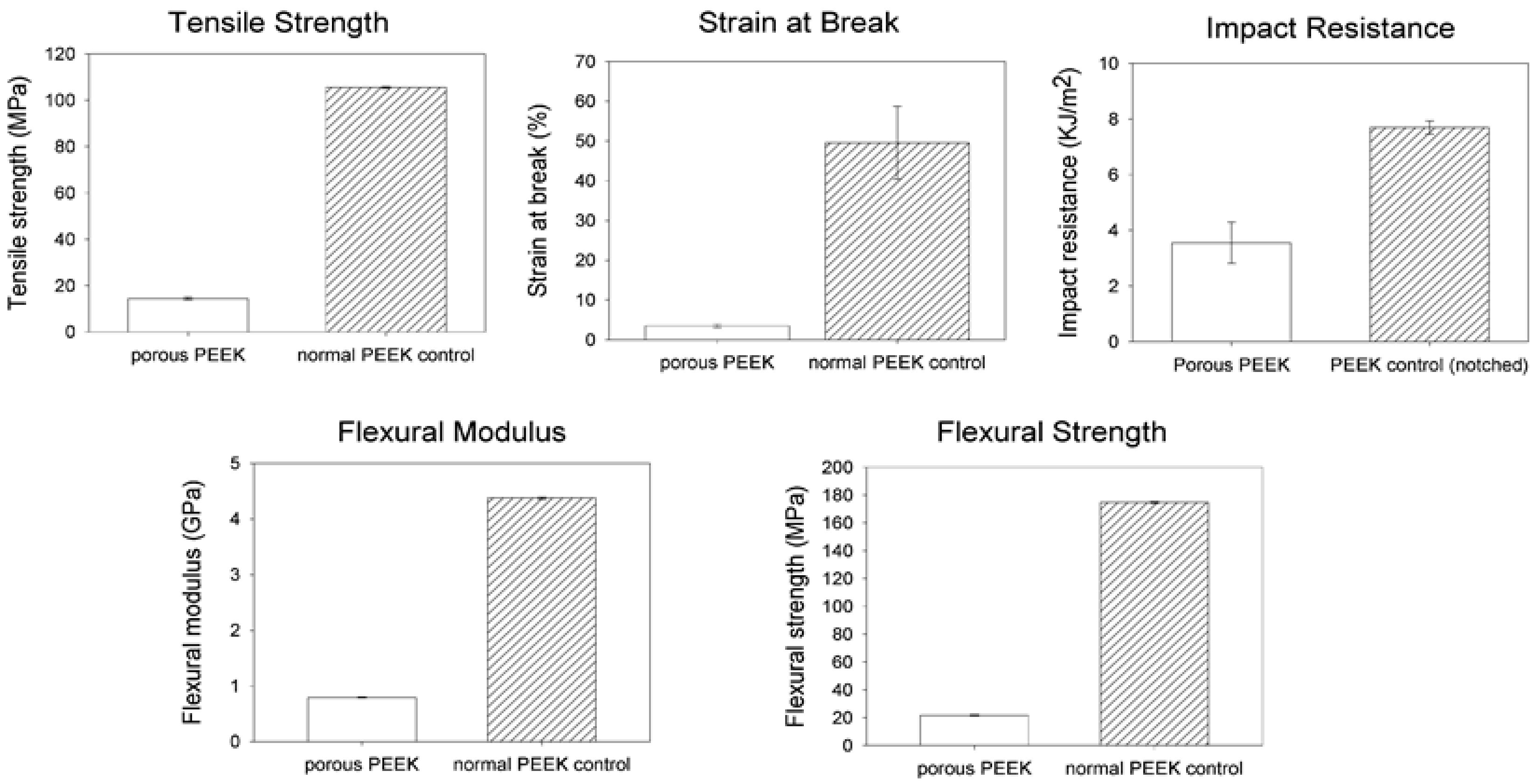

Figure 3.10: Results of mechanical testing showing the reduced mechanical properties of porous PEEK compared to normal solid PEEK.

3.3.3 Mechanical Testing

Using ISO standards mechanical properties were measured. The testing procedures (n=5) resulted in the following mean properties(Figure 3.10): tensile strength (14.5 MPa for porous and 105.5 MPa for control), strain at break (3.5% porous and 49.5% control), impact strength (3.6 kJ/m^2 porous and 7.7 kJ/m^2 control), flexural strength (21.6 MPa porous and 174.6 MPa control) and flexural modulus (0.8 GPa porous 4.4 GPa control.)

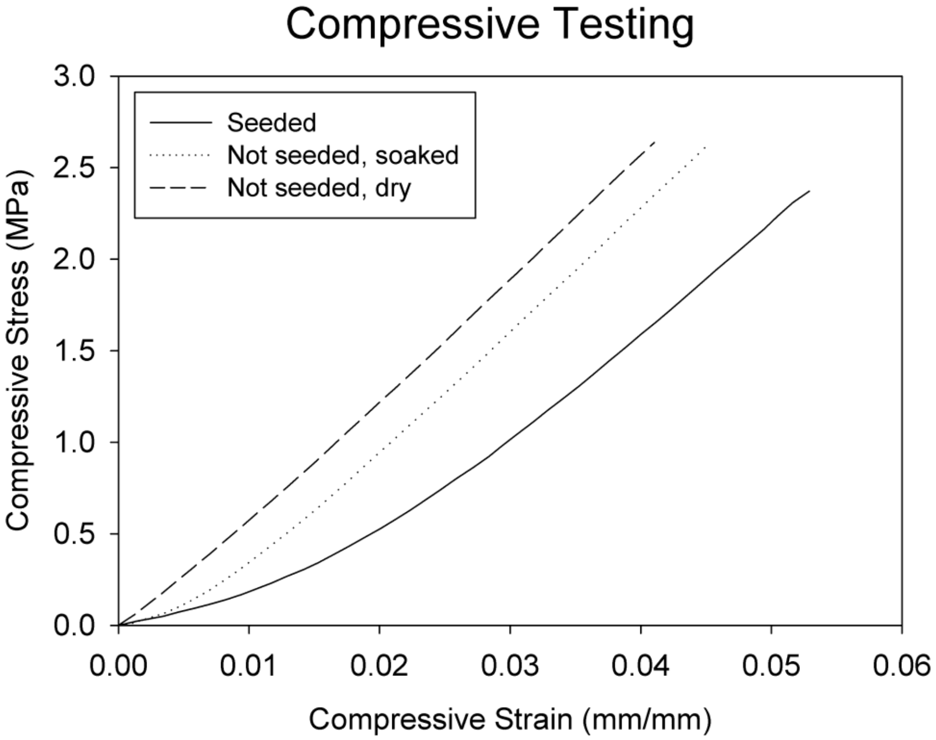

Figure 3.11: Compressive stress and strain for a dry, not seeded PEEK construct, a not seeded PEEK construct which had been soaked for 21 days in culture media, and a representative curve of the four constructs which were cultured *in vitro* for 21 days.

Compression strength was tested on a dry, uncultured sample of the porous PEEK biomaterial, a wet, 21 day soaked sample, and on multiple 21 day, MSC cultured samples (Figure 3.11). Cultured and media soaked samples exhibited reduced compressive modulus compared to dry uncultured samples which also showed a more linear stress-strain relationship. While soaking appeared to have an effect on stress-strain relationship a stronger augmentation of the relationship was observed with the cultured samples. ASTM D695/ISO604 and dynamic fatigue test ASTM *F2077-03-Test method for intervertebral body fusion devices* resulted in a permanent compressive deformation (~25 µm) after 5 million cycles over 6 days (Figure 3.12.)

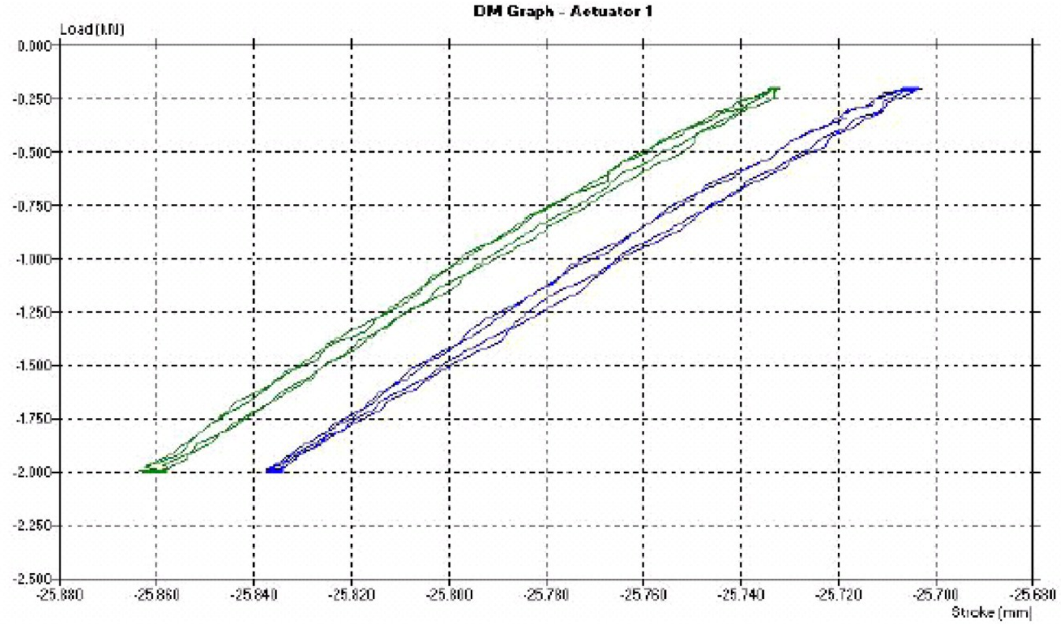

Figure 3.12: Dynamic compressive fatigue testing on the porous PEEK foam according to ASTM D695/ISO604 and Dynamic fatigue test ASTM F2077-03-Test method for intervertebral body fusion device. The blue line is the start of the compressive loading of the porous PEEK foam and the green denotes the end loading of the material. A ~25 µm permanent deformation of the material is observed.

3.4 Discussion

How cells interact with materials is important in deciding a material's potential as a biomaterial. To access this interaction for a new porous form of PEEK as a potential for orthopedic material, MSC, which are native to bone marrow, were cultured *in vitro* on porous foam PEEK scaffolds for periods up to 21 days. Observations were focused on the cell material interaction and intrusion into the pores of the material.

Even though PEEK is greatly hydrophobic, having a contact angle of 80°, making it seem less than ideal for tissue engineering(144), PEEK has favorable cell attachment and elicits a minimal immune response(150-154). It seems that changes in the material's processing that produced porous foam PEEK have not changed this. Observed cell morphologies shifted to the spherical forms MSCs are known for that of a flat polygonal shape that is similar to osteoblasts(155). Because porous PEEK and standard PEEK have the same chemical makeup, the positive result may be attributed to changes in surface topography. Previous studies have shown that a slightly rougher surface has slight affects on adhesion and mineralization of osteoblasts(156).

SEM imaging showed cells accepting and laying against the surface and creating ordered tissues with cell-cell boundaries by day 7 of *in vitro* culturing. With increasing culture time cells began to be more organized and deposit extracellular matrix. The matrix was able to easily mineralize and work towards being a more mature bone-like ECM that almost evenly covered the scaffold surface by 21 days of culture. Cells seemed to grow into the pore spaces at the surface of the material as culture time progressed. EDS mapping showed increasing coverage of the tissue surface in calcium and phosphorus which are major components of mature tissue mineralization. EDS elemental spectra peaks also increased in correlation with calcium assays showing increases in calcium from 7 to 21 day cultures. Even though no statistical difference was seen in scaffold cellularity from assays, images showed increasing amount of cells over the culture periods. These results show that porous PEEK allow for MSC differentiation, matrix formation, and matrix mineralization. There may have been early differentiation of the MSC which reduces proliferation which could have caused the lack of change in DNA content throughout culturing(157-158). This accelerated differentiation assumption is supported by the increase in alkaline phosphatase activity after the first week of culture and the constant levels of osteopontin. This consistency in osteopontin levels throughout culturing suggest the cells may have been at the early stages of osteoblastic differentiation at day 7. If this accelerated rate of differentiation and the constant level of tissue formation are carried over to *in vivo* implantation, the material could cause favorable reductions in scar formation between the tissue and the material and establish a firm contact with adjacent bone tissue. With porous PEEK's base form favoring bone tissue cytocompatibility, modification of the surface by plasma or physical wet chemistry could improve cell-material interactions even further(159-162). For the porous PEEK to be considered more greatly osteoconductive its porosity would need to be increased from 50%, the pore diameters would need to be increased from 100 µm, and pore interconnectivity would need to be increased also. These things would favor tissue ingrowth more highly.

The currently incorporated pores have reduced the mechanical properties significantly from those observed for solid PEEK. Further augmentation of the pore space would more greatly affect mechanical properties and reduce the materials implantation options down to non-load-bearing applications. The mechanical data showed similar compressive moduli above a strain rate of 2%. Culturing and media soaking of the materials caused increased amounts of deviation of the compressive modulus. The soaked sample's slightly lower initial modulus could be consistent with the theory of reduced material crystallinity of PEEK with water uptake (typically around 0.1- 0.5%)(163-164). It was for this reason that the sample was soaked for 21 days to be more comparable to the cultured sample, which had been submerged in cell culture media for that period. Cultured samples showed the most deviation from the final modulus. Because the tissue growth was along the surface the device would have impacted the tissue matrix first. The major component of deposited bone-like neotissue is collagen which has a much lower compressive modulus than pure PEEK. This could attribute to the deviation to that of the soaked sample. The porous constructs also withstood the dynamic device specific application test, cycling between 0.2 to 2.0 kN. The fatigue properties of the material meet the requirements for cervical interbody cages. Because of the materials mechanical properties, the new porous form of PEEK could also be potentially used in other areas of tissue engineering where osteoconductivity is not required.

3.5 Conclusions

The porous PEEK foams created by twin screw compounding and supercritical extraction showed greatly different mechanical properties to that of its solid form. Favorable biocompatibility with MSCs allowed for osteogenic differentiation, matrix production and ECM mineralization. While the cytocompatibility shows that the new form of porous PEEK retains it ability to be osteoconductive, the mechanical properties may be of benefit for implants that require reduced modulus.

3.6 Disclosure

Cell culture, mechanical testing of cellularized scaffolds, and much of the assay analysis were performed by Bonnie C. Landy. Medical application material testing was performed and data was provided from Marcus Jarman-Smith from Invibio.

Chapter 4: Scaffold Architecture Influences on Culturing of Preosteoblastic Cells Under Continuous Fluid Shear

4.1 Introduction

A common promising technique in the development of BTE supplements involves the seeding and culture of MSCs on porous polymer scaffolds within a flow perfusion bioreactor(8, 15, 39, 128, 165-167). As discussed in Chapter 2, perfusion bioreactors make use of mechanical stimulation by passing media through porous scaffolds that cells have been seeded upon which exposes cells to fluid shear stresses(15, 99, 107, 119, 168-172). The continuous fluid movement also allows for greater nutrient transfer to cells within a scaffold network. This combination of shear stresses and improved nutrient transfer promotes cell proliferation, differentiation and production of extracellular matrix (ECM)(107, 144, 169). The extent or type of cellular stimulation has been seen to be dependent on the magnitude of fluid shear stresses exerted upon the construct(107, 119).

Chapter 2 discussed the manufacture of porous polymer scaffolds for tissue engineering of bone where some of the most popular techniques of scaffold production are solvent casting/particulate leaching, rapid prototyping, gas foaming, electrospinning and membrane lamination(8, 51, 56-59). These different modes of production commonly produce scaffolds of high porosity (~70- 90%) to allow for proper oxygen and nutrient transport, but contain diverse internal architectures. These individual architectures could produce different internal shear stresses for flow rates of equal magnitude that affect the growth and proliferation of cells seeded onto the scaffolds. Although the use of porous polymer scaffolds has shown to facilitate the proliferation and differentiation of cells(169, 173) and generalizations of internal fluid shear environments of idealized structures have been proposed(174), shear stress distributions within scaffold architectures have not been fully investigated and are not well understood.

Fluid shear stress, until recently, has been estimated by creating simplified assumptions about the pore structure and the velocity profiles of fluid movement within the pore structures(99). These analytical solutions do not take into account the non-ideal micro-structure of the actual scaffold internal network. This in turn creates only estimates of flow conditions without producing distributions of the shear stresses experienced inside of the scaffold architecture. To get past these disadvantages Porter et al(175). used micro-computed tomography (μCT) to image trabecular bone in conjunction with the lattice Boltzmann method (LBM) to calculate the local shear stresses inside of natural 3D scaffolds. Since then, μCT has been used in conjunction with fluid dynamics simulations to characterize shear stress distributions within different types of scaffolds(176-179).

The main goal of this study is to elucidate the significance of porous scaffold architecture in the growth and osteoblastic differentiation of MSC cultured under flow perfusion. For this purpose we: 1) characterize the fluid dynamic environments of two different scaffold architectures, solvent cast/particulate leached porous foams and nonwoven fiber meshes, composed of the same material (PLLA) with comparable porosities and surface area to solid volume ratios and 2) identify the influence of scaffold architecture and shear forces on the proliferation and differentiation along the osteoblastic lineage of mesenchymal stem cells seeded on both types of scaffolds and cultured under static or dynamic conditions in a perfusion bioreactor. These goals were approached through combined computational and experimental analysis. Computational analysis was achieved with LBM coupled with nondestructive μCT imaging(180-182). The computations produced detailed flow fields developed inside of the scaffolds and shear stresses were computed locally within the void space of the architecture where media flow was passed. Experimental analysis was performed by seeding and culturing scaffolds with MSCs then examining the cultured cell/scaffold constructs using cellularity, alkaline phosphatase activity, and calcium assays along with scanning electron microscopy. These analyses produced information on proliferation, differentiation, extracellular matrix production, and extracellular matrix mineralization.

4.2 Methods and Materials

4.2.1 Porous Foam Scaffold Manufacturing

Porous foam scaffolds were prepared using solvent casting/particulate leaching method(8, 183-185). Briefly, poly(L-lactic acid) (PLLA, 114,500 MW, 1.87 PDI, Birmingham Polymers) was dissolved into chloroform 5% w/v. The solution was then poured over a bed of sodium chloride crystals (NaCl, 250-350 μm). Solvent was allowed to evaporate for 24h. The resulting salt-polymer composite was inserted into an 8 mm diameter cylindrical mold and compressed at 500 psi. During compression, the composite was heated to 130 °C and held at constant temperature and pressure for 30 min. Using a diamond wheel saw (Model 650, South Bay Technology, Inc.), the resulting composite rod was cut into 2.3 mm thick discs. The discs were placed into deionized water (DIH_2O) under agitation for 2 days to leach out NaCl. Entire DIH_2O volumes were replaced twice per day. Leached discs were then removed from DIH_2O and placed under vacuum to remove moisture from the scaffolds. The resulting product was ~85% porous, 8 mm diameter, 2.3 mm thick discs. Porosity of scaffolds was determined by measuring the solid volume (mass of the scaffold divided by the density of PLLA) and comparing to the total scaffold volume (assuming a cylindrical scaffold shape.)

4.2.2 Nonwoven Fiber Mesh Scaffold Manufacturing

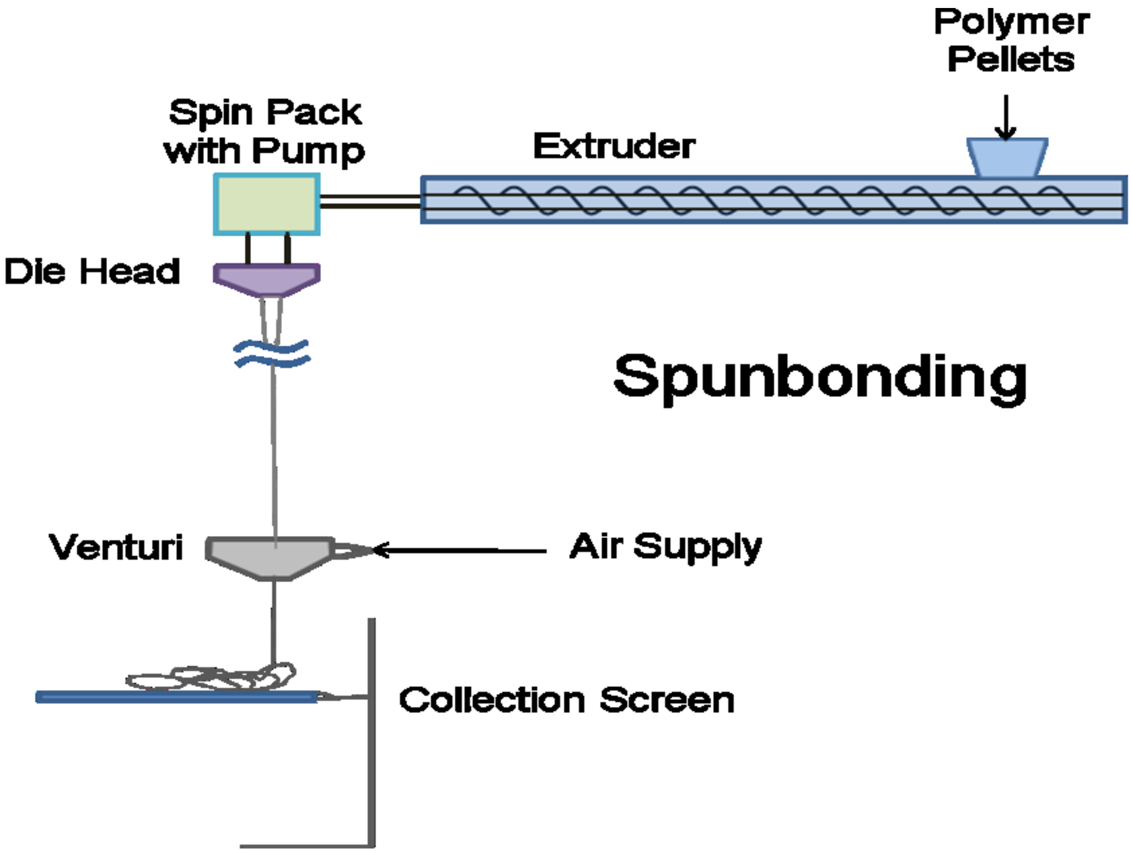

Figure 4.1: Spunbonding apparatus used to produce PLLA nonwoven fiber meshes for scaffolds

Nonwoven fiber mesh scaffolds were constructed using PLLA micro-fibers produced with the technique known as spunbonding(186-190). A schematic of the spunbonding apparatus is shown in Figure 4.1. In spunbonding, a hot polymer melt is extruded from a heated die and then fed through a high speed air venturi to attenuate the polymer strand to a fine diameter fiber. The polymer used in the production of fibers was PLLA (grade 6251D, 1.4% D enantiomer 108,500 MW, 1.87 PDI, NatureWorks LLC.) In the present work, a custom Brabender extruder of 19.1 mm (0.75 in.) diameter and 381 mm length was used to melt and pressurize the polymer. The barrel of the extruder had a 20:1 L/D ratio and a 3:1 compression ratio. The polymer exiting from the extruder was then fed to a modified Zenith pump which pumped controlled quantities of molten polymer through a heated die which has a single polymer capillary of 0.420 mm inside diameter. The die assembly was heated using two 250 W cartridge heaters. Polymer flow rates were varied from 0.13 to 0.81 g/min. The polymer strand exits the die and feeds through an air venturi 100 cm below the die nozzle. Room temperature air flow to the venturi was measured and controlled using a rotameter. During spunbonding, a collection screen was placed 175 cm below the die face. The collection screen was manually circulated in order to obtain even layering of the fibers. This procedure resulted in a random lay down of fibers known as nonwoven. Layers of fibers were stacked and measured until the stack reached a mass of 9.0 ± 0.1 g within an area of 162.8 cm^2. From the collected nonwoven fiber stack, a center cut sheet having a 7 cm diameter was collected. This procedure was the same as that used by de Rovere and Shambaugh(186). Finally using an 8 mm diameter die, discs were punched from the layered 7 cm diameter fiber sheets. The resultant scaffolds were ~85% porous with an 8 mm diameter and ~2.3 mm thickness. Collected fibers' diameters were measured optically using a Nikon HFX-II microscope. Eleven fiber diameters were taken and averaged for each sample. For the nonwoven fiber scaffolds produced for this study, the average diameter of the fibers was 34.8 ± 1.85 μm. Porosity was determined by the same method as porous foams: the solid volume (mass of the scaffold divided by the density of PLLA) was measured and compared to the total scaffold volume (assuming a cylindrical scaffold shape.)

4.2.3 Cell Culture

Preliminary cell culture was performed similar to Chapter 3 except when cells were plated flasks were supplemented with osteogenic media and when cell cultures reached ~80% confluency were washed with phosphate buffered saline, lifted with trypsin (Invitrogen), centrifuged at 400 g for 5 min, re-suspended in osteogenic media and used for seeding.

4.2.4 Scaffold Pre-Wetting

Before seeding, scaffolds were sealed into a beaker containing ethanol with a septum stopper. Vacuum was applied to the vessel until air ceased to visibly escape the scaffolds. Penetration of the scaffolds by ethanol pre-wetted the scaffolds reducing surface tension to allow the scaffolds to ubiquitously be penetrated by cell suspensions and media during seeding and culturing(185). The scaffolds were immediately removed from the beaker and press fit into cassettes.

4.2.5 Dynamic Seeding and Culture

Cassettes containing pre-wet scaffolds were placed into a flow perfusion bioreactor(172). The perfusion bioreactor has been previously used for culture of MSCs in 3-dimensional scaffolds(107, 119, 169). To rinse and cure the system, 200 mL of osteogenic media was perfused through scaffolds and bioreactor for 1 hour. Using oscillatory flow perfusion 500,000 MSCs per scaffold were seeded(121, 184). Briefly, MSCs suspended at 500,000 cells per 0.25 mL of osteogenic media were pipetted over each scaffold. Cells were perfused though the scaffolds at a flow rate of 0.15 mL/min for 5 min until the suspension volume passed through the scaffolds. The direction of flow was reversed and the cells were passed back through the scaffolds. This procedure was repeated for 2 hours. Flow was then stopped and the cells were allowed to rest and adhere for 2 hours. After the resting period, cassettes containing scaffolds for static culture were removed from the bioreactor and placed in a 6 well plate and submerged with 10.5 mL of osteogenic media. Cassettes for dynamic culture were left in the bioreactor and a continuous unidirectional flow of 0.5 mL/min/scaffold was applied. All cultures were incubated at 37 °C and 5% CO_2 with media being replaced with fresh ostogenic media every 3 days. Seeded scaffolds were cultured periods of 4 and 8 days.

4.2.6 Scaffold Analysis

Once culture periods concluded, scaffolds were removed from cassettes, washed with PBS and placed in sample vessels containing 3 mL of DIH_2O. Foam scaffolds in DIH_2O were broken down into small pieces and fiber scaffolds in DIH_2O had their structures opened up. Samples were then subjected to 3 freeze/thaw cycles to lyse the cells. Samples were then analyzed for scaffold cellularity, ALP activity, and calcium content similar to chapter 3.

4.2.7 Statistical Analysis

Three samples were used ($n = 3$) for all experiments. Values were reported as the average of all samples in an experimental group, and error was reported as the standard error of the mean. Data was analyzed using ANOVA and multiple pair-wise comparisons were carried out using the Tukey method at a confidence level of 95%.

4.2.8 Scaffold Imaging via SEM

Once culture periods concluded, scaffolds were removed from cassettes and washed twice with PBS. The washed scaffolds were then fixed with 10% PBS buffered formalin (Sigma) at 4 °C overnight. Next, they were washed twice with PBS and passed through serial dehydration using ethanol-water. Samples were then critical point dried using an autosamdri-814 (Tousimis Research Corporation, Rockville, MD), mounted to metal stubs and sputter coated with gold-palladium using a Hummer VI triode sputtering system (Anatech LTD., Union City, CA). Noncellular porous foam and nonwoven fiber mesh scaffold samples were also mounted on metal stubs and sputter coated. Imaging was performed on a Zeiss 960 scanning electron microscope (SEM, Carl Zeiss SMT Inc., Oberkochen, Germany) with a tungsten filament. Digital imaging was made possible by the EDS 2008 program (IXRF Systems, Inc., Houston, Texas). SEM imaging allows for visualization of polymer scaffold structure, cellularity, ECM production, and cell morphology.

4.2.9 Scaffold Imaging via μCT

Two PLLA scaffolds of each architecture (one nonwoven fiber mesh and one porous foam) were analyzed via μCT by a ScanCo VivaCT40 (ScanCo Medical, Bassersdorf, Switzerland) to obtain 10μm resolution, 2D intensity image slices at optimum settings of 88 μA intensity and 45 kV energy. Acquired X-ray images were filtered for noise reduction and assembled into 3D reconstructions of the scaffolds using custom Matlab® code. The scans were segmented using a global thresholding technique, which resulted in the porosity of the scaffolds being within 1% of the experimentally measured values. The surface area of scaffolds was calculated using 3D reconstructions of μCT data based on an algorithm that has been reported elsewhere.(191)

Verification of average fiber diameter for the nonwoven fiber mesh scaffold was obtained by 3 different methods: 1) based on the surface area per solid volume ratio using Equation 1; 2) by fitting circles to fiber cross-sections on the μCT images using a Matlab® edge detection technique; 3) optically using a microscope. The area per solid volume or “specific surface area” of the medium for cylinders is given as:

$$S = \frac{4}{D} \tag{1}$$

where D is the fiber diameter.

The average pore size was estimated for the two types of scaffolds using their hydraulic radius, R_h. The hydraulic radius was calculated using the equation for a packed bed or porous medium

$$R_h = \frac{\varepsilon}{(1-\varepsilon)S_0} \tag{2}$$

where ε is the porosity and S_0 is the ratio of the surface area to the volume. These values were obtained from μCT image reconstructions. The hydraulic diameter, D_h, which is a reflection of the average pore diameter for each of the scaffolds, was then calculated as

$$D_h = 4(R_h) \tag{3}$$

Values for R_h and D_h are reported in Table 4.1.

For each scaffold, a single cuboid portion was obtained from the center of the digital reconstruction, in order to avoid end effects in the flow simulations. The exact size of the reconstruction "cut-out" was similar with 5.41 mm x 5.41 mm x 1.53 mm for the porous foam scaffold, and 5.41 mm x 5.41 mm x 1.37 mm for the nonwoven fiber mesh scaffold.

4.2.10 Fluid Flow Simulations: Lattice Boltzmann Method

The lattice Boltzmann method (LBM) is a numerical technique for simulating fluid flow that consists of solving the discrete Boltzmann equation(192-194). In addition to computational advantages [e.g., LBM is inherently parallelizable on high-end parallel computers(195-196), and it is rather easily implemented], LBM techniques have been used in a wide spectrum of applications [turbulence(197), non-Newtonian flows(198-200), and multiphase flows(201).] More importantly, for the present application, LBM is especially appropriate for modeling pore-scale flow through porous media (such as scaffolds) due to the simplicity with which it handles complicated boundaries.

A custom-written, in-house code was developed for this work (see Voronov et al.(191) for further details.) The 3D, 15-velocity lattice (D3Q15) for LBM(202), in conjunction with the single-relaxation time approximation of the collision term given by Bhatnagar, Gross and Krook(203), was used to perform simulations. Periodic boundary conditions were applied in all three directions, in order to approximate an infinite domain. The no-slip boundary condition was applied at the wall faces using the "bounce-back" technique(193). In order to take advantage of the inherent LBM parallelizability, the domain was decomposed using message passing interface. The LBM results were validated for several flow cases for which analytical solutions are available: forced flow in a slit, flow in a pipe, and, since the application of interest is flow through porous media, the LBM code was validated for flow through an infinite array of spheres(191).

The calculation of the shear stress was conducted following the scheme suggested by Porter et al.(175), where the full shear stress tensor is calculated first, and then the maximum eigenvalue is evaluated using a Jacobi iteration technique. The cell culture media was assumed to be a Newtonian fluid and the shear stresses within a scaffold was estimated as

$$\underline{\underline{\sigma}} \approx \mu\left(\frac{1}{2}\right)\left(\nabla\vec{U} + \nabla\vec{U}^{T}\right) \qquad (4)$$

where $\underline{\underline{\sigma}}$ is the shear stress tensor, and $\vec{U}$ is the local velocity vector. The fluid dynamic viscosity was 0.01 g/cm s, which is close to that of α-MEM supplemented with 10% FBS which is typically used in cell culturing experiments(204). Velocity vectors used in calculations were derived from flow rates of 0.5 mL/min (used in experiments conducted in this study) and 1 mL/min, both similar to commonly employed flow rates for the culturing MSCs in the flow perfusion bioreactors(100, 107, 119, 168, 205). The shear stresses reported herein are the largest eigenvalues of $\underline{\underline{\sigma}}$.

4.3 Results and Discussion

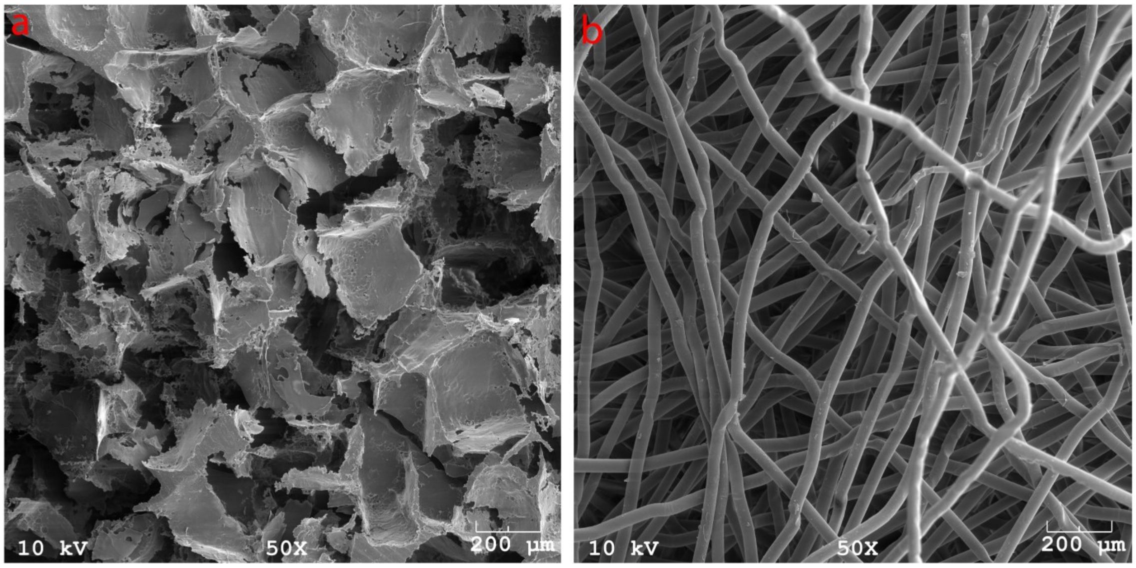

Figure 4.2: SEM images of a plain noncellular a) porous foam scaffold created by solvent casting/particulate leaching and a b) nonwoven fiber mesh scaffold created by spunbonding. The images were taken at 50x magnification and the scale bars are 200 µm.

4.3.1 Polymer Scaffolds

Porous foams made by solvent casting/particulate leaching and nonwoven fiber meshes have distinctively different architectures. This can be seen from the SEM images of the plain scaffold surfaces in Figure 4.2. The porous foams can be distinguished by their characteristic thin walls and the cuboidal structure of the pore space. The fiber meshes can be distinguished by their series of randomly overlaying cylinders. 3D reconstructions from μCT scans further illustrate these architectural distinctions (Figure 4.3.) The 3D reconstructions also revealed highly interconnected porous networks contained within both of the scaffolds types. The accuracy of the global threshold chosen for μCT image segmentation was verified by comparisons between the diameter of the PLLA fibers obtained from the μCT reconstructions and the diameter of the fibers measured with other methods (microscope and SEM). Table 4.1 is a summary of various other geometric characteristics of the two scaffold types, showing similarities between the scaffolds. The average pore size, estimated using D_h, was one of these similarities. The value of 271.28 μm for porous foams falls within the range of values of the salt grain size (250-355 μm) that was used to create the void space of the scaffold.

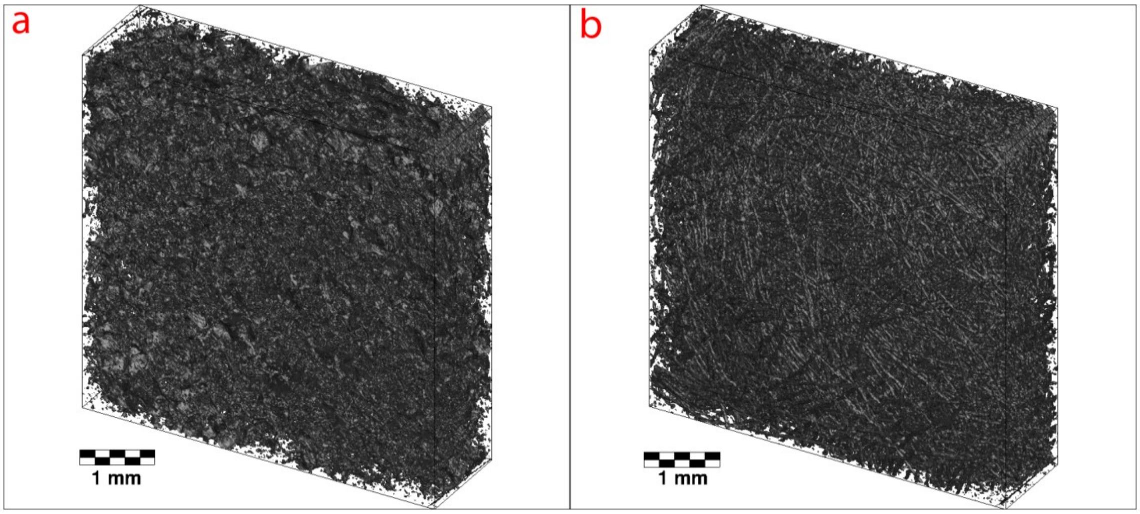

Figure 4.3: Matlab® 3D reconstructions from μCT imaging of a a)porous foam scaffold created by solvent casting/particulate leaching and a b)nonwoven fiber mesh scaffold created by spunbonding

	Nonwoven Fiber Mesh	Porous Foam
Void Fraction	0.85	0.85
Surface Area / Solid Volume [cm^{-1}]	1046.47	835.52
Surface Area / Total Volume [cm^{-1}]	157.33	125.08
Mean Diameter From Specific Area [μm]	38.22	-
Mean Diameter From Edge Detection [μm]	33.01 ± 5.73	-
Mean Diameter From Microscope [μm]	34.8 ± 1.85	-
Hydraulic Radius [μm]	54.15	67.82
Hydraulic Diameter [μm]	216.60	271.28

Table 4.1: Scaffold comparison based on geometric characteristics

4.3.2 Shear Stress Distribution within the Pore Space

In order to compare the two scaffold types (nonwoven fiber mesh and porous foam) on geometrically equivalent basis, two scaffolds were prepared with roughly equivalent specific surface area and volume fraction parameters (see Table 4.1). The surface stress was calculated for both scaffolds using LBM and the results are summarized in Table 4.2. Figure 4.4 contains images of Matlab® 3D reconstructions of average surface shear stresses on the porous foam and nonwoven fiber mesh scaffolds.

	0.5 mL/min		1 mL/min	
	Nonwoven Fiber Mesh	Porous Foam	Nonwoven Fiber Mesh	Porous Foam
Mean Surface Stress [$g/cm\ s^2$]	0.12	0.13	0.27	0.25
Standard Deviation [$g/cm\ s^2$]	0.09	0.11	0.21	0.18
Standard Deviation as % of Mean	74.84	78.18	78.19	74.85

Table 4.2: Surface stress calculation results for nonwoven fiber mesh scaffold made by spunbonding and porous foam scaffold made by solvent casting/particulate leaching obtained from LBM for 0.5 mL/min and 1 mL/min flow rates

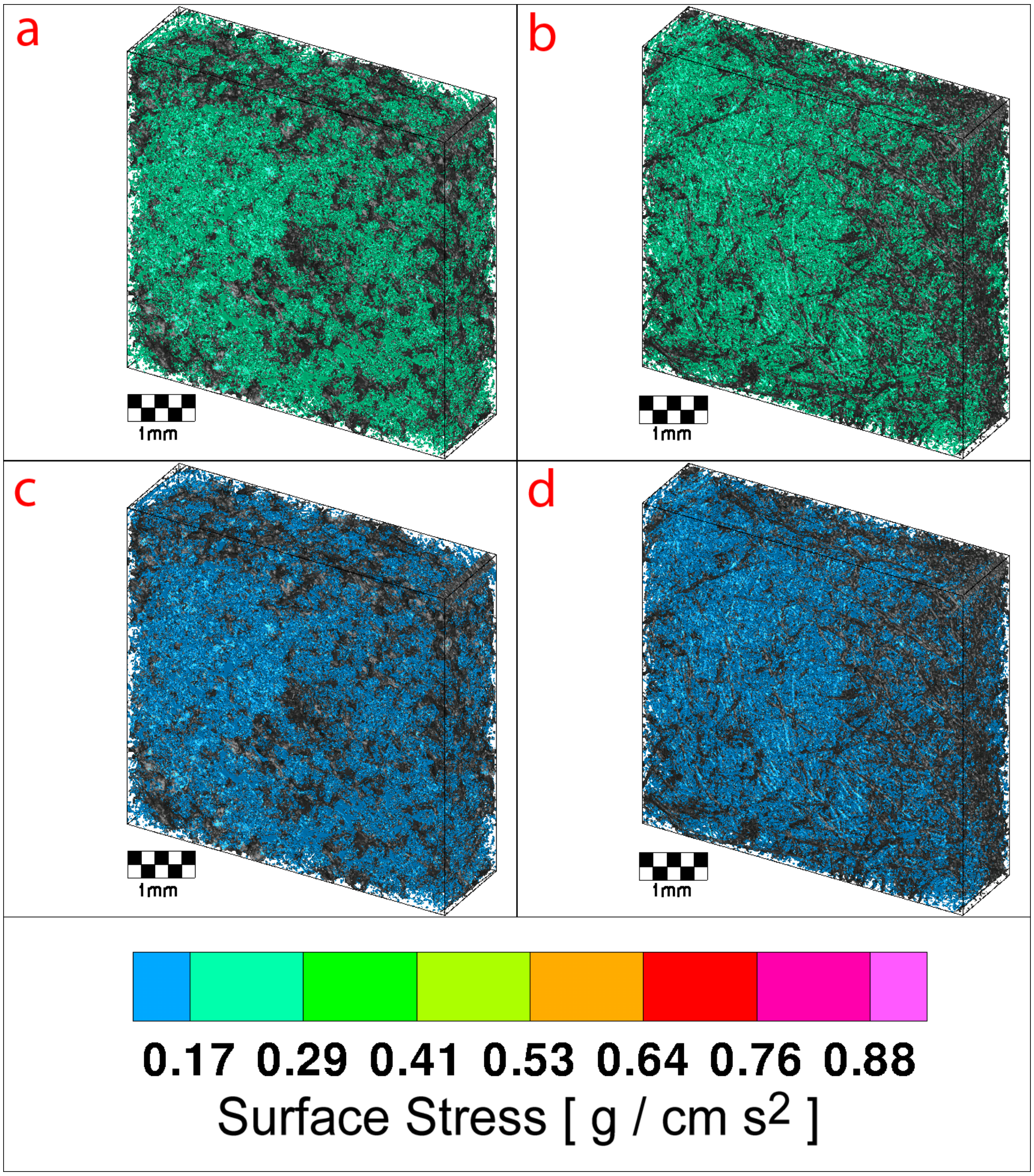

Figure 4.4: Matlab® 3D reconstructions from µCT imaging showing average surface shear stresses for a 1 mL/min flow rate in a a) porous foam scaffold created by solvent casting/particulate leaching and a b) nonwoven fiber mesh scaffold created by spunbonding and 0.5 mL/min flow rate in a c) porous foam scaffold created by solvent casting/particulate leaching and d) nonwoven fiber mesh scaffold created by spunbonding.

Since it is apparent from Table 4.2 that there is no appreciable difference between the mean surface stress values for the two differing scaffold geometries, the distribution of the surface stress was examined next. This is the distribution of shear stresses that cells would experience if they were attached to the scaffold surface in a single cell layer which is an idealized case during initial stages of culturing. The probability density function (PDF) that the surface stress follows inside the porous foam and nonwoven fiber mesh scaffolds is shown in Figure 4.5. From these figures it can be concluded that the shape of the PDF of the surface stress of the two different scaffold geometries does not display a significant difference. Both of the PDFs are skewed to the right. Increasing the flow rate results in an elevated mean shear stress, as expected, and a wider distribution of shear stresses with increased skewness toward higher shear stress values for scaffolds of both architectures.

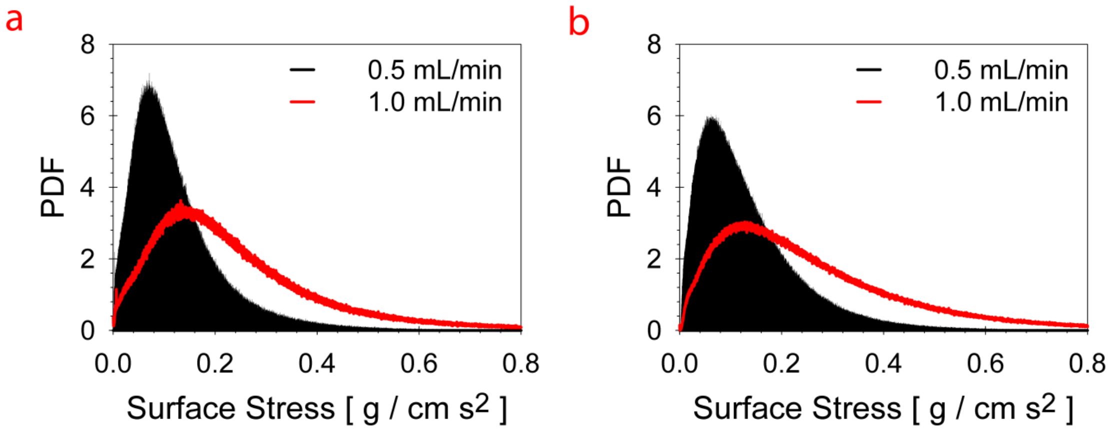

Figure 4.5: Probably density functions (PDF) of the surface stress in a) porous foam scaffold produced using solvent casting/particulate leaching method and b) nonwoven fiber mesh scaffold made by spunbonding method obtained from calculations using LBM method for a flow rate of (shaded)0.5 mL/min with (red line)1 mL/min overlay.

LBM can also used to calculate permeability, another important parameter that is often measured for porous materials. These calculations can be easily compared to semi-empirical correlations further validating the LBM method. A multitude of analytical solutions for creeping flow through geometrically simple cylinder arrangements, as well as semi-empirical correlations for creeping flow through more geometrically complicated cylinder arrangements exist(206-208). Table 4.3 contains a comparison of the permeability values obtained from LBM to the Blake-Kozeny-Carman (BKC) equation

$$K = \frac{\varepsilon^3}{(1-\varepsilon)^2} \frac{1}{S^2 k} \tag{5}$$

where ε is the medium void fraction, S is $4/D$ for cylinders if D is the diameter of cylinders, and k is the Kozeny constant ($k \approx 5$ from experiment(209).) Since the BKC equation is well established, simple to use and versatile, it appears that it can be used for the estimation of the permeability of high-porosity scaffolds such as the ones used in this study. Detailed fluid dynamics simulations can provide the local shear stress field and the shear stress distribution. The S used in BKC calculations is the same obtained from our algorithm used in 3D reconstructions of μCT data (see 4.2.9 Scaffold Imaging via μCT) The permeability of the foam scaffold is about 45% higher than the permeability of the fiber mesh scaffold, which is a reflection of the higher specific area of the fiber mesh (see Table 4.1.)

	Nonwoven Fiber Mesh Permeability [cm^2]	% Difference from LBM	Porous Foam Permeability [cm^2]	% Difference from LBM
LBM [cm^2]	5.29×10^{-6}	-	7.70×10^{-6}	-
BKC Equation (Assuming k = 5) (208-209)	4.96×10^{-6}	6.32	7.86×10^{-6}	2.08

Table 4.3: Comparison of scaffold permeability obtained from LBM to prediction from the BKC equation for porous foam scaffolds and nonwoven fiber mesh scaffolds.

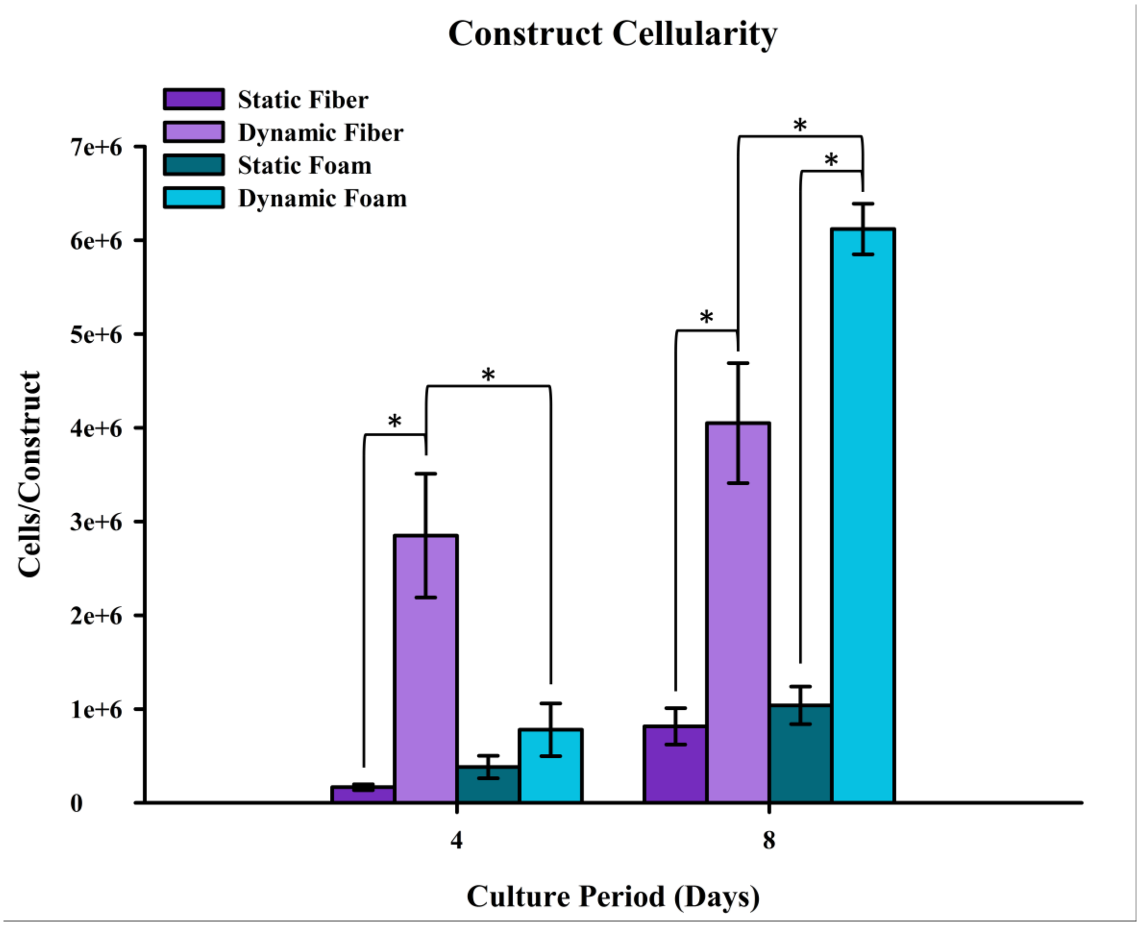

Figure 4.6: Cellularity of cell/polymer nonwoven fiber mesh scaffolds made by spunbonding and porous foam scaffolds made by solvent casting/particulate leaching for 4 and 8 day periods of dynamic culture in the flow perfusion bioreactor and static culture. The results are presented as means ± standard error of the mean for *n* = 3. (* indicates significance p<0.05)

4.3.3 Scaffold Cellularity

As seen in Figure 4.6, dynamically cultured scaffolds were seen to have higher cellularity for both culture periods compared to statically cultured scaffolds. These results are comparable to previously performed studies(107, 119, 168, 205) and denote the significant benefits of flow perfusion cultures on the cellular growth of preosteoblastic cells seeded onto 3D porous scaffolds. Dynamically cultured fibers were seen to have over 3.5 times higher scaffold cellularity at 4 days than porous foams cultured dynamically. This observation was then reversed for 8 day dynamically cultured scaffolds showing porous foam scaffolds with 1.5 times higher scaffold cellularity then fiber samples. These cellular proliferation observations in dynamic cultures may be because cells seeded onto nonwoven fiber scaffolds were able to grow to and between neighboring fibers allowing for higher initial cellular proliferation on fibers interconnected by cell growth. These interconnected cellular networks are necessary for advancing the tissue formation beyond the material surface where cells are originally seeded. Cells seeded upon porous foam scaffolds needed to lay down ECM and migrate to make intracellular connections before cellular proliferation and differentiation could occur more rapidly. No significant difference in scaffold cellularities were seen between statically cultured fiber scaffolds and statically cultured porous foam scaffolds for both culture periods.

4.3.4 Alkaline Phosphatase Activity

Increases in alkaline phosphatase activity have shown to be a good indication of commitment towards osteoblastic differentiation(15, 149). From Figure 4.7, MSCs dynamically cultured on fiber scaffolds were seen to have significantly higher ALP activity, 3.7 to 4.2 times higher, then fiber scaffolds cultured statically. Cells dynamically and statically cultured on porous foam scaffolds exhibited similar ALP activity to one another at 4 days of culture. After 8 days of culture, cells dynamically cultured on porous foam scaffolds showed 3.6 times higher ALP activity over cells statically cultured on porous foam scaffolds. Thus, after 8 days of culture flow perfusion significantly enhanced the osteoblastic differentiation of MSC compared to their respective static controls in good agreement with previous studies(99, 107, 119, 168, 205).

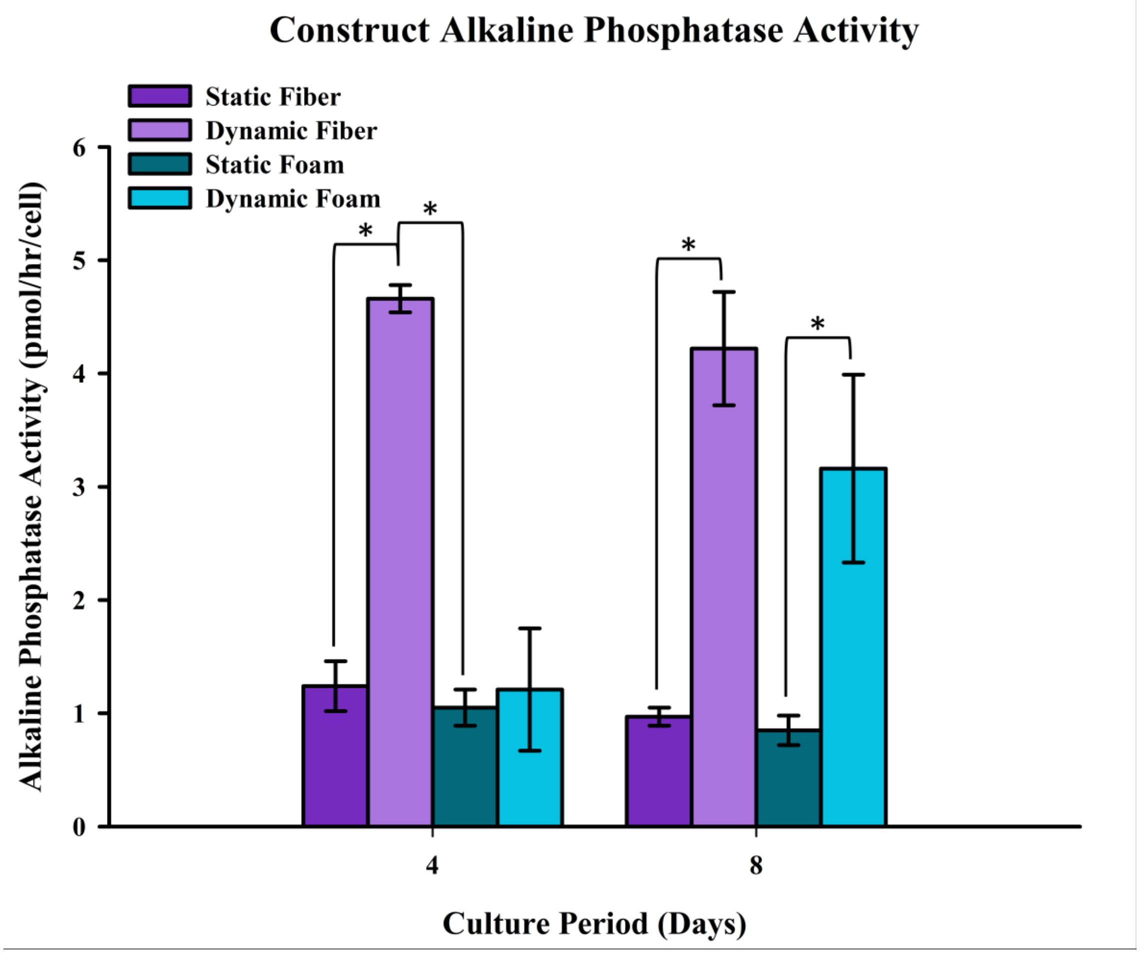

Figure 4.7: ALP activity of cell/polymer nonwoven fiber mesh scaffolds made by spunbonding and porous foam scaffolds made by solvent casting/particulate leaching for 4 and 8 day periods of dynamic culture in the flow perfusion bioreactor and static culture. The results are presented as means ±standard error of the mean for *n* = 3. (* indicates significance $p<0.05$)

Interestingly, after 4 days of culture only the perfused MSCs seeded onto the nonwoven fibers demonstrate enhanced osteoblastic differentiation implying that the observed rapid proliferation on these scaffolds under flow perfusion was accompanied by accelerated differentiation unlike the foams where the cells appeared to require a rearrangement of their microenvironment before they could get into the proliferative and differentiation phase as seen in the day 8 cultures. Under similar dynamic conditions, as seen in the study of 99% porous PLLA nonwoven fiber meshes scaffolds(168), more time is taken to get to a highly proliferative phase with an enhanced commitment towards the osteoblastic lineage. The porous foams used in this study and the highly porous nonwoven fiber meshes from the previous study both appear to require the cells to overcome larger open distances to establish an interconnected network. This overcoming of intercellular distances with cell proliferation and tissue growth and later cell differentiation may have been the cause of this culture timing. This timing has been commonly seen with other materials under similar culture conditions(100, 107, 119, 205). The task of establishing a cellular network may be easier in nonwoven fiber mesh scaffolds of lower porosity, like the 85% porous ones used in this study, due to the availability of numerous fiber-fiber contact points that permit the deposition of ECM with greater ease.

Cells cultured on fibers were seen to have 3.8 times greater ALP activity over cells on porous foams after 4 days of dynamic culture but at 8 days of dynamic culture, cells cultured on fiber scaffolds had statistically similar ($p>0.05$) ALP activity to cells cultured on porous foam scaffolds. These results are aligned with the cell proliferation data and denote the need of the MSCs to establish a widespread ECM network on the two types of scaffolds. This task appears to require a longer period for cultures on the salt leached foams. After this occurrence in both scaffold types cultured under flow perfusion, shear forces become the dominant mechanism for induction of osteoblastic differentiation (as seen in day 8 ALP data). Finally, no significant difference in ALP activities was seen between cells statically cultured on fiber scaffolds and cells statically cultured on porous foam scaffolds at both time points as expected since the material that the cells were grown in both cases was PLLA.

4.3.5 Calcium Deposition

The determination of the presence and/or amount of calcium gives indication of the degree of mineralization of deposited extracellular matrix. The presence of increased amounts of mineralized extracellular matrix gives indication of maturing osteoblastic cultures(15, 149). All samples, except for the 8 day dynamically cultured fiber constructs, displayed measurements in the noise region, indicating no notable amounts of calcium. 8 day dynamically cultured nonwoven fiber scaffolds had 225 ± 7 μg Ca^{2+}/scaffold. This presence of calcium coincides with the increased presence of ALP activity for the dynamic fibers at 4 days of culture, indicating a quick maturity. Artificial scaffolds cultured under similar conditions have shown little or no calcium deposition present at about 8 days(100, 119, 168). This demonstrates the MSCs preference for quicker differentiation and mineralization under flow conditions on the nonwoven fiber mesh scaffolds.

4.3.6 SEM Imaging

SEM images provided visualization of cellularity, ECM production, and cell morphology of cultured cellular constructs. Static cultures showed cells exhibiting both rounded appearances signifying morphologies similar to that of MSCs (Figure 4.8e) and flat cuboidal shapes signifying the morphology of osteoblastic like cells. Cells on statically cultured scaffolds were isolated into multiple smaller individual communities and cells. Dynamic cultures displayed more cells and ECM along the surface compared

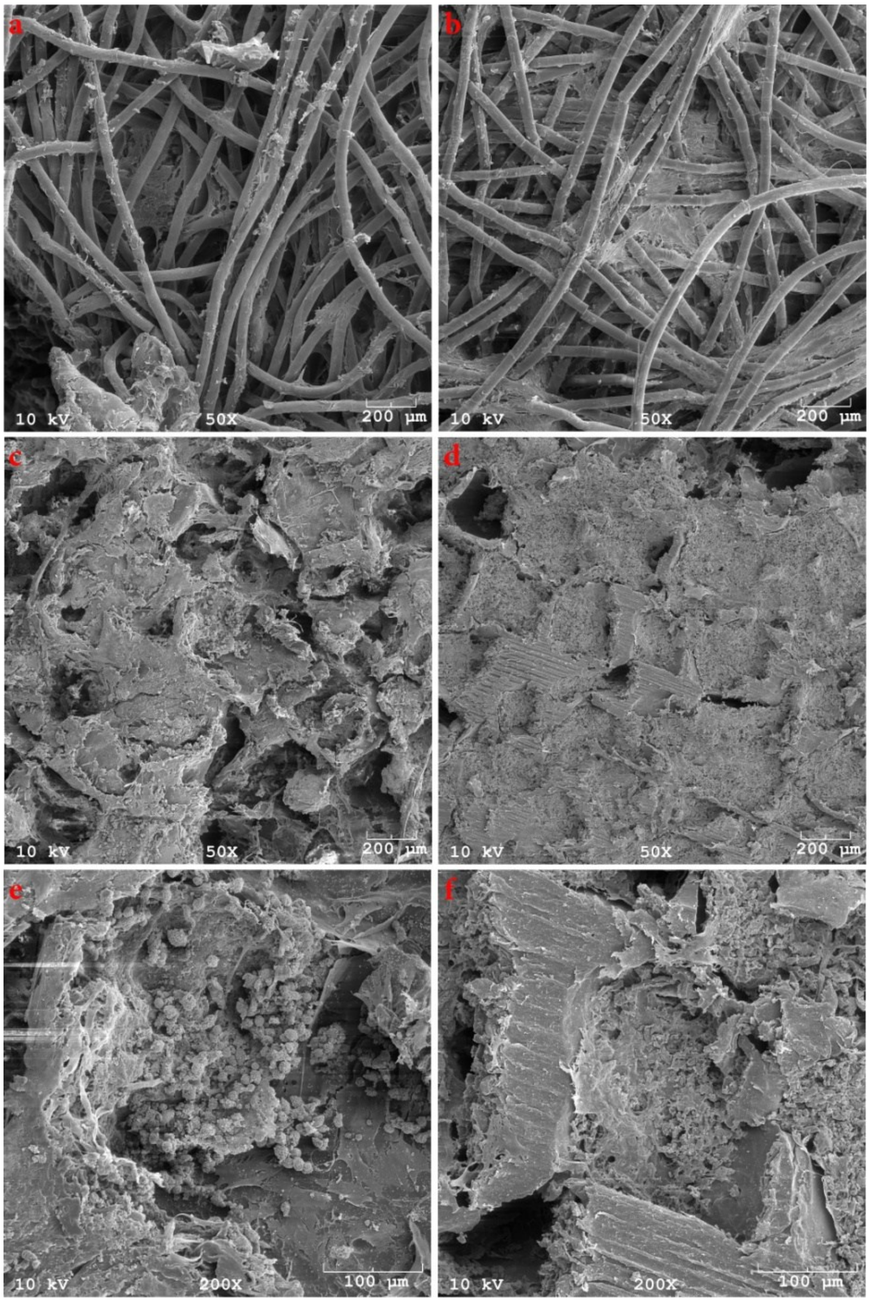

Figure 4.8: SEM images of the top/inlet surfaces of long term cultured scaffolds. a) Statically cultured fiber scaffold, b) dynamically cultured fiber scaffold, c) statically cultured foam scaffold, d) dynamically cultured foam scaffold, e) statically cultured foam scaffold showing rounded cells similar to the morphology of MCSs, and f) dynamically cultured foam scaffold showing cells with a flat cuboidal shape within extracellular matrix exhibiting the morphology of an osteoblastic cell culture which is a good indication of osteoblastic differentiation. Images a-d taken at 50x magnification and scale bar is 200 µm. Images e and f taken at 200x magnification and scale bar is 100 µm.

to static cultures and all cells visualized had morphologies similar to those of osteoblastic like cells (Figure 4.8f). The scaffold base side (denoting the exit of flow perfused media) of dynamically cultured scaffolds also had a higher presence of cells compared to statically cultured scaffolds, which were almost absent of cells (images not included). This lack of rounded cells and increase in the amount of cells and ECM present on dynamically scaffolds show the promotion of proliferation and differentiation from fluid shear. Images of dynamically cultured nonwoven fiber mesh scaffolds (Figure 4.8b) showed cells settled into communities around spaces were fibers were near, touching, or crossing one another. Cells that attached to independent fibers that had no close neighboring fibers, laid down to the surface of the fiber they were attached with minimal ECM formation. Analysis of SEM images of dynamically cultured porous foams (Figure 4.8d) displayed cells penetrating the interior of pores. Interestingly cell growth and matrix deposition seems disproportionate in some pores. This could lead to clogging and changes to fluid flow characteristics in longer culture periods. Cell growth on fiber mesh scaffolds appears to be more evenly distributed.

4.4 Conclusions

As seen with previous studies, dynamic cultured MSCs using flow perfusion enhances growth and differentiation over statically cultured MSCs within the first 8 days. This was also found to be independent of architecture for scaffolds made from the same material, PLLA, with similar porosity, 85%, and surface to solid volume ratio.

Given similar porosities and surface area to solid volume ratios, the differences in architecture between scaffolds made by solvent casting/particulate leaching and spunbonding do not cause a significant difference in the LBM results for the average value of the wall shear stress of for the shape of the probability density function that the shear stress follows. Therefore, the differences observed experimentally in the cell behavior should be attributed mostly on the cell's response to the architecture of the scaffold, and not to the differences in fluid-induced shear stress experienced by the cells.

MSCs seeded onto nonwoven fiber mesh scaffolds made by spunbonding were able to grow to neighboring fibers allowing for higher initial cellular proliferation and quicker differentiation while cells seeded upon porous foam scaffolds made by solvent casting/particulate leaching probably needed to first lay down ECM and then migrate to make cellular connections before cellular proliferation and differentiation could occur. The generalized results of this study may be applicable to many other similar polymer scaffolds using flow perfusion. The computational methodology used in this study could be applied to a wide variety of scaffold systems independent of structural and material properties.

4.5 Disclosure

Microfiber fabrication was performed by Taren Blue. μCT reconstructions and computational modeling were performed by Dr. Roman Voronov.

Chapter 5: Influences of Chemical and Mechanical Stimuli on the Detachment of Mesechymal Stem Cells Seeded on PLLA Scaffolds

5.1 Introduction

The adherence of cells to scaffolds is an important first step in the long term *in vitro* culturing of BTE constructs. Mechanostimulation of preosteoblastic cells by fluid shear has been found to promote differentiation and the production and calcification of extracellular matrix(15, 102, 210). However, high shear rates may also cause the detachment of cells from the scaffold surface immediately after seeding(121). This shows that the fluid shear that is considered beneficial in BTE could also be a highly destructive force. If too many cells are removed from the scaffold, the cells will not proliferate and produce neotissue. There must be a balance between the destructive and constructive qualities of fluid flow that will allow optimum development of a tissue *in vitro*.

Chemical supplements have been used many times to stimulate the differentiation and development of bone-like matrix(37, 60). The main additives that are attributed to the encouragement of preosteoblastic cells to differentiate are dexamethasone and BMP-2. Dexamethasone was one of the first chemicals used to encourage osteoblastic differentiation and mineralized matrix production(15, 211). Dexamethasone is usually provided in media with ascorbic acid and beta-glycerophosphate. The genesis of collagen fibrils increases in the presence of ascorbic acid, which is already found in culture media, and is provided in increased levels as a source of encouragement for the development of ECM. Beta-glycerophosphate's role in media is to provide a rich phosphate source to allow genesis of mineralized tissue(211). While the combination of dexamethasone, ascorbic acid and beta-glycerophosphate's osteoinductive abilities are well documented in BTE(1, 13, 16-17, 102, 119, 210, 212-213), all their effects upon the cells are not fully understood. Our main hypothesis is that one or more of these supplements could cause rapid changes to cells and affect cellular adhesion in a positive or negative way.

In order to try and characterize these cellular detachment phenomena in a flow perfusion system, preosteoblastic MSCs were seeded on PLLA scaffolds using both static seeding and dynamic seeding within a flow perfusion bioreactor. During the seeding process, cells were exposed to either basic culture media (αMEM) or osteogenic media containing the supplements dexamethasone, ascorbic acid, and beta-glycerophosphate. The resulting seeded scaffolds were then exposed to fluid flow shear forces up to 48 hours. The following is a detailed description of this set of experiments.

5.2 Materials and Methods

5.2.1 Cell Culture

MSC's were obtained from rats by the same methods used in chapter 3. At ~70% confluency, flasks of 3rd passage MSC's were lifted from the surface with 0.25% Trypsin (Invitrogen) and resuspended in either basic culture media (αMEM, Atlanta Biologicals) or osteogenic media (αMEM supplemented with 10^{-8}M dexamethasone, 10mM β-glycerophosphate, and 50mg/L ascorbic acid (all supplements from Sigma-Aldrich)) for seeding.

5.2.2 Scaffold Manufacturing

Porous foam PLLA scaffolds, of 85% porosity, were prepared using solvent casting/particulate leaching method(8, 183-185) which has been outlined in chapter 4.

5.2.3 Seeding

To enable effective scaffold seeding, Porous foam PLLA scaffolds were pre-wet with ethanol according to the methods outlined in chapter 4. Then the pre-wet scaffolds were seeded either statically or dynamically. For static seeding scaffolds press fit into cassettes were placed in a 6-well culture plates. 1×10^6 MSC's suspended in 0.25 mL of either basic αMEM or osteogenic media were pipetted over the top surface of the scaffolds. The well plates where then placed in a cell culture incubator (37° C and $5\% CO_2$) and cells were allowed to attach to the scaffold for 4 hours. For dynamic seeding, scaffolds were seeded in a flow perfusion bioreactor(127) using oscillatory seeding(121) which has been outlined in chapter 4. For dynamic seeding 1×10^6 MSC's suspended in either basic αMEM or osteogenic media were placed over each scaffold. The media that was used in the bioreactors coincided with the media used for suspension.

5.2.4 Cell Detachment by Fluid Shear

To facilitate detachment of cells from the surface of the PLLA porous foams, scaffolds were subjected to a continuous unidirectional flow rate of 1 mL/min/scaffold (0.25 ± 0.18 $g/cm \cdot s^2$ shear stress(214)) within a flow perfusion bioreactor after seeding(121). Detachment periods were either 8 or 48 hours. Scaffolds were removed from flow at evenly spaced intervals along the full detachment period. For 8 hour detachment periods scaffold samples were pulled at 0, 4, and 8 hours. For 48 hour detachment periods sample scaffolds were removed from flow taken, at 0, 24, and 48 hours. 4 scaffolds were taken at per each time point detachment experiments were performed twice. ($n = 4 \times 2 = 8$)

5.2.5 Scaffold Cellularity Analysis

DNA analysis using PicoGreen® was used quantify the removal of cells from the scaffolds. The method of scaffold preparation and DNA analysis has been described in chapter 4.

5.2.6 Statistical Analysis

Values were reported as the average of all samples within an experimental group with error reported as the standard error of the mean. Data analysis was performed using ANOVA and multiple pair-wise comparisons were conducted using the Tukey method with a confidence level of 95%.

5.3 Results

To analyze initial seeding effects, MSCs were seeded on scaffolds either statically or dynamically using both αMEM and osteogenic media (n=6). Seeding efficiencies for statically seeded scaffolds were 25.9±0.8% αMEM and 31.4±3.4% osteogenic and for dynamically seeded scaffolds seeding efficiencies were 25.7±5.1% αMEM and 20.8±3.0% osteogenic. No significant differences were observed between statically seeded and dynamically seeded scaffolds using αMEM. A significant difference ($p<0.001$) was observed in scaffold cellularity between statically seeded and dynamically seeded scaffolds when osteogenic media was used (Figure 5.1). Also when seeding staticly, the use of osteogenic media statistically increases ($p<0.005$) the number of cells attached a scaffold when compared to the use of αMEM. This is effect is inverted during dynamic seeding with scaffolds seeded using αMEM having higher cellularity to those seeded using osteogenic media ($p<0.05$).

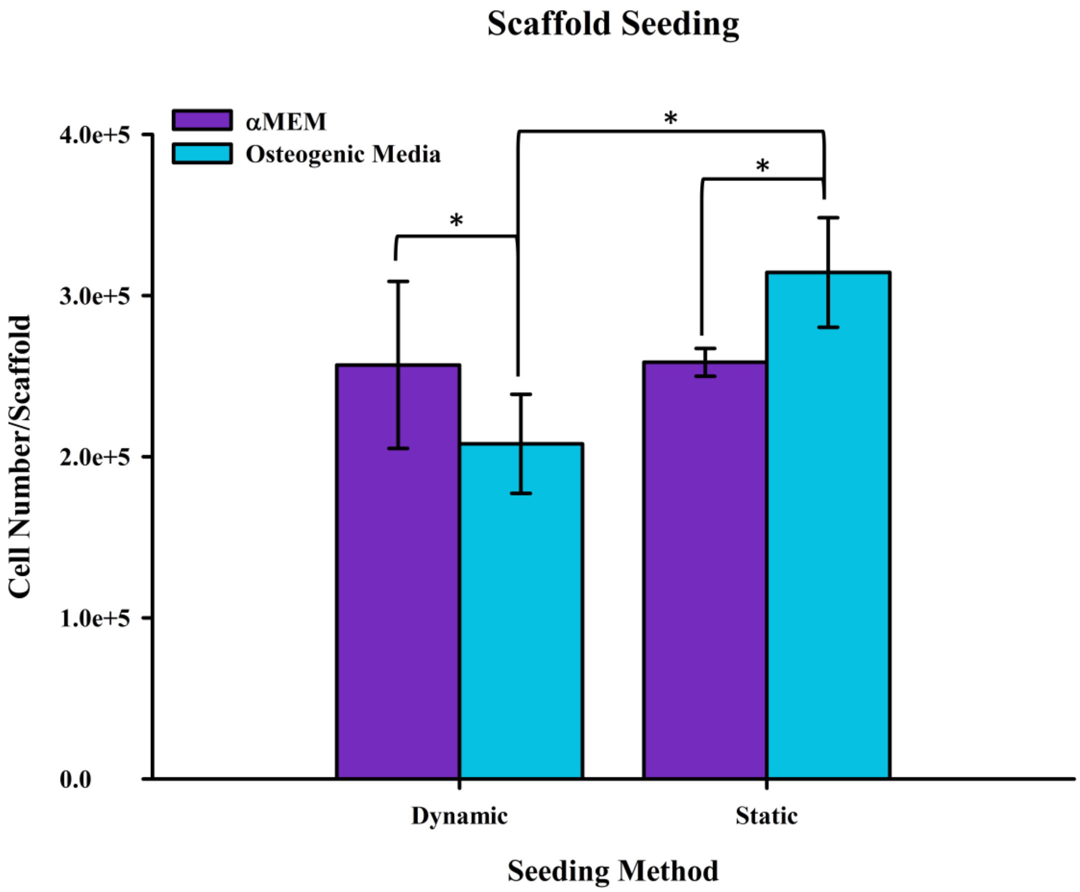

Figure 5.1: Graph of scaffold cellularities after seeding PLA porous foams either statically or dynamically in a perfusion bioreactor. Seeding was performed using either αMEM or osteogenic media. As seen from the graph, scaffold cell numbers are not significantly different when either seeding method was used with αMEM. When using osteogenic media. a static method of seeding results in more cells upon the scaffold over dynamic seeding. There is also an inverse relationship between the type of media used and the method of seeding where there are increased cell numbers with dynamic seeding with αMEM and static seeding with osteogenic media. (* indicates significance $p<0.05$)

The detachment of cells from the surface of scaffolds was examined for $1x10^6$ MSCs seeded upon PLA foam scaffolds either dynamically or statically and with either αMEM or with osteogenic media. When statically seeded scaffolds were subjected to a detachment flow rate of 1 mL/min/scaffold for 8 hours, the statically seeded scaffolds did not produce consistent results (data not shown). The cause of this may be due to the

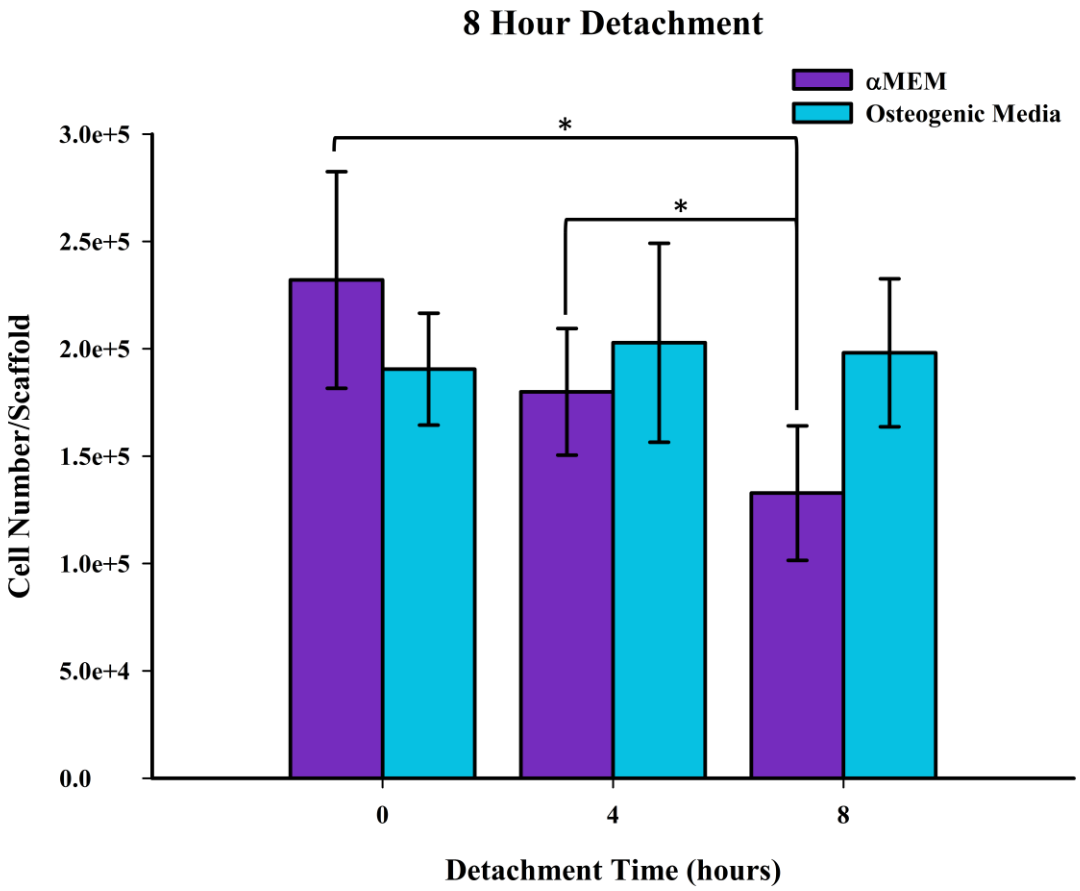

Figure 5.2: Graph depicting 8 hour detachment of MSCs from PLLA scaffolds using a 1 mL/min/scaffold fluid flow rate. MSCs were dynamically seeded on PLLA porous foams using either αMEM or osteogenic media. While the cellularities of scaffolds seeded in the presence of osteogenic media did not change significantly over an 8 hour detachment period, scaffolds seeded using αMEM showed a significant decrease in cellularity. (* indicates significance $p<0.05$)

uncontrollable nature of cell placement on the scaffold in which highly variable numbers of multicellular structures are bound to the scaffold surface via a small number of cell-material interactions. These large clusters may detach at even modest shear rates. When dynamically seeded scaffolds were subjected to the same 1mL/min/scaffold detachment flow, scaffolds seeded with osteoblastic media showed no change in cellularity(Figure 5.2). However, scaffolds seeded dynamically with αMEM had a statistically significant decrease ($p<0.005$) in scaffold cellularity with a drop from $2.32 \pm 0.26 \times 10^5$ cells at seeding to $1.33 \pm 0.31 \times 10^5$ cells after 8 hours of detachment flow.

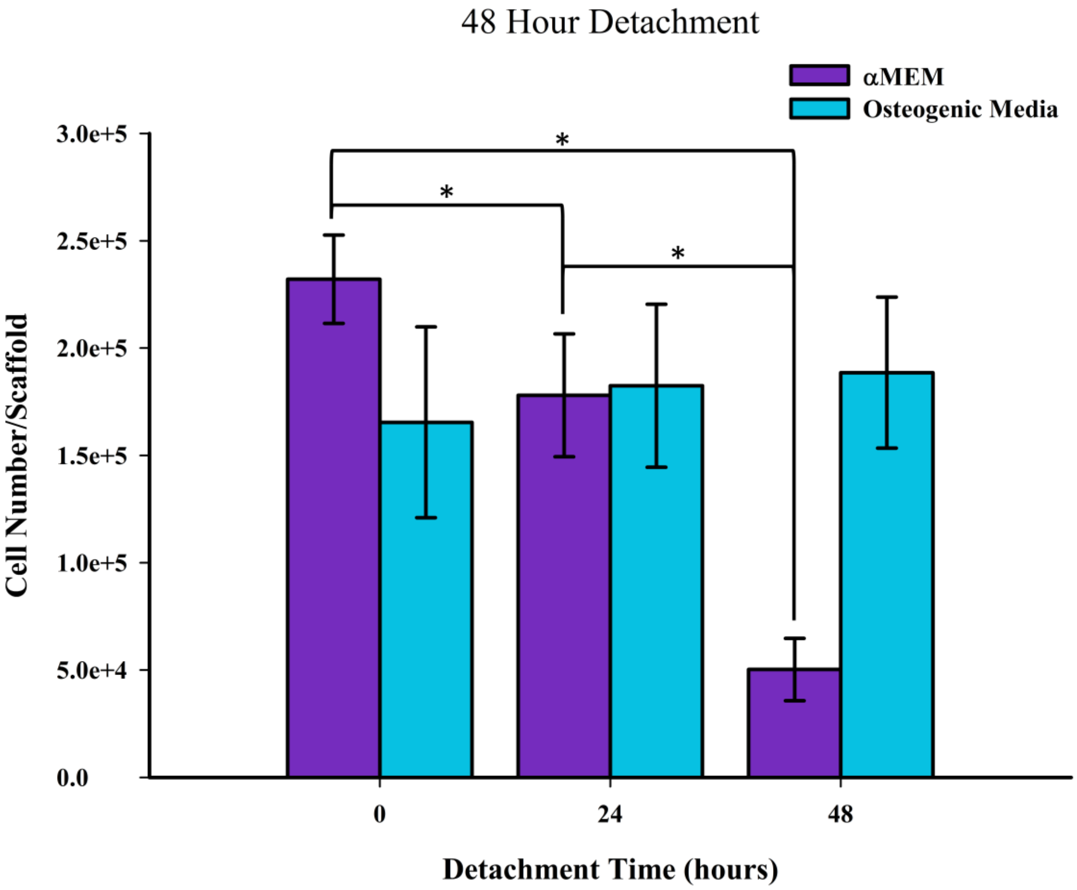

Figure 5.3: Graph depicting 48 hour detachment of MSCs from PLLA scaffolds using a 1 mL/min/scaffold fluid flow rate. MSCs were dynamically seeded on PLLA porous foams using either αMEM or osteogenic media. It is seen from the graph that while cellularities of scaffolds seeded in the presence of osteogenic media did not change a significant drop in scaffold cellularity is seen between 24 and 48 hours of detachment for scaffolds seeded using αMEM.

In order to try to achieve cellular detachment from scaffolds seeded using dynamic seeding with osteoblastic media, detachment periods were extended to 48 hours at a flow rate of 1 mL/min/scaffold (Figure 5.3.) Once again, scaffolds seeded dynamically using osteogenic media showed no change in scaffold cellularity over a 48 hour detachment period. A significant drop in scaffold cellularity ($p \ll 0.001$) was seen after 48 hours of unidirectional flow perfusion for scaffolds seeded using αMEM. The most significant drop occurred between 24 and 48 hours of detaching flow were scaffold cellularities dropped from $1.78\pm0.29\text{x}10^5$ cells to $0.50\pm0.15\text{x}10^5$ cells, equating to a 42.7±24.6% loss of cells.

5.4 Discussion

Although previous studies have reported increased cellular attachment using oscillatory seeding(121, 123), it was only seen in this study with the use of αMEM. In the case of seeding using osteogenic media, the resulting scaffold cellularities found were actually contrary to previous data with statically seeded scaffolds having higher cellularites ($3.14\pm0.34\text{x}10^5$ cells/scaffold) than dynamically seeded scaffolds ($2.08\pm0.31\text{x}10^5$ cells/scaffold). This may be attributed to inefficient washing of scaffolds after static seeding. This could have resulted in cell numbers being misrepresented by the inclusion of non-adherent cells that were trapped inside the porous network of the statically seeded scaffolds. The data also showed that inclusion of osteogenic supplements improved seeding by static methods but lowered the number of cells attached by dynamic seeding. Overall, the seeding efficiencies of all scaffolds (31.4±3.4% to 20.8±3.0%) were within expected ranges of ~20-30% for seeding on PLLA scaffolds.

A 1mL/min/scaffold flow rate was chosen in order to detach cells from the scaffolds because it has previously been used to develop BTE scaffolds using this bioreactor system. This denotes that the flow rate has the potential ability to encourage cellular proliferation within the same system(119, 127). When statically seeded MSC's were subjected to shearing flow, scaffold cellular retention was inconsistent. This may be because of the way cells set on the upper surface of scaffolds that are statically seeded(17). Cells that are statically seeded tend to attach near one another creating cell-cell bonds. This could cause the cells to come off in chunks or globs making data sporadic. Analysis of this phenomenon will have to be characterized by histology with sectioning of the scaffolds in line with the flow path or by fluorescent or SEM imaging of the surfaces of statically seeded scaffolds subjected to fluid shear flow. Because of the inconclusive data that came from trying to detach cells from the statically seeded scaffolds in an 8 hour period, 48 hour detachment experiments were not performed on statically seeded scaffolds.

Cells that were seeded dynamically appeared to be more adhered to the surface of scaffolds when compared to statically seeded scaffolds. This was apparent by the lack of cellular detachment observed in the 8 hour detachment runs performed on the dynamically seeded scaffolds using osteogenic media. Mechanical stimuli from fluid flow might be playing a role in the attachment of cells to polymer scaffolds. The trend that was observed in the 8 hour detachments lead to the extension of the detachment period. With 48 hours of detaching flow, a statistically observable drop in cellularity, a 78.4±7.5% loss, was seen for scaffolds seeded dynamically with αMEM. This indicates that there could be a problem associated higher flow rates when trying to culture MSC under flow perfusion. If cells continue to detach the ability for the scaffold to generate tissue would be greatly affected. Lower flow rates would have to be investigated to find a flow rate which creates a point of homeostasis. This would become the upper threshold for fluid flow in the system. Flow rates below this point would be useful in the culturing of MSCs using αMEM.

The lack in observable change in scaffold cellularity from the influence from detachment flow applied for 8 hours continued to 48 hour detachments of MSCs seeded dynamically with osteogenic media. This denotes a negligible cellular detachment from the polymer scaffolds. These observations show that the supplements provided in osteogenic media not only encourage preosteblastic differentiation and matrix production but also have an effect on cellular attachment. Because this is coupled with mechanical stimulus provided by fluid movement, a complex system of cellular attachment is presented.

Because of the mixture of chemical and mechanical stimuli, it cannot be ascertained what directly causes the observed lack of cellular detachment when osteogenic media is used to seed scaffolds dynamically. Detachment experiments where only one or combinations of two of the supplements are added to αMEM media could potentially elucidate if the detachment effects observed are linked to one of the chemical stimuli. More isolation experimentation will have to be performed.

5.5 Conclusions

Supplementation of basal media with the osteogenic additives dexamethasone, beta-glycerophosphate, and ascorbic acid causes a decrease in dynamic scaffold seeding. While this is observed, when osteogenic media is coupled with dynamic seeding, MSCs attached to 3D PLLA scaffolds resist detachment from fluid shear forces. Because there is a mixture of mechanical and chemical stimuli in the system, experiments that will isolate the supplements and mechanical forces will have to be developed and performed. Also, fluid shear in perfusion bioreactors seems to have a damaging effect on scaffold cellularity when MSCs are seeded dynamically onto PLLA scaffolds using αMEM. Seeking out a flow rate that will create a homeostasis for scaffold cellularity would create a culturing flow rate threshhold. Although these experiments present some interesting data, more research will need to be done to isolate solutions to the observed effects.

Chapter 6: 3D Bone Tissue Engineered Construct Analysis via Conventional High Resolution µCT without X-Ray Contrast

6.1 Introduction

There is a great range of materials, scaffold structures, seeding techniques and culturing methods used in 3D tissue engineering. In order to evaluate and compare the combinations of development techniques, many constructs must be destroyed. This raises a need for proficient and accurate methods of analyzing tissue scaffold integrations to allow for comparisons.

When trying to evaluate construct characteristics such as cell and tissue distribution histology by physical sectioning is the current gold standard of analysis. If someone wanted to generate a 3D representation of a scaffold using conventional histology, they would have to manually image multiple sections by optical microscopy. To do this would take massive amounts of time physically sectioning samples and imaging. The final reconstruction would likely be incomplete and not properly represent the actual 3D tissue formation within the scaffold due to limitations in slice thickness, distortion artifacts, and tissue separation during sectioning. Because of its noninvasive nature and speed, interest in high resolution X-ray micro-computed tomography (µCT) as an alternative in the characterization of tissue engineering constructs has arisen. µCT has been shown to as an impressive instrument to evaluate constructs because it possesses excellent resolution which is preferred for the detection of tissue synthesis and vascular in-growth into scaffolds(215). Additionally, other researchers have reported that cells have tolerated µCT scanning well, which could allow for the opportunity of repeated nondestructive scans without interfering with an experiment(216-218).

However, X-ray based imaging techniques do have their drawbacks. In μCT, a material's ability to be imaged is based on it attenuation of X-rays. This means that radio-dense materials (e.g. rock, metal, and mineralized bone) appear with greater intensity, while radiolucent materials (e.g. polymers, water, and soft tissue) result in low intensity and are barely to not visible at all. This also presents a problem if two materials that have closely similar X-ray attenuations are next to one another or intertwined. The two items "bleed" into one another and sometimes trying to distinguish the two objects is futile. These problems have led to the uses of such things as synchrotron radiation-based μCT (SR-μCT) which uses phase contrasting and X-ray contrasting stains (e.g. iodine-based agents, Au/Ag, and OsO_4) which can be used to analyze materials that would be difficult if not impossible to image or distinguish from one another(219). These solutions are come with their own set of problems. In order to perform SR-μCT, the μCT machine must have access to a particle accelerator is not always readily found or easy to use piece of equipment. X-ray contrasting agents can be costly and many of them are toxic so imaging of tissue using the contrast agents would require the sacrificing of a sample. Specific staining of materials is not always easy. In the case of porous scaffolds used in tissue engineering you cannot be sure that a stain will reach all the way into a scaffold's interior where a target may lay.

The goal of this study was to introduce a straightforward and practical approach to use conventional high resolution μCT to perform 3D virtual histology without the assistance of X-ray contrasting agents or use of exotic equipment. Polymeric based BTE constructs were chosen for analysis by this new method because of its incorporation 4 different materials that be distinguished. The materials are cells, soft organic tissue, mineralized tissue and a polymer scaffold. The constructs were generated by seeding and *in vitro* culturing MSCs on a PLA non-woven fiber mesh scaffold within a flow perfusion bioreactor using osteogenic media(8, 15, 39, 128, 165-167, 220). As proof of concept this study will show that established image processing methods can reconstruct a 3D histological view of an engineered scaffold containing cells and tissue using conventional high resolution μCT.

6.2 Materials and Methods

6.2.1 Scaffold Production

Porous non-woven scaffolds were produced and evaluated in the same fashion as chapter 4. Average fiber diameter was found to be 34.8 ± 1.85 μm.

6.2.2 Cell Culture

MSCs were extracted and precultured on 75 cm^2 culture flasks similar to the methods used in Chapter 4.

6.2.3 Scaffold Seeding and Culture

Cassettes containing pre-wet non-woven fiber scaffolds were placed into a flow perfusion bioreactor(119, 169, 172, 221). Using oscillatory flow perfusion, MSCs were seeded on each non-woven fiber mesh scaffold(121, 184). Seeding suspensions were 1 million cells per scaffold for non-cultured samples, and 500,000 cells per scaffold for long term cultured samples. Culturing was performed by applying a continuous unidirectional flow of 0.5 mL/min/scaffold for 16 days post seeding. All cultures were incubated at 37 °C and 5% CO_2. During long term culturing, osteogenic media was replaced with fresh media every 3 days. At the conclusion of seeding or culturing, cell/scaffold constructs were removed from their cassettes and washed twice with PBS. The washed constructs were then fixed with 10% PBS buffered formalin (Sigma) at 4 °C overnight. Next, they were washed twice with PBS and passed through serial dehydration using ethanol-water. Samples were then critical point dried using a Tousimis Research Corporation autosamdri-814.

6.2.4 Scaffold Cellularity

After seeding had concluded, the fiber scaffolds were removed from cassettes and processed to find DNA content with PicoGreen®like in Chapter 4. DNA assays were performed on 6 scaffolds (N=6) to obtain cell numbers.

6.2.5 μCT Imaging

Non-woven fiber mesh PLA scaffolds taken just after seeding and after 16 days of perfusion culture were imaged via high resolution μCT by an Xradia MicroXCT 400. The images that were obtained corresponded to the maximum resolution of the machine and had an isotropic spatial resolution of 0.9108 μm. Intensity image slices were obtained at optimum settings of 200 μA intensity and 40 kV energy. Acquired 2D X-ray images were filtered for noise reduction and assembled into 3D reconstructions of the scaffolds using a custom Matlab® code. Verification of average fiber diameter for the non-woven fiber mesh scaffold can be found in a previous publication(222).

6.2.6 Scanning Electron Microscopy Imaging

Scanning electron microscopy (SEM) imaging was performed on the same samples that were imaged with μCT for the validation of the virtual histology results. After cell seeded scaffolds were imaged via μCT, scaffolds were mounted on metal stubs and sputter coated with gold-palladium using an Anatech Hummer VI triode sputtering system. SEM imaging was then performed on a JEOL JSM-840A scanning electron microscope with a tungsten filament. Digital imaging was produced using the IXRF Systems EDS 2008 program.

6.2.7 Proposed Segmentation Algorithm

A representative 2D slice of raw data obtained from the μCT machine can be seen Figure 6.2A. Each pixel contains a 16-bit grayscale intensity value that is representative of the X-ray beam attenuation at that particular spatial coordinate. Immediately it becomes obvious that there are two materials in the image that are easily distinguishable: the PLA fibers that have a circular-to-ellipsoid cross-section and account for most of the solid material in the image, and the mineralized tissue which is nearly white in color due to its high attenuation of X-rays. The latter can be segmented from the rest due to the much higher pixel intensity, because no other material "bleeds" into this range. The PLA fibers, on the other hand, have the lowest pixel intensity, as is expected for polymeric materials. Knowledge of the PLA intensity threshold, combined with the observation that the PLA fiber cross-sections occupy a much larger area than any other object in the image that is not mineralized tissue, allow for segmentation of the scaffold material from the rest of the image. This leaves the cells and the soft tissue that have been produced. Although there is a slight difference in intensity between cells and ECM, there is a "bleed" of intensity at the borders where cells and ECM meet. Because of this trait, cells that are encapsulated in ECM require special attention, as is discussed later in the manuscript. The procedure outlined above is described in an algorithmic form below and an overview of it is depicted in Figure 6.1:

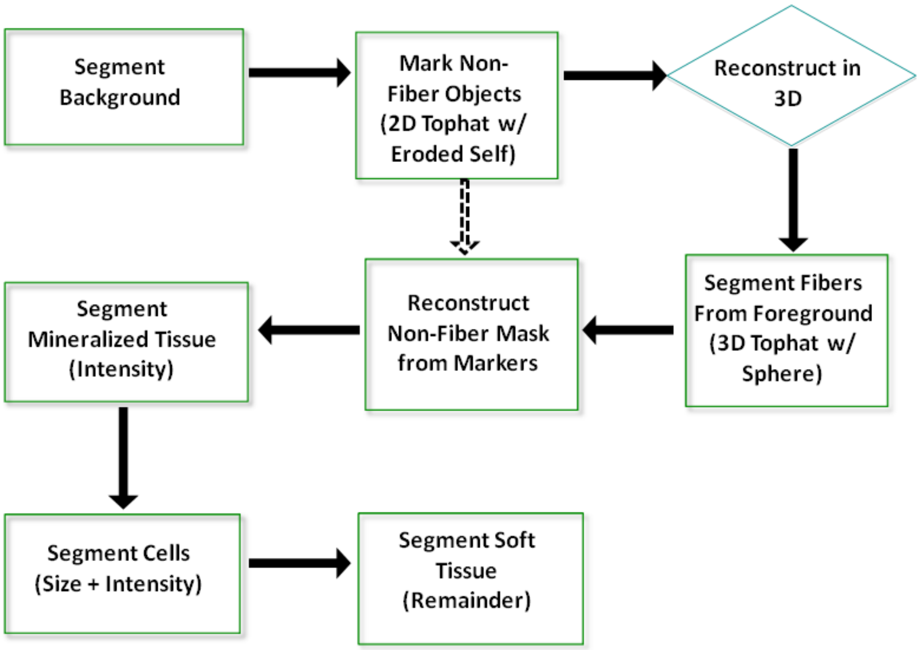

Figure 6.1: Process flow diagram outlining the proposed µCT image segmentation algorithm.

TWO DIMENSIONAL PRE-PROPROCESSING

REMOVE BACKROUND: a) Contrast stretch image (saturate 1% of low and high intensities) to improve signal-to-noise ratio and remap the new intensities weighed towards brighter pixels by using a gamma value of 3 b) Fill "holes" in grayscale image to obtain outlines of foreground objects. c) Use simple thresholding to obtain a black & while (BW) mask of foreground. An intensity of 25,000 was used as the global threshold for the brightened images from step 'a' and excluded pixels belonging to the BW mask from step 'b' from the thresholding d) Filter foreground mask for "salt" noise (remove lone pixels).

CREATE MARKERS FOR NON-FIBER OBJECTS: a) Estimate locations of non-fiber objects for future use using the tophat procedure with a special structuring element. The structuring element is created individually for each foreground object in the BW foreground mask by eroding the object itself until about 50% of its original area is left. The result of the tophat procedure gives the objects on fiber surfaces.

THREE DIMENSIONAL SEGMENTATION

SEGMENT NON-FIBER MATERIAL FROM FOREGROUND: Segmented fibers from the rest of the materials present in the image by performing a 3D “tophat” procedure on the foreground BW mask with a spherical structuring element, where sphere diameter is taken to be the maximum expected cell diameter of 15µm. The tophat algorithm “rolls” the structuring element along the inner fiber boundary and whatever cannot be reached by the sphere is considered to be non-fiber. An intensity threshold of 18,000 applied to the original (non-brightened) images can further help to refine the segmentation results, since most of the non-fiber objects are brighter than this value.

RECONSTRUCT NON-FIBER 3D MASK: a) Filter the non-fiber material mask for fiber voxels that have been erroneously segmented in the previous step (isolated voxels, surface voxels, etc). b) Use non-fiber object markers from Step 2 to perform image reconstruction into the cleaned mask from part a.

SEGMENT MINERALIZED TISSUE FROM NONFIBER FOREGROUND: Threshold the mineralized tissue based solely on the significant intensity difference relative to the rest of the materials in the image. An intensity threshold of 30,000 for the images worked well in this step, because all of the mineralized tissue is brighter and all the other objects are dimmer than this value.

6) SEGMENT CELLS FROM NONFIBER FOREGROUND: Since at this point the only remaining non-fiber materials in the image should be cells and soft tissue, segment the former by utilizing differences in intensity and some prior knowledge of the cell

size/morphology. The optimum intensity threshold between cells and soft tissue was identified as about 1.2 times the soft tissue average intensity: roughly 25,000. Apply this threshold globally to segment cell matter, and from these, isolate individual cells by applying a cell size “search window”: minimum and maximum volume bounds that correspond to spherical objects between 4-15µm diameter (at this point assumption of a spherical shape is only used for the volume estimation).

SEGMENT SOFT TISSUE FROM NONFIBER FOREGROUND: Once the cells and the mineralized tissue have been segmented, by the process of elimination, the only remaining non-fiber materials in the image should be soft tissue.

A representative 2D slice of the segmented data using the above algorithm can be seen in the Figure 6.2B.

6.2.8 Spatial Comparison Measurement: Equivalent Sphere Diameter

Experimental measurements of Equivalent Sphere Diameter (ESD) were performed on 2D SEM images using ImageJ software. To estimate ESD from SEM images, three edge-to-edge cross sectional measurements of multiple cells were made. The first measurement was across the largest edge-to-edge cross section, if the cell had a visibly larger cross section. The second measurement was made at a 90° angle from the first. The third measurement was made by bisecting the two first measurements. This resulted in measurements of 45°s from one another. The 3 edge-to-edge measurements were then averaged and considered to be the ESD of the cell from SEM imaging. An illustration of a typical ESD measurement made from SEM is shown in Figure 6.4A. These were compared to ESDs measured from the µCT images. The latter were calculated by apply the volume of a sphere formula to the 3D reconstructions of cells attached to the scaffold surface.

6.2.9 Spatial Comparison Measurement: Nearest Neighbor Distance

Experimental measurements of Nearest Neighbor Distance (NND) were performed on 2D SEM images using ImageJ software. Planar NNDs in the SEM images were measured from a cell's center to the center of the nearest neighboring cell. An illustration of a typical NND measurement made from SEM is shown in Figure 6.5A. These were compared to NNDs measured from the μCT images. The latter were calculated by taking the distances (not necessarily planar) between the centers of mass of cells nearest to each other in the 3D reconstructions.

6.2.10 Statistics

Values were reported as the average from all samples taken from an experimental group ± standard error. Data sets for scaffold cellularity were analyzed using single factor ANOVA at a confidence level of 95%. A two-sample Kolmogorov-Smirnov test was conducted on spatial comparison measurement, ESD and NND, data with a confidence level of 95%.

6.3 Results

In order to evaluate the performance of the virtual histology algorithm, scaffolds seeded with cells that without culturing were evaluated first. A total of 8 scaffolds were seeded with cells and 3 sub-volumes (592.4 μm x 92.0 μm x 592.4 μm) were scanned in different areas of each scaffold, bringing the total number of μCT samples examined to N=24. The Figure 6.3A shows a typical 2D μCT slice of one of the non-cultured scaffolds with only cells and fibers present in the image (note the difference with Figure 6.2, which also contains soft and mineralized tissues). It is apparent from Figure 6.3A that the fibers and the MSCs (marked with green boxes) are clearly distinguishable from each other by the human eye. However, to test whether the proposed algorithm is up to the challenge, the Matlab code was applied to the μCT image stacks and created 3D representations of the scanned scaffold sub-volumes. Figure 6.3B shows one such reconstruction resulting from the algorithm, where the MSCs are again labeled in green. From this figure it is apparent that the size and the shape of the MSCs relative to that of the PLA fibers is appropriate and no unexpected objects appear in the reconstruction.

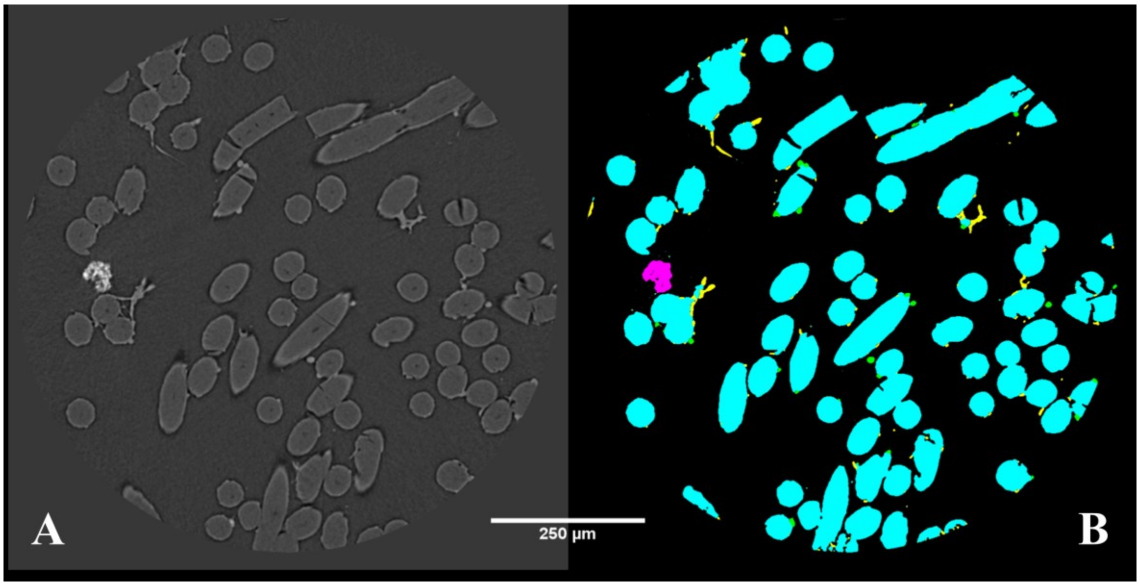

Figure 6.2: Segmentation of different materials in a 2D μCT image of a 16 day cultured sample: A) original image obtained from the μCT machine; B) segmented image using the algorithm described in this paper. Cyan is PLA fibers, Green is cells, Yellow is soft tissue, and Magenta is mineralized tissue (Scale bar is 250 μm).

As a way to validate against experiment, cellularity obtained from the virtual histology was compared to that obtained from the PicoGreen® dsDNA quantification assay. The cellularity obtained from the μCT imaging and reconstructions (when scaled to the full scaffold size) was 268,000 ± 35,000 cells/scaffold, while the DNA assay for samples from the same experimental group gave a cellularity of 247,000 ± 31,000 cells/scaffold. The number of structures observed as cells from μCT imaging are not significantly different (P = 0.68) from the cellularity found using the widely accepted

PicoGreen® assay thus providing a validation of the methodology. This can be observed in Figure 6.6.

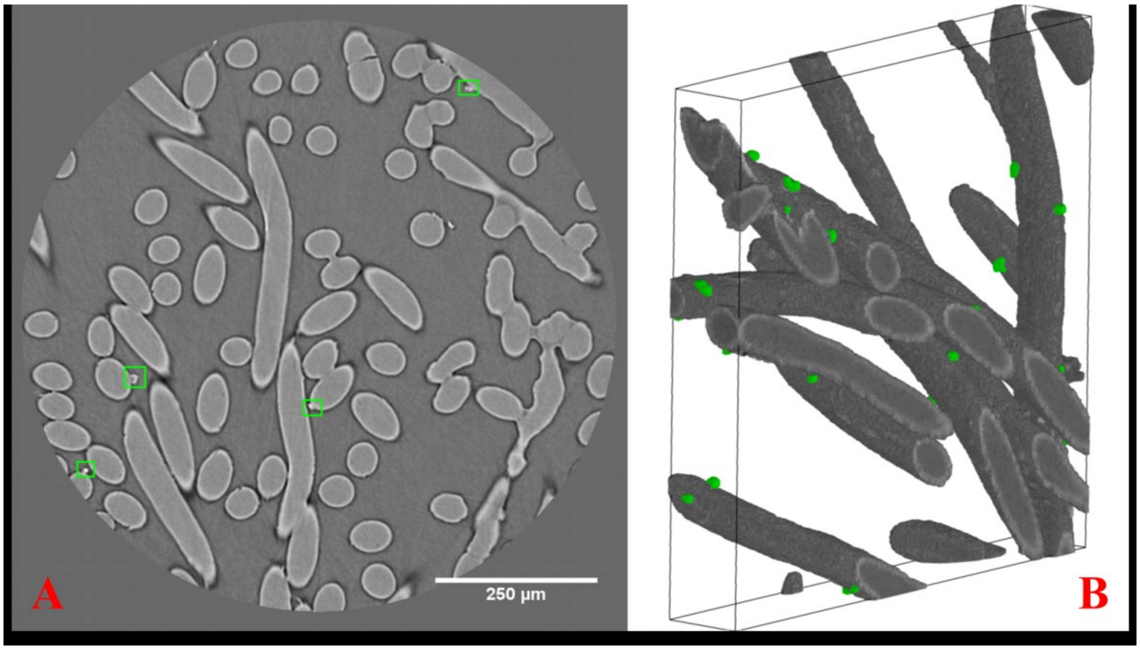

Figure 6.3: Images from µCT showing cells attached to fibers of non-woven fiber mesh scaffolds. A) 2D µCT image of the nonwoven fiber mesh scaffold with MSCs seeded on the PLA fibers. The cells are seen within the green boxes to be round, and brighter than the fibers (Scale bar is 250 µm). B) 3D reconstruction using µCT images of cells on PLA fibers from a 1 million cell-seeded non-woven fiber mesh scaffold: Cells segmented using the proposed algorithm are shown in green color (only cells ~10µm in size are shown for clarity; image size is 592.4 µm x 92.0 µm x 592.4 µm).

For further validation of the virtual histology algorithm against experiment two spatial comparison criteria were tested: scaffold cellularity, ESD and NND. A comparison of µCT to SEM results for ESD and NND appear in Figure 6.4B and Figure 6.5B, respectively. Both of the spatial comparison criteria show statistical agreement between the µCT and SEM imaging results, with ESD and NND, respectively. This finding further validates the reliability of the proposed methodology to differentiate between at least two object types, in this case, cells and polymer scaffold. Results from µCT are presumed to be a more accurate representation of the actual ESD and NND measurements, due to the fact that they are based on 3D measurements and a larger sample size, explaining moderate differences to those observed from SEM.

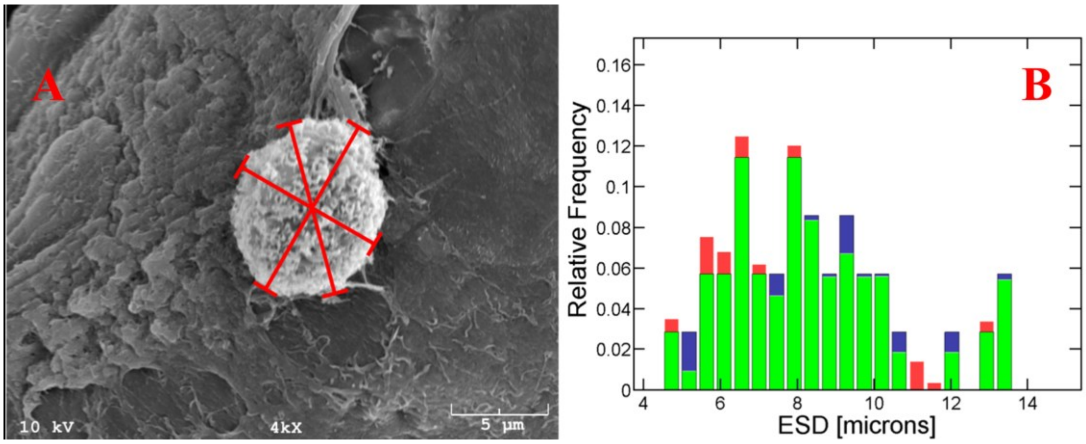

Figure 6.4: Visual equivalent sphere diameter (ESD) measurement using SEM images of cells on a cell seeded non-woven fiber scaffold. A) Example measurements for an ESD calculation appear as edge-to-edge bars in red (Scale bar is 5 µm). B) Histogram comparing equivalent sphere diameter (ESD) calculations of cells from µCT and SEM imaging; illustrating validation of the proposed methodology. The red color is µCT, light blue is SEM, and green is the overlap between the two.

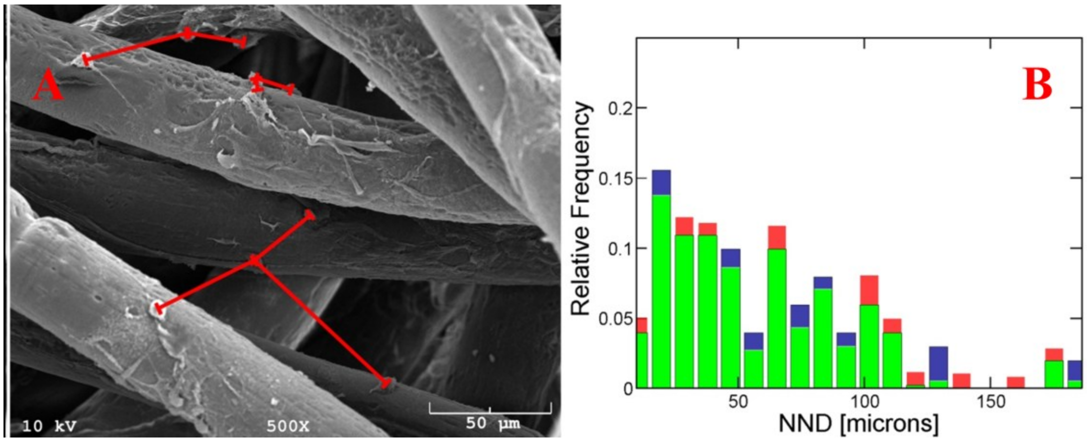

Figure 6.5: A) Visual nearest neighbor distance (NND) measurement using SEM images of cells on a cell seeded non-woven fiber scaffold. Example measurements for a NND calculation appear as edge-to-edge bars in red (Scale bar is 50 µm). B) Histogram comparing nearest neighbor distance (NND) calculations of cells from µCT and SEM imaging; illustrating validation of the proposed methodology. The red color is µCT, light blue is SEM, and green is the overlap between the two.

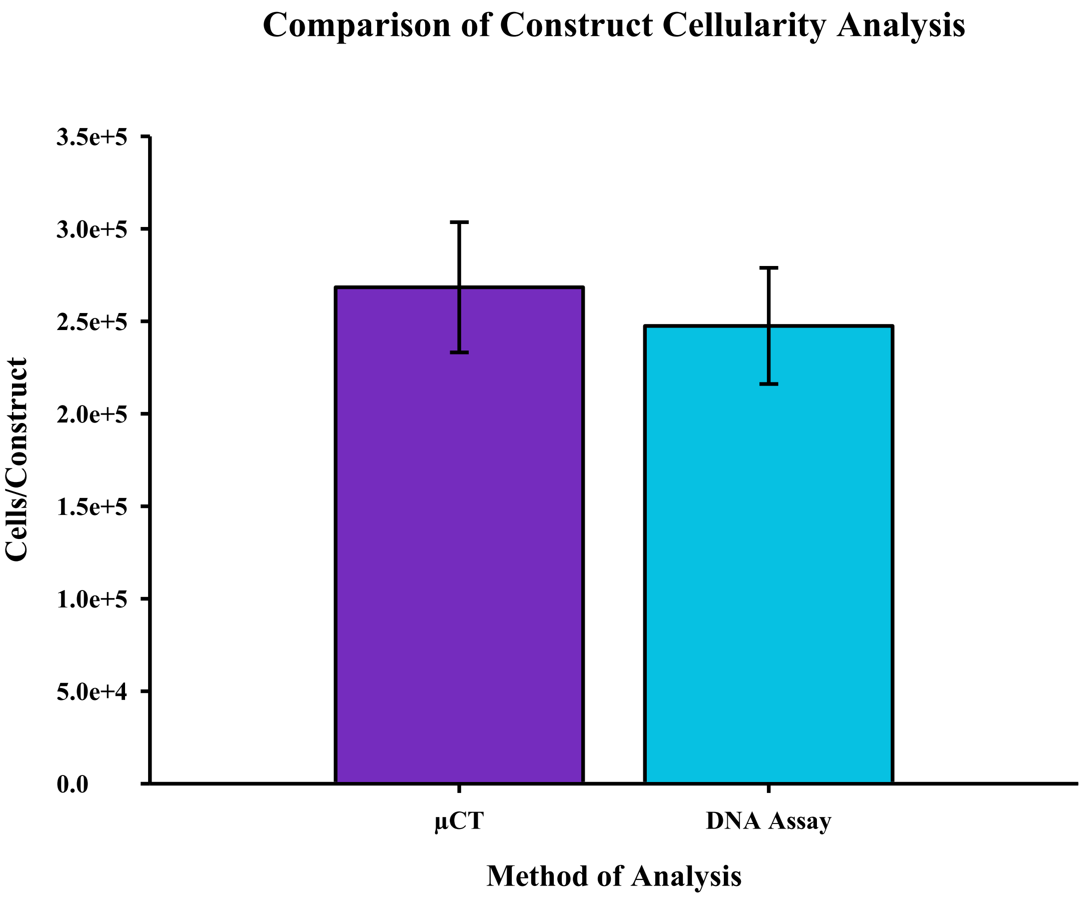

Figure 6.6: Graph of scaffold cellularities observed from analysis of μCT virtual histology and from PicoGreen® DNA assay. The graph depicts an 8% difference between the mean cellularity found by the DNA assay and the mean cellularity found by virtual histology. This difference is within commonly observed noise ranges for similar experimental cell measurements. Also, it can be seen from the graph that the mean cellularities are not statistically different from one another (P = 0.68).

For the case of cultured scaffolds, the complexity of the image-processing task increases two-fold: there are now four different materials in the μCT images instead of two that must be distinguished without the help of any foreign agents. Luckily, the mineralized tissue is readily separable via simple intensity thresholding, as is immediately apparent from Figure 6.2. Thus, given that scaffolds can be easily segmented based on their size and shape, and mineralized tissue based on its intensity, the most challenging image-processing task that remains for the histology of cultured scaffolds is to differentiate between cells and soft tissue. However, by taking advantage of a few simple characteristics of cell morphology and intensity, these two similar materials can be successfully segmented. This is illustrated in Figure 6.7.

Figure 6.7 shows four different cases of cells embedded in soft tissue, where the small size (~10μm in diameter) and slightly higher intensity (>1.2 x surrounding soft tissue intensity) of the cells distinguish it from the tissue. By utilizing these differences, cultured scaffolds can too be reconstructed in a histological manner, with all four of the materials segmented from each other. Figure 6.8 is a representative final result of one such reconstruction that clearly shows the complex interplay between the newly formed tissue, the cells and the scaffold material, as are identified by the algorithm. From Figure 6.8 it is apparent that there are individual cells (marked in green) outside of ECM along with mineralized (red) or soft (yellow) tissue located on the PLA fibers. These are summarized in Table 6.1.

Material	Volume %
Mineralized Tissue	1.9 ± 0.5
MSCs	2.32 ± 0.04
Soft Tissue	4.31 ± 0.03
PLA Fibers	22.6 ± 0.1

Table 6.1: Volume percent occupied by materials as resulted from segmented 3D reconstruction of the μCT data taken from representative 16 day cultured construct

6.4 Discussion

This study demonstrated, as a proof of concept, that conventional high resolution μCT combined with image processing techniques and a clever choice of geometry can be used to study spatial cell arrangement and tissue formation within scaffolds, which are of fundamental importance to developing tissue engineering strategies. A BTE non-woven PLA fiber mesh scaffold seeded with rat MSCs was chosen as the first test sample. The choice of the PLA fiber mesh was strategic: the characteristic cylindrical fiber shape and PLA radio lucency both assist in the image segmentation process. Since the cells are the smallest, and therefore, the most challenging objects to capture accurately, the proposed approach was initially tested by using non-cultured scaffolds that were seeded with MSCs. The cell/scaffold constructs were removed from the bioreactor immediately following the dynamic seeding in order to prevent the cells from proliferating and producing tissue. The motivation to try this simple case first was that by having just two different materials in the image (scaffold and cells) would allow for a more stringent validation of the algorithm's accuracy against experimental methods.

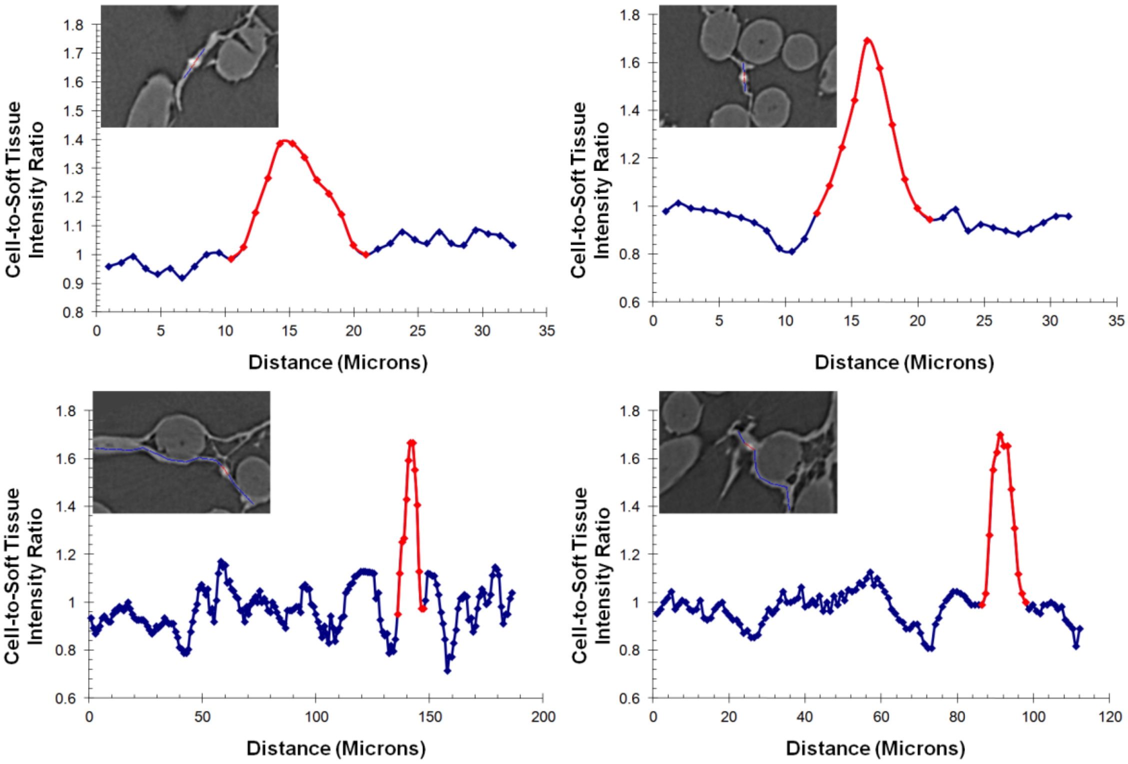

Figure 6.7: Segmentation procedure for cells embedded in soft tissue: comparison of cell intensities relative to those of soft tissue around them for four different cases. Grayscale insets show the actual μCT images being analyzed; Color traces the path of the intensity profile in each image (Red marks the cells and Blue marks the soft tissue).

Although, a typical cell seeding density for a BTE culturing experiment is 500,000 cells per scaffold, the non-cultured scaffolds were purposely over-seeded with twice the density: 1 million cells per scaffold. This was done in order to make the problem more challenging by having a larger number of cells that are closely spaced to each other. Assuming a typical seeding efficiency of about 20-30%, a total of ~250,000 cells were expected to be attached to the scaffold(121). This would imply that if a uniform cell distribution within the scaffold volume that comes from the dynamic seeding technique were assumed(121), a 2D slice of the scaffold with the dimensions of the disc shown in Figure 6.3A would be expected to roughly have single digits of cells. This is consistent with the findings of this study. When compared the cellularities obtained from the PicoGreen® assay (reported here as the mean over 6 scaffolds ± standard error) and the μCT virtual histology reconstructions (reported here as the mean over 8 scaffolds ± standard error), their means are within 8% of one another. This is well within the noise range commonly observed in the measurement of cell numbers in biological specimens. The slightly higher average given by the virtual histology is attributed to the fact that the subvolumes were scanned near the centers of the scaffolds; while the PicoGreen® assay takes into account the more porous scaffold periphery where there can be less cells. Also, some DNA is lost during the processing of constructs for the PicoGreen® assay. Finally, when the two-sample Komogorov-Smirnov tests was performed for both of the spatial comparison criteria, ESD and NND, it was able to be shown that the null hypothesis that the distributions are not different from one another could not be rejected at the 5% significance level for either case, further validating the reliability of the algorithm to identify cells on fibers. Although small differences exist between the μCT and the SEM results, they are likely due to the fact that the former is a true 3D measurement, while the latter results are inferred from 2D images.

The next step after validation of the algorithm for the simple case of non-cultured scaffolds was to test it on a realistic scenario of a cultured BTE sample. In order to do this a scaffold was seeded at the typical seeding density of 500,000 cells per scaffold and cultured for 16 days. Once cultured, the imaging algorithm was again put to the test. This sample had significant amounts of soft and mineralized tissue present in their μCT images (see Figure 6.2). In this case the isolated cells and the fibers were segmented as before, while the mineralized tissue was segmented based solely on the significantly higher intensity difference relative to anything else in the images. The soft tissue and cells embedded into it, however, required special attention. As is depicted in Figure 6.7, cells identified as embedded in soft tissue can be accurately picked out by their characteristic morphology (roughly 4-15μm in diameter with a mostly circular cross-section) and intensity (higher than ~1.2 times the average surrounding soft tissue, or >25,000 intensity). Using this strategy, cells embedded into the soft tissue were also successfully segmented. The resulting 3D reconstruction depicted in Figure 6.8 showed that soft tissue is present in larger amounts and seems to cover the fibers, while also making connections between them. The mineralized tissue was identified to be present in large locally-concentrated globular chunks, near the soft tissue. And the cells were mostly isolated on fibers, with a few of them being embedded in the soft tissue. The relative amounts of volume occupied by each material (summarized in Table 6.1) showed that the non-woven fiber mesh scaffold became compressed from its original 85% porosity down to ~77.4% due to the flow perfusion seeding and culturing. All of these observations are consistent with what is expected from *in vitro* bone-like tissue formation and demonstrate the usefulness of the tool proposed in this publication in monitoring the intra-BTE construct microenvironment. Since the goal of this manuscript was to show as *proof of concept* that virtual contrast free histology is possible, the reader can be left with the following final thoughts, without submerging into further analysis of the cultured BTE sample beyond the intentions of the manuscript.

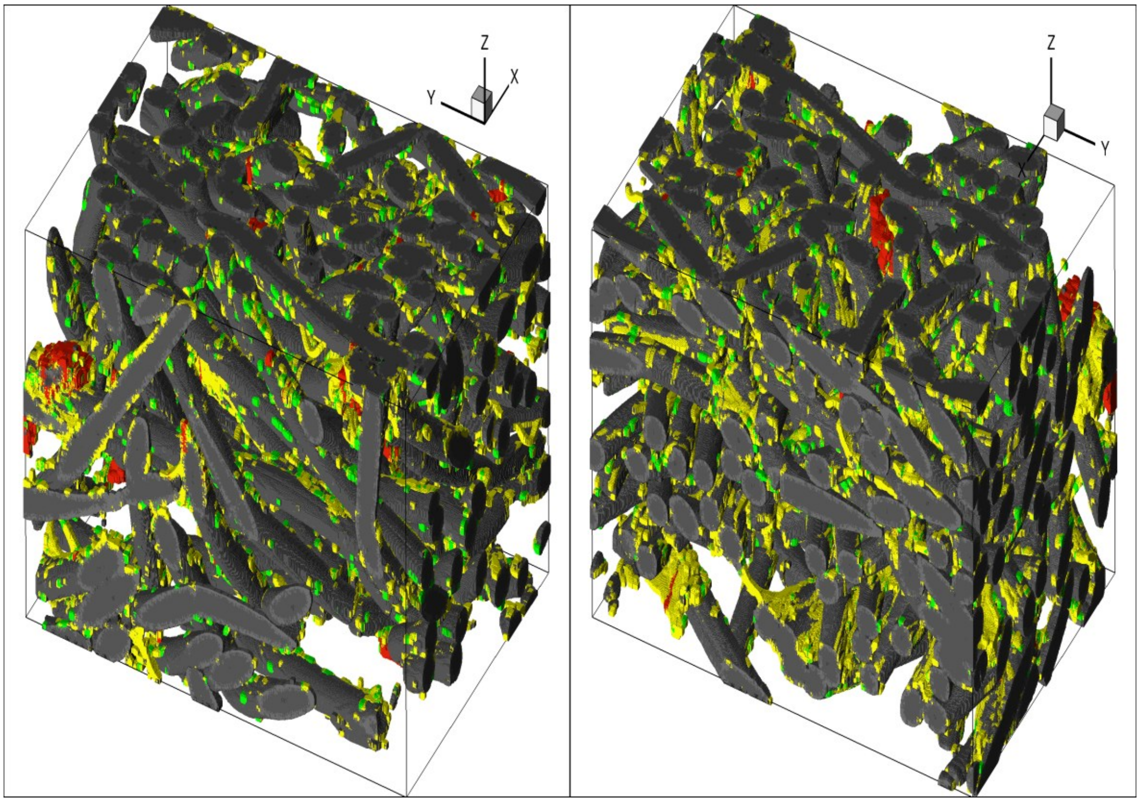

Figure 6.8: Final 3D reconstruction (image size is 0.62 mm x 0.91 mm x 0.62 mm) of µCT an imaged 16 day long term cultured BTE construct viewed from two different angles: Gray – PLA non-woven fiber mesh scaffold, Green – Cells, Yellow – Soft Tissue, Red – Mineralized Tissue.

We have proposed and validated an approach to perform 3D virtual histology by conventional means and without X-ray contrasts. The usefulness of this method is that tissue engineers could study the *in vitro* culturing process non-destructively and without resorting to burdensome techniques such as histology by sectioning. It is also important to note that our algorithm makes minimal assumptions about the cell size and shape when segmenting them from fibers or from soft tissue (arguably the most challenging image processing task in this method). Thus, it is able to capture cells that have assumed a non-spherical shape, even when they are embedded in soft tissue. Having said that, there is still room for improvement to the algorithm, for example, separating cells in larger globule formations (25+ cells) remains an unsolved issue. There are also several limitations to the proposed approach. Namely, it is currently limited to scans of small sub-volumes (~1/5th of total scaffold volume per scan) due to the intense computational power that is required to process images at such fine resolution. The approach is also prone to errors such as irregularities in scaffold manufacturing, or contaminants/foreign objects in the sample. However, application of rigorous manufacturing methods, development of machine learning imaging algorithms, and advances in supercomputing; all of these obstacles can be overcome in the near future. Additionally, even though fine resolutions can be achieved and almost all of the mass of cells and tissue are observed, some features of cells and tissue smaller than the highest achievable resolution of the μCT machine could be potentially missed. Yet, even at the current state of things, this methodology offers valuable insight into the *in vitro* tissue growing process at the ease of conventional means. Therefore, it can be foreseen as becoming an integral part in the future development of tissue engineering techniques.

6.5 Conclusion

This work demonstrated as proof of concept the ability to perform 3D histological analysis by using conventional μCT equipment without the use of X-ray contrasts. Critical to this goal was the prior knowledge of the regular cylindrical geometry of the fiber mesh scaffolds used in this study. Although there is more work to be done on improving this approach, it can be expected that the ability to nondestructively image new tissue formation within polymer scaffolds will propel advancements in tissue engineering and will allow for an objective comparison between the numerous tissue engineering protocols that exist today. This study appears to be the first of its kind where virtual histology via conventional high resolution μCT has been used to directly measure the relative amounts of cells, soft and mineralized tissue within BTE scaffolds. It is hoped that this methodology that incorporates conventional high resolution μCT, which is becoming increasingly available, will encourage the use of virtual histology on a wide variety of cell/tissue/scaffolds and improve the evaluation of tissue engineering strategies.

6.6 Disclosure

Microfiber fabrication was performed by Taren Blue and Venkatesh Meenakshisundaram. μCT reconstructions using multi-masking virtual histology technique, and computerized spatial comparisons were performed by Dr. Roman Voronov.

Chapter 7: Conclusions and Future Directions

Within this dissertation are many studies that have been performed on polymeric scaffolds used in BTE applications. First a new porous PEEK scaffold structure that was osteoconductive and could allow for surface ingrowth of tissue was examined. It was determined that the porous PEEK material could be incorporated into implantable devices that required reduced modulus and minor interlacing with surrounding tissues. Next, the influences from different PLA scaffolds with random architectures on the development of MSCs into bone like tissues while cultured in a flow perfusion bioreactor was described. It was first noted that despite the differences in structure, non-woven fiber mesh scaffolds manufactured by spunbonding and porous foams manufactured by solvent casting and particulate leaching, both having the same porosity and mass volume ratio, exhibited similar fluid shear flow characteristics when used in a flow perfusion bioreactor. My experimental results found that non-woven fiber meshes facilitated faster osteogenic differentiation of MSC than porous foams but tissues generated on both scaffolds had similar characteristics after 8 days. After that, a study into the detachment of MSCs from PLA porous foam scaffolds by fluid flow in a perfusion bioreactor was conducted. In this detachment study it was observed that cells seeded dynamically in a perfusion bioreactor using media with osteogenic supplements were more resistant to elevated shear forces than scaffolds that were seeded dynamically using basal media. The study went on to find that fluid flow shear forces could severely damage seeded cells opportunity of forming a tissue by detaching over 75% of the scaffold cells within 2 days. Lastly, a technique using computer analysis of μCT images was able to perform virtual histology on PLA non-woven fiber mesh scaffolds that had MSCs cultured upon it in a flow perfusion bioreactor. The technique was able to segment cells, polymer scaffold, soft tissue, and mineralized tissue from one another and create 3D representations of the cell and tissue growth within the scaffold.

The array of studies presented in this manuscript is evidence of the multitude of options being explored through BTE. Even though these projects generated a plethora of conclusions, more research can be done. The porous PEEK that was explored presents some good options for continued work. An increase in the material porosity could open up more possibilities. An increase in the amount of porogen during the manufacturing process should be able to achieve this. An increase in porosity should increase the potential of interconnectivity of the internal porous network. This increase in interconnectivity should allow for increased nutrient transport in the scaffold. This will in turn also allow the material to be used in perfusion experiments. Also even if the material's mechanical properties potentially drop as expected, I think the development of porous material coating for implants used in orthopedic applications would be useful. This could first be tested *in vitro* as before then move into testing the material *in vivo* for long bone grafts in rabbits and dogs with the goal of having fusion of the long bone to the graft.

In the case of the culturing of MSCs on non-woven fiber meshes vs the porous foam scaffolds under flow perfusion, I would look into modification of the surface chemistry of the scaffolds. A coating of the surface with type I collagen will change the initial adhesion of cells to the construct by increasing the amount of initial cells attached after seeding. The already deposited matrix could also allow for faster cell differentiation within the porous foams but also could accelerate cell differentiation in non-woven fiber meshes also. The coating would have to be thin because softer materials do not always stand up to fluid shear forces well. Because of this, incorporation of glycosaminoglycans or the molecule arginyl-glycyl-apartic acid (RGD) entrapped with a linker into the surface of the scaffolds may be beneficial for investigation. Another option would be to use PLA ordered structures that have similar surface areas and fluid shear profiles or similar surface areas and different fluid shear profiles. For this, ordered structures would need to have fluid dynamic modeling to find compatible structures or in an inversed experiment, the fluid dynamic environment profile would need to be optimized and a scaffold designed to fit it.

Much additional work could be done to extend out the research on the detachment of MSCs that have been seeded on PLA scaffolds by fluid shear. First I would run some 48 hour detachments using media that contained just one supplement and a combination of two of the supplements. This potentially could identify the supplement responsible for the observed behavior, if it is just one of the supplements causing it or a combination of them. The 8 hour detachment runs for the static seeded scaffold should be rerun and imaging that looks at the surface of the scaffolds should be conducted. The morphologies of the cells that are present after seeding and the cells that are present after detachment could shed light upon why the cells detach as they do. Another option would be to put membrane filters on the exit ports to capture cells. The captured cells could be taken from the membrane and analyzed by flow cytometry for size to see if individual cells are detaching or if the cells that are removed from the scaffolds are conglomerations. The use of flow cytometry would also be helpful in identifying the cells that detach from the surface of the dynamically seeded scaffolds with basal media. Looking for expressions of surface adhesion molecules in detached and attached cells could lead to better understanding of what keeps cells attached to the scaffolds. Another thing that could be considered is to expose cells to osteogenically supplemented media for 2-4 hours before lifting the cells from a culture flask with trypsin. The lifted cells could be seeded with αMEM and then subjected to detachment experiments. This may lead to insight into if the presence of osteogenic supplements is needed at the time of seeding to improve cell adherence. Experiments to find the threshold flow rate for cellular detachment of MSCs would also help expand the uses of flow perfusion bioreactors for use in some soft tissue applications. The reduced flow rate could improve nutrient delivery with minimal stimulatory affects from mechanical stimuli generated by fluid shear.

The use of virtual histology with conventional high resolution μCT has many areas to expand upon. First, a flow perfusion bioreactor could be designed from highly radio opaque materials so it may be placed in a μCT machine. This would remove the need of opening up a reactor and taking constructs out from culture. Using this new technology would allow the same scaffold to be scanned multiple times throughout culturing while maintaining sterile conditions. Then using virtual histology, the scaffolds could be reconstructed and the scaffold elements identified. A problem with obtaining images from μCT is that it is very difficult to scan the very same sub volume. If placement of a construct is off by a few mm and entire new sub volume can be imaged. Creation of a matching algorithm to align scaffold reconstructions after imaging would allow for direct comparison of scaffold sub volumes to themselves during a culture period. With this, mapping of fluid shear forces in a localized area could be correlated to cellular attachment, cell migration and tissue development giving better insight into how forces and nutrient delivery affect the development of tissue constructs.

Tissue engineering is like a puzzle where we know what the end picture is but we don't know what all the pieces look like. Improvements in materials, tissue development, and methods of analysis will help put the picture together. Bone tissue engineering continues to evolve through the advancement of techniques and technologies. This dance of changes and matching of technologies to help produce and analyze bone tissue constructs shows great promise towards the development of functional bone substitutes. A substitute that could be developed *in vitro* and be ready for implantation when it is crucially needed when diseased and damaged bone must be removed would be ideal. By continued research, we boldly move towards these advancements.

References

1. Bostrom, R.D. and A.G. Mikos, *Tissue Engineering of Bone*, in *Synthetic biodegradable polymer scaffolds*, A. Atala and D.J. Mooney, Editors. 1997, Birkhäuser: Boston. p. 215 - 234p.^^

2. Brown, K.L. and R.L. Cruess, *Bone and cartilage transplantation in orthopaedic surgery. A review.* J Bone Joint Surg Am, 1982. **64**(2): p. 270-9.

3. Freeland, A.E. and J.P. Rehm, *Autogenous bone grafting for fractures of the hand.* Tech Hand Up Extrem Surg, 2004. **8**(2): p. 78-86.

4. Bonassar, L.J. and C.A. Vacanti, *Tissue engineering: the first decade and beyond.* J Cell Biochem Suppl, 1998. **30-31**: p. 297-303.

5. Langer, R. and J.P. Vacanti, *Tissue engineering.* Science, 1993. **260**(5110): p. 920-6.

6. Saltzman, W.M., *Cell Interactions with Polymers*, in *Principles of tissue engineering*, R.P. Lanza, R.S. Langer, and W.L. Chick, Editors. 1997, Academic Press; R.G. Landes: San Diego & Austin. p. 221-236p.

7. Vacanti, J.P., et al., *Transplantation of cells in matrices for tissue regeneration.* Adv Drug Deliv Rev, 1998. **33**(1-2): p. 165-182.

8. Liu, X. and P.X. Ma, *Polymeric scaffolds for bone tissue engineering.* Ann Biomed Eng, 2004. **32**(3): p. 477-86.

9. Zhang, L., et al., *Development of bone marrow mesenchymal stem cell culture in vitro.* Chin Med J (Engl), 2012. **125**(9): p. 1650-5.

10. Bruder, S.P., et al., *The effect of implants loaded with autologous mesenchymal stem cells on the healing of canine segmental bone defects.* J Bone Joint Surg Am, 1998. **80**(7): p. 985-96.

11. Vilquin, J.T. and P. Rosset, *Mesenchymal stem cells in bone and cartilage repair: current status.* Regen Med, 2006. **1**(4): p. 589-604.

12. Steinert, A.F., et al., *Concise review: the clinical application of mesenchymal stem cells for musculoskeletal regeneration: current status and perspectives.* Stem Cells Transl Med, 2012. **1**(3): p. 237-47.

13. Boeckel, D.G., et al., *Cell culture-based tissue engineering as an alternative to bone grafts in implant dentistry: a literature review.* J Oral Implantol, 2012. **38 Spec No**: p. 538-45.

14. Salter, E., et al., *Bone tissue engineering bioreactors: a role in the clinic?* Tissue Eng Part B Rev, 2012. **18**(1): p. 62-75.

15. Sikavitsas, V.I., J.S. Temenoff, and A.G. Mikos, *Biomaterials and bone mechanotransduction.* Biomaterials, 2001. **22**(19): p. 2581-2593.

16. Abousleiman, R.I. and V.I. Sikavitsas, *Bioreactors for tissues of the musculoskeletal system.* Adv Exp Med Biol, 2006. **585**: p. 243-59.

17. Alvarez-Barreto, J.F. and V.I. Sikavitsas, *Tissue Engineering Bioreactors*, in *Tissue Engineeirng and Artificial Organs*, J.D. Bronzino, Editor. 2006, CRC/Taylor & Francis: Boca Raton. p. 44-41.

18. Turner, C.H., *Biomechanical Aspects of Bone Formation*, in *Bone Formation*, F. Bronner and M. Farach-Carson, Editors. 2004, Springer: London ; New York. p. 79-105.

19. Bilezikian, J.P., L.G. Raisz, and G.A. Rodan, *Principles of bone biology*. 2nd ed. 2002, San Diego: Academic Press. 2 v. (xxiv, 1696 p.).

20. Stocum, D.L., *Regeneration of Musculoskeletal Tissues*, in *Regenerative Biology and Medicine*. 2012, Academic Press: San Diego. p. 127-160.^^

21. Puzas, J.E., *Site-specific Mineralized Matrix Formation by Osteoblasts*, in *Bone Formation*, F. Bronner and M. Farach-Carson, Editors. 2004, Springer: London ; New York. p. 71-78.

22. Bukka, P., M.D. McKee, and A.C. Karaplis, *Molecular Regularion of Osteoblast Differentiation*, in *Bone Formation*, F. Bronner and M. Farach-Carson, Editors. 2004, Springer: London ; New York. p. 1-17.

23. Bronner, F., M.C. Farach-Carson, and J. Rubin, *Bone resorption*. Topics in bone biology v. 2. 2005, London: Springer. xiii, 189 p.

24. O'Connor, R.D., M.C. Farach-Carson, and N.C. Schanen, *Genetic and Epigenetic Aspects of Bone Development*, in *Bone and development*, F. Bronner, M.C. Farach-Carson, and H.I. Roach, Editors. 2010, Springer-Verlag: London. p. 1-23.^^

25. Kronenberg, H.M. and U.-i. Chung, *The parathyroid hormone-related protein and Indian hedgehog feback loop in the growth plate*, in *The molecular basis of skeletogenesis*, G. Cardew and J. Goode, Editors. 2001, Wiley: Chichester ; New York. p. 144-157.^^

26. Colnot, C. and T. Alliston, *Tissue Interactions in Long Bone Development*, in *Bone and development*, F. Bronner, M.C. Farach-Carson, and H.I. Roach, Editors. 2010, Springer-Verlag: London. p. 25-37.

27. Bronner, F. and M. Farach-Carson, *Bone formation*. Topics in bone biology v.1. 2004, London ; New York: Springer. xv, 160 p.

28. Bronner, F., M.C. Farach-Carson, and H.I. Roach, *Bone and development*. Topics in bone biology. 2010, London: Springer-Verlag. xxvii, 305 p.

29. Baron, R. and W.C. Horne, *Regulation of Osteoclast Activity*, in *Bone resorption*, F. Bronner, M.C. Farach-Carson, and J. Rubin, Editors. 2005, Springer: London. p. 34-57.

30. AAOS, *United States Bone and Joint Decade: The Burden of Musculoskeletal Diseases in the United States.* 2008, American Academy of Orthopaedic Surgeons: Rosemont, IL.

31. Giannoudis, P.V., H. Dinopoulos, and E. Tsiridis, *Bone substitutes: an update.* Injury, 2005. **36 Suppl 3**: p. S20-7.

32. Fodor, W.L., *Tissue engineering and cell based therapies, from the bench to the clinic: the potential to replace, repair and regenerate.* Reprod Biol Endocrinol, 2003. **1**: p. 102.

33. Laurencin, C., Y. Khan, and S.F. El-Amin, *Bone graft substitutes.* Expert Review of Medical Devices, 2006. **3**(1): p. 49-57.

34. Toolan, B.C., *Current concepts review: Orthobiologics.* Foot & Ankle International, 2006. **27**(7): p. 561-566.

35. VanGordon, S., W. Yates, and V.I. Sikavitsas, *Mechanostimulation in Bone and Tendon Tissue Engineering*, in *Mechanobiology handbook*, J. Nagatomi, Editor. 2011, Taylor & Francis: Boca Raton. p. 415-438.

36. Parfitt, A.M., *The cellular basis of bone remodeling: the quantum concept reexamined in light of recent advances in the cell biology of bone.* Calcif Tissue Int, 1984. **36 Suppl 1**: p. S37-45.

37. Jaiswal, N., et al., *Osteogenic differentiation of purified, culture-expanded human mesenchymal stem cells in vitro.* J Cell Biochem, 1997. **64**(2): p. 295-312.

38. Rosenbaum, A.J., D.A. Grande, and J.S. Dines, *The use of mesenchymal stem cells in tissue engineering: A global assessment.* Organogenesis, 2008. **4**(1): p. 23-7.

39. Stiehler, M., et al., *Effect of dynamic 3-D culture on proliferation, distribution, and osteogenic differentiation of human mesenchymal stem cells.* J Biomed Mater Res A, 2009. **89**(1): p. 96-107.

40. Holtorf, H.L., J.A. Jansen, and A.G. Mikos, *Flow perfusion culture induces the osteoblastic differentiation of marrow stroma cell-scaffold constructs in the absence of dexamethasone.* J Biomed Mater Res A, 2005. **72**(3): p. 326-34.

41. Colnot, C., *Cell sources for bone tissue engineering: insights from basic science.* Tissue Eng Part B Rev, 2011. **17**(6): p. 449-57.

42. Werntz, J.R., et al., *Qualitative and quantitative analysis of orthotopic bone regeneration by marrow.* J Orthop Res, 1996. **14**(1): p. 85-93.

43. Bruder, S.P., et al., *Bone regeneration by implantation of purified, culture-expanded human mesenchymal stem cells.* J Orthop Res, 1998. **16**(2): p. 155-62.

44. Castano-Izquierdo, H., et al., *Pre-culture period of mesenchymal stem cells in osteogenic media influences their in vivo bone forming potential.* J Biomed Mater Res A, 2007. **82**(1): p. 129-38.

45. Hadjipanayi, E., R.A. Brown, and V. Mudera, *Interface integration of layered collagen scaffolds with defined matrix stiffness: implications for sheet-based tissue engineering.* J Tissue Eng Regen Med, 2009. **3**(3): p. 230-41.

46. Glowacki, J. and S. Mizuno, *Collagen scaffolds for tissue engineering.* Biopolymers, 2008. **89**(5): p. 338-44.

47. Hollinger, J.O. and G.C. Battistone, *Biodegradable bone repair materials. Synthetic polymers and ceramics.* Clin Orthop Relat Res, 1986(207): p. 290-305.

48. Nienhuijs, M.E., et al., *Bone-like tissue formation using an equine COLLOSS E-filled titanium scaffolding material.* Biomaterials, 2006. **27**(16): p. 3109-14.

49. Holy, C.E., M.S. Shoichet, and J.E. Davies, *Engineering three-dimensional bone tissue in vitro using biodegradable scaffolds: investigating initial cell-seeding density and culture period.* J Biomed Mater Res, 2000. **51**(3): p. 376-82.

50. Bose, S., M. Roy, and A. Bandyopadhyay, *Recent advances in bone tissue engineering scaffolds.* Trends Biotechnol, 2012. **30**(10): p. 546-54.

51. Hutmacher, D.W., *Scaffolds in tissue engineering bone and cartilage.* Biomaterials, 2000. **21**(24): p. 2529-2543.

52. Fong, E.L., et al., *Building bridges: leveraging interdisciplinary collaborations in the development of biomaterials to meet clinical needs.* Adv Mater, 2012. **24**(36): p. 4995-5013.

53. Woo, K.M., et al., *Nano-fibrous scaffolding promotes osteoblast differentiation and biomineralization.* Biomaterials, 2007. **28**(2): p. 335-43.

54. Deng, M., et al., *Nanostructured polymeric scaffolds for orthopaedic regenerative engineering.* IEEE Trans Nanobioscience, 2012. **11**(1): p. 3-14.

55. Lienemann, P.S., M.P. Lutolf, and M. Ehrbar, *Biomimetic hydrogels for controlled biomolecule delivery to augment bone regeneration.* Adv Drug Deliv Rev, 2012. **64**(12): p. 1078-89.

56. Boudriot, U., et al., *Electrospinning approaches toward scaffold engineering--a brief overview.* Artificial Organs, 2006. **30**(10): p. 785-92.

57. Hutmacher, D.W., et al., *State of the art and future directions of scaffold-based bone engineering from a biomaterials perspective.* J Tissue Eng Regen Med, 2007. **1**(4): p. 245-60.

58. Hutmacher, D.W., M. Sittinger, and M.V. Risbud, *Scaffold-based tissue engineering: rationale for computer-aided design and solid free-form fabrication systems.* Trends Biotechnol, 2004. **22**(7): p. 354-62.

59. Christenson, E.M., et al., *Nanobiomaterial applications in orthopedics.* Journal of Orthopaedic Research, 2007. **25**(1): p. 11-22.

60. Kern, S., et al., *Comparative analysis of mesenchymal stem cells from bone marrow, umbilical cord blood, or adipose tissue.* Stem Cells, 2006. **24**(5): p. 1294-301.

61. Sekiya, I., et al., *Dexamethasone enhances SOX9 expression in chondrocytes.* J Endocrinol, 2001. **169**(3): p. 573-9.

62. Marie, P.J., F. Debiais, and E. Hay, *Regulation of human cranial osteoblast phenotype by FGF-2, FGFR-2 and BMP-2 signaling.* Histol Histopathol, 2002. **17**(3): p. 877-85.

63. Yamaguchi, A., T. Komori, and T. Suda, *Regulation of osteoblast differentiation mediated by bone morphogenetic proteins, hedgehogs, and Cbfa1.* Endocr Rev, 2000. **21**(4): p. 393-411.

64. Li, C., et al., *Electrospun silk-BMP-2 scaffolds for bone tissue engineering.* Biomaterials, 2006. **27**(16): p. 3115-24.

65. Shin, H., S. Jo, and A.G. Mikos, *Biomimetic materials for tissue engineering.* Biomaterials, 2003. **24**(24): p. 4353-64.

66. Alvarez-Barreto, J.F. and V.I. Sikavitsas, *Improved mesenchymal stem cell seeding on RGD-modified poly(L-lactic acid) scaffolds using flow perfusion.* Macromol Biosci, 2007. **7**(5): p. 579-88.

67. Cook, A.D., et al., *Characterization and development of RGD-peptide-modified poly(lactic acid-co-lysine) as an interactive, resorbable biomaterial.* J Biomed Mater Res, 1997. **35**(4): p. 513-23.

68. Cui, Y.L., et al., *Biomimetic surface modification of poly (L-lactic acid) with gelatin and its effects on articular chondrocytes in vitro.* J Biomed Mater Res A, 2003. **66**(4): p. 770-8.

69. Wolff, J., *The Law of Bone Remodeling*. 1986, New York: Berlin Heidelberg, Springer.

70. Cowin, S.C., *Bone poroelasticity.* J Biomech, 1999. **32**(3): p. 217-38.

71. Bonewald, L.F. and M.L. Johnson, *Osteocytes, mechanosensing and Wnt signaling.* Bone, 2008. **42**(4): p. 606-15.

72. Riddle, R.C. and H.J. Donahue, *From streaming-potentials to shear stress: 25 years of bone cell mechanotransduction.* J Orthop Res, 2009. **27**(2): p. 143-9.

73. Burger, E.H. and J. Klein-Nulend, *Mechanotransduction in bone--role of the lacuno-canalicular network.* FASEB J, 1999. **13 Suppl**: p. S101-12.

74. Basso, N. and J.N. Heersche, *Characteristics of in vitro osteoblastic cell loading models.* Bone, 2002. **30**(2): p. 347-51.

75. Mullender, M., et al., *Mechanotransduction of bone cells in vitro: mechanobiology of bone tissue.* Med Biol Eng Comput, 2004. **42**(1): p. 14-21.

76. Jacobs, C.R., *Primary cilia.* J Musculoskelet Neuronal Interact, 2007. **7**(4): p. 297-8.

77. Malone, A.M., et al., *Primary cilia in bone.* J Musculoskelet Neuronal Interact, 2007. **7**(4): p. 301.

78. Malone, A.M., et al., *Primary cilia mediate mechanosensing in bone cells by a calcium-independent mechanism.* Proc Natl Acad Sci U S A, 2007. **104**(33): p. 13325-30.

79. Whitfield, J.F., *Primary cilium--is it an osteocyte's strain-sensing flowmeter?* J Cell Biochem, 2003. **89**(2): p. 233-7.

80. Whitfield, J.F., *The solitary (primary) cilium--a mechanosensory toggle switch in bone and cartilage cells.* Cell Signal, 2008. **20**(6): p. 1019-24.

81. Pavalko, F.M., et al., *A model for mechanotransduction in bone cells: the load-bearing mechanosomes.* J Cell Biochem, 2003. **88**(1): p. 104-12.

82. Ingber, D.E., *Tensegrity: the architectural basis of cellular mechanotransduction.* Annu Rev Physiol, 1997. **59**: p. 575-99.

83. Jaasma, M.J., et al., *Adaptation of cellular mechanical behavior to mechanical loading for osteoblastic cells.* J Biomech, 2007. **40**(9): p. 1938-45.

84. Di Palma, F., et al., *Modulation of the responses of human osteoblast-like cells to physiologic mechanical strains by biomaterial surfaces.* Biomaterials, 2005. **26**(20): p. 4249-57.

85. Weyts, F.A., et al., *ERK activation and alpha v beta 3 integrin signaling through Shc recruitment in response to mechanical stimulation in human osteoblasts.* J Cell Biochem, 2002. **87**(1): p. 85-92.

86. Cheng, B., et al., *PGE(2) is essential for gap junction-mediated intercellular communication between osteocyte-like MLO-Y4 cells in response to mechanical strain.* Endocrinology, 2001. **142**(8): p. 3464-73.

87. Cherian, P.P., et al., *Effects of mechanical strain on the function of Gap junctions in osteocytes are mediated through the prostaglandin EP2 receptor.* J Biol Chem, 2003. **278**(44): p. 43146-56.

88. Cherian, P.P., et al., *Mechanical strain opens connexin 43 hemichannels in osteocytes: a novel mechanism for the release of prostaglandin.* Mol Biol Cell, 2005. **16**(7): p. 3100-6.

89. Saunders, M.M., et al., *Gap junctions and fluid flow response in MC3T3-E1 cells.* Am J Physiol Cell Physiol, 2001. **281**(6): p. C1917-25.

90. Saunders, M.M., et al., *Fluid flow-induced prostaglandin E2 response of osteoblastic ROS 17/2.8 cells is gap junction-mediated and independent of cytosolic calcium.* Bone, 2003. **32**(4): p. 350-6.

91. Yamaguchi, D.T., et al., *Parathyroid hormone-activated calcium channels in an osteoblast-like clonal osteosarcoma cell line. cAMP-dependent and cAMP-independent calcium channels.* J Biol Chem, 1987. **262**(16): p. 7711-8.

92. Ryder, K.D. and R.L. Duncan, *Parathyroid hormone enhances fluid shear-induced [Ca2+]i signaling in osteoblastic cells through activation of mechanosensitive and voltage-sensitive Ca2+ channels.* J Bone Miner Res, 2001. **16**(2): p. 240-8.

93. Li, J., et al., *L-type calcium channels mediate mechanically induced bone formation in vivo.* J Bone Miner Res, 2002. **17**(10): p. 1795-800.

94. Liu, D., et al., *Activation of extracellular-signal regulated kinase (ERK1/2) by fluid shear is Ca(2+)- and ATP-dependent in MC3T3-E1 osteoblasts.* Bone, 2008. **42**(4): p. 644-52.

95. Altman, G.H., et al., *Cell differentiation by mechanical stress.* FASEB Journal, 2002. **16**: p. 270-272.

96. Hurley, M.M. and J.A. Larenzo, *Systemic and Local Regulators of Bone Remodeling*, in *Bone Formation*, F. Bronner and M. Farach-Carson, Editors. 2004, Springer: London ; New York. p. 44-70.

97. Pavlin, D., et al., *Mechanical loading stimulates differentiation of periodontal osteoblasts in a mouse osteoinduction model: effect on type I collagen and alkaline phosphatase genes.* Calcif Tissue Int, 2000. **67**(2): p. 163-72.

98. Hillsley, M.V. and J.A. Frangos, *Bone tissue engineering: the role of interstitial fluid flow.* Biotechnol Bioeng, 1994. **43**(7): p. 573-81.

99. Goldstein, A.S., et al., *Effect of convection on osteoblastic cell growth and function in biodegradable polymer foam scaffolds.* Biomaterials, 2001. **22**(11): p. 1279-1288.

100. Gomes, M.E., et al., *Effect of flow perfusion on the osteogenic differentiation of bone marrow stromal cells cultured on starch-based three-dimensional scaffolds.* Journal of Biomedical Materials Research Part A, 2003. **67**(1): p. 87-95.

101. Freed, L.E., et al., *Advanced Tools for Tissue Engineering: Scaffolds, Bioreactors, and Signaling.* Tissue Engineering, 2006. **12**(12): p. 3285-3305.

102. Yeatts, A.B. and J.P. Fisher, *Bone tissue engineering bioreactors: dynamic culture and the influence of shear stress.* Bone, 2011. **48**(2): p. 171-81.

103. Kaspar, D., et al., *Dynamic cell stretching increases human osteoblast proliferation and CICP synthesis but decreases osteocalcin synthesis and alkaline phosphatase activity.* J Biomech, 2000. **33**(1): p. 45-51.

104. Neidlinger-Wilke, C., H.J. Wilke, and L. Claes, *Cyclic stretching of human osteoblasts affects proliferation and metabolism: a new experimental method and its application.* J Orthop Res, 1994. **12**(1): p. 70-8.

105. Nagatomi, J., et al., *Cyclic pressure affects osteoblast functions pertinent to osteogenesis.* Ann Biomed Eng, 2003. **31**(8): p. 917-23.

106. Rath, B., et al., *Compressive forces induce osteogenic gene expression in calvarial osteoblasts.* J Biomech, 2008. **41**(5): p. 1095-103.

107. Sikavitsas, V.I., et al., *Mineralized matrix deposition by marrow stromal osteoblasts in 3D perfusion culture increases with increasing fluid shear forces.* Proc Natl Acad Sci U S A, 2003. **100**(25): p. 14683-8.

108. Darling, E.M. and K.A. Athanasiou, *Articular cartilage bioreactors and bioprocesses.* Tissue Eng, 2003. **9**(1): p. 9-26.

109. Vunjak-Novakovic, G., et al., *Dynamic cell seeding of polymer scaffolds for cartilage tissue engineering.* Biotechnol Prog, 1998. **14**(2): p. 193-202.

110. Zhao, F. and T. Ma, *Perfusion bioreactor system for human mesenchymal stem cell tissue engineering: dynamic cell seeding and construct development.* Biotechnol Bioeng, 2005. **91**(4): p. 482-93.

111. Sucosky, P., et al., *Fluid mechanics of a spinner-flask bioreactor.* Biotechnol Bioeng, 2004. **85**(1): p. 34-46.

112. Sikavitsas, V.I., G.N. Bancroft, and A.G. Mikos, *Formation of three-dimensional cell/polymer constructs for bone tissue engineering in a spinner flask and a rotating wall vessel bioreactor.* J Biomed Mater Res, 2002. **62**(1): p. 136-48.

113. Vunjak-Novakovic, G., et al., *Microgravity studies of cells and tissues.* Ann N Y Acad Sci, 2002. **974**: p. 504-17.

114. Begley, C.M. and S.J. Kleis, *The fluid dynamic and shear environment in the NASA/JSC rotating-wall perfused-vessel bioreactor.* Biotechnol Bioeng, 2000. **70**(1): p. 32-40.

115. Williams, K.A., S. Saini, and T.M. Wick, *Computational fluid dynamics modeling of steady-state momentum and mass transport in a bioreactor for cartilage tissue engineering.* Biotechnol Prog, 2002. **18**(5): p. 951-63.

116. Yoshioka, T., et al., *Repair of large osteochondral defects with allogeneic cartilaginous aggregates formed from bone marrow-derived cells using RWV bioreactor.* J Orthop Res, 2007. **25**(10): p. 1291-8.

117. Duke, P.J., E.L. Daane, and D. Montufar-Solis, *Studies of chondrogenesis in rotating systems.* J Cell Biochem, 1993. **51**(3): p. 274-82.

118. Freed, L.E., et al., *Chondrogenesis in a cell-polymer-bioreactor system.* Exp Cell Res, 1998. **240**(1): p. 58-65.

119. Bancroft, G.N., et al., *Fluid flow increases mineralized matrix deposition in 3D perfusion culture of marrow stromal osteoblasts in a dose-dependent manner.* Proc Natl Acad Sci U S A, 2002. **99**(20): p. 12600-5.

120. Cartmell, S.H., et al., *Effects of medium perfusion rate on cell-seeded three-dimensional bone constructs in vitro.* Tissue Eng, 2003. **9**(6): p. 1197-203.

121. Alvarez-Barreto, J.F., et al., *Flow perfusion improves seeding of tissue engineering scaffolds with different architectures.* Ann Biomed Eng, 2007. **35**(3): p. 429-42.

122. Chung, C.A., et al., *Enhancement of cell growth in tissue-engineering constructs under direct perfusion: Modeling and simulation.* Biotechnol Bioeng, 2007. **97**(6): p. 1603-16.

123. Wendt, D., et al., *Oscillating perfusion of cell suspensions through three-dimensional scaffolds enhances cell seeding efficiency and uniformity.* Biotechnol Bioeng, 2003. **84**(2): p. 205-14.

124. Mizuno, S., F. Allemann, and J. Glowacki, *Effects of medium perfusion on matrix production by bovine chondrocytes in three-dimensional collagen sponges.* J Biomed Mater Res, 2001. **56**(3): p. 368-75.

125. Zhao, F., R. Chella, and T. Ma, *Effects of shear stress on 3-D human mesenchymal stem cell construct development in a perfusion bioreactor system: Experiments and hydrodynamic modeling.* Biotechnol Bioeng, 2007. **96**(3): p. 584-95.

126. Zhao, F., et al., *Effects of oxygen transport on 3-d human mesenchymal stem cell metabolic activity in perfusion and static cultures: experiments and mathematical model.* Biotechnol Prog, 2005. **21**(4): p. 1269-80.

127. Bancroft, G.N., V.I. Sikavitsas, and A.G. Mikos, *Design of a flow perfusion bioreactor system for bone tissue-engineering applications.* Tissue Engineering, 2003. **9**(3): p. 549-54.

128. Meinel, L., et al., *Bone tissue engineering using human mesenchymal stem cells: Effects of scaffold material and medium flow.* Annals of Biomedical Engineering, 2004. **32**(1): p. 112-122.

129. Xie, Y., et al., *Three-dimensional flow perfusion culture system for stem cell proliferation inside the critical-size beta-tricalcium phosphate scaffold.* Tissue Eng, 2006. **12**(12): p. 3535-43.

130. Voronov, R.S., et al., *Efficient Lagrangian scalar tracking method for reactive local mass transport simulation through porous media.* International Journal for Numerical Methods in Fluids, 2011. **67**(4): p. 501-517.

131. Martin, I., D. Wendt, and M. Heberer, *The role of bioreactors in tissue engineering.* Trends Biotechnol, 2004. **22**(2): p. 80-6.

132. Meinel, L., et al., *Engineering bone-like tissue in vitro using human bone marrow stem cells and silk scaffolds.* J Biomed Mater Res A, 2004. **71**(1): p. 25-34.

133. Li, Y., et al., *Effects of filtration seeding on cell density, spatial distribution, and proliferation in nonwoven fibrous matrices.* Biotechnol Prog, 2001. **17**(5): p. 935-44.

134. Williams, D.F., A. McNamara, and R.M. Turner, *Potential of polyetheretherketone (PEEK) and Carbon-fibre-reinforced PEEK in medical applications.* Journal of Materials Science Letters, 1987. **6**(2): p. 188-190.

135. Bradley, G.W., et al., *Effects of flexural rigidity of plates on bone healing.* J Bone Joint Surg Am, 1979. **61**(6A): p. 866-72.

136. Simmons, C.A., N. Valiquette, and R.M. Pilliar, *Osseointegration of sintered porous-surfaced and plasma spray-coated implants: An animal model study of early postimplantation healing response and mechanical stability.* J Biomed Mater Res, 1999. **47**(2): p. 127-38.

137. Terjesen, T. and K. Apalset, *The influence of different degrees of stiffness of fixation plates on experimental bone healing.* J Orthop Res, 1988. **6**(2): p. 293-9.

138. Woo, S.L., et al., *A comparison of cortical bone atrophy secondary to fixation with plates with large differences in bending stiffness.* J Bone Joint Surg Am, 1976. **58**(2): p. 190-5.

139. Trexel, I. *Trexel MuCell Processes*. 2006 [cited 2012; Available from: http://www.trexel.com/company/index.php.

140. Kramschuster, A. and L.S. Trung, *Highly Porous Injection-Molded Biodegradable Polymer Foams for Tissue Engineering Scaffolds*, in *BioFoams*. 2007: Capri, Italy.

141. Morrissette, D. and P. Croteau, *Porous Material and Method for Fabricating Same*, U. States, Editor. 2009, PPD Meditech: US. p. 13.

142. Converse, G.L., et al., *Hydroxyapatite whisker-reinforced polyetherketoneketone bone ingrowth scaffolds.* Acta Biomater, 2010. **6**(3): p. 856-63.

143. Converse, G.L., T.L. Conrad, and R.K. Roeder, *Mechanical properties of hydroxyapatite whisker reinforced polyetherketoneketone composite scaffolds.* J Mech Behav Biomed Mater, 2009. **2**(6): p. 627-35.

144. Datta, N., et al., *Effect of bone extracellular matrix synthesized in vitro on the osteoblastic differentiation of marrow stromal cells.* Biomaterials, 2005. **26**(9): p. 971-7.

145. Vilamitjana-Amedee, J., et al., *Human bone marrow stromal cells express an osteoblastic phenotype in culture.* In Vitro Cell Dev Biol Anim, 1993. **29A**(9): p. 699-707.

146. Manduca, P., et al., *Differential expression of alkaline phosphatase in clones of human osteoblast-like cells.* Journal of Bone and Mineral Research, 1993. **8**(3): p. 291-300.

147. Ogston, N., et al., *Dexamethasone and retinoic acid differentially regulate growth and differentiation in an immortalised human clonal bone marrow stromal cell line with osteoblastic characteristics.* Steroids, 2002. **67**(11): p. 895-906.

148. Jaiswal, N., et al., *Osteogenic differentiation of purified, culture-expanded human mesenchymal stem cells in vitro.* Journal of Cellular Biochemistry, 1997. **64**(2): p. 295-312.

149. Lian, J.B. and G.S. Stein, *Concepts of Osteoblast Growth and Differentiation - Basis for Modulation of Bone Cell-Development and Tissue Formation.* Critical Reviews in Oral Biology & Medicine, 1992. **3**(3): p. 269-305.

150. Hunter, A., et al., *Attachment and proliferation of osteoblasts and fibroblasts on biomaterials for orthopaedic use.* Biomaterials, 1995. **16**(4): p. 287-95.

151. Katzer, A., et al., *Polyetheretherketone--cytotoxicity and mutagenicity in vitro.* Biomaterials, 2002. **23**(8): p. 1749-59.

152. Macnair, R., et al., *Application of confocal laser scanning microscopy to cytocompatibility testing of potential orthopaedic materials in immortalised osteoblast-like cell lines.* Cells and Materials, 1996. **6**(1-3): p. 71-78.

153. Morrison, C., et al., *In vitro biocompatibility testing of polymers for orthopaedic implants using cultured fibroblasts and osteoblasts.* Biomaterials, 1995. **16**(13): p. 987-92.

154. Wenz, L.M., et al., *In vitro biocompatibility of polyetheretherketone and polysulfone composites.* J Biomed Mater Res, 1990. **24**(2): p. 207-15.

155. Maniatopoulos, C., J. Sodek, and A.H. Melcher, *Bone formation in vitro by stromal cells obtained from bone marrow of young adult rats.* Cell Tissue Res, 1988. **254**(2): p. 317-30.

156. Sagomonyants, K.B., et al., *The in vitro response of human osteoblasts to polyetheretherketone (PEEK) substrates compared to commercially pure titanium.* Biomaterials, 2008. **29**(11): p. 1563-72.

157. Aubin, J.E., et al., *Mesenchymal Stem Cells and Osteoblast Differentiation*, in *Principles of Bone Biology*, J.P. Bilezikian, L.G. Raisz, and G.A. Rodan, Editors. 2002, Academic Press: San Diego. p. 59-81.

158. Owen, T.A., et al., *Progressive development of the rat osteoblast phenotype in vitro: reciprocal relationships in expression of genes associated with osteoblast proliferation and differentiation during formation of the bone extracellular matrix.* J Cell Physiol, 1990. **143**(3): p. 420-30.

159. Cook, S.D. and A.M. Rust-Dawicki, *Preliminary evaluation of titanium-coated PEEK dental implants.* J Oral Implantol, 1995. **21**(3): p. 176-81.

160. Noiset, O., Y.J. Schneider, and J. Marchand-Brynaert, *Fibronectin adsorption or/and covalent grafting on chemically modified PEEK film surfaces.* J Biomater Sci Polym Ed, 1999. **10**(6): p. 657-77.

161. Pino, M., N. Stingelin, and K.E. Tanner, *Nucleation and growth of apatite on NaOH-treated PEEK, HDPE and UHMWPE for artificial cornea materials.* Acta Biomater, 2008. **4**(6): p. 1827-36.

162. Poulsson, A.H.C. and R.G. Richards, *Enhancement of human primary osteoblast adhesion and function by plasma surface modification of PEEK.* Eur Cell Mater, 2009. **18**(Suppl. 2): p. 34.

163. Kurtz, S.M. and J.N. Devine, *PEEK biomaterials in trauma, orthopedic, and spinal implants.* Biomaterials, 2007. **28**(32): p. 4845-4869.

164. Boinard, E., R.A. Pethrick, and C.J. MacFarlane, *The influence of thermal history on the dynamic mechanical and dielectric studies of polyetheretherketone exposed to water and brine.* Polymer, 2000. **41**(3): p. 1063-1076.

165. Mikos, A.G., et al., *Engineering complex tissues.* Tissue Engineering, 2006. **12**(12): p. 3307-3339.

166. Yaszemski, M.J., et al., *Evolution of bone transplantation: Molecular, cellular and tissue strategies to engineer human bone.* Biomaterials, 1996. **17**(2): p. 175-185.

167. Tuan, R.S., G. Boland, and R. Tuli, *Adult mesenchymal stem cells and cell-based tissue engineering.* Arthritis Research & Therapy, 2003. **5**(1): p. 32-45.

168. Sikavitsas, V.I., et al., *Flow perfusion enhances the calcified matrix deposition of marrow stromal cells in biodegradable nonwoven fiber mesh scaffolds.* Ann Biomed Eng, 2005. **33**(1): p. 63-70.

169. Holtorf, H.L., J.A. Jansen, and A.G. Mikos, *Flow perfusion culture induces the osteoblastic differentiation of marrow stromal cell-scaffold constructs in the absence of dexamethasone.* Journal of Biomedical Materials Research Part A, 2005. **72A**(3): p. 326-334.

170. Gomes, M.E., et al., *In vitro localization of bone growth factors in constructs of biodegradable scaffolds seeded with marrow stromal cells and cultured in a flow perfusion bioreactor.* Tissue Engineering, 2006. **12**(1): p. 177-188.

171. Datta, N., et al., *In vitro generated extracellular matrix and fluid shear stress synergistically enhance 3D osteoblastic differentiation.* Proceedings of the

National Academy of Sciences of the United States of America, 2006. **103**(8): p. 2488-2493.

172. Bancroft, G.N., V.I. Sikavitsas, and A.G. Mikos, *Design of a flow perfusion bioreactor system for bone tissue-engineering applications.* Tissue Eng, 2003. **9**(3): p. 549-54.

173. Hollister, S.J., *Porous scaffold design for tissue engineering.* Nat Mater, 2005. **4**(7): p. 518-24.

174. Boschetti, F., et al., *Prediction of the micro-fluid dynamic environment imposed to three-dimensional engineered cell systems in bioreactors.* Journal of Biomechanics, 2006. **39**(3): p. 418-425.

175. Porter, B., et al., *3-D computational modeling of media flow through scaffolds in a perfusion bioreactor.* Journal of Biomechanics, 2005. **38**(3): p. 543-549.

176. Cioffi, M., et al., *Modeling evaluation of the fluid-dynamic microenvironment in tissue-engineered constructs: a micro-CT based model.* Biotechnol Bioeng, 2006. **93**(3): p. 500-10.

177. Raimondi, M.T., et al., *The effect of hydrodynamic shear on 3D engineered chondrocyte systems subject to direct perfusion.* Biorheology, 2006. **43**(3-4): p. 215-22.

178. Cioffi, M., et al., *Computational evaluation of oxygen and shear stress distributions in 3D perfusion culture systems: macro-scale and micro-structured models.* J Biomech, 2008. **41**(14): p. 2918-25.

179. Maes, F., et al., *Modeling fluid flow through irregular scaffolds for perfusion bioreactors.* Biotechnol Bioeng, 2009. **103**(3): p. 621-30.

180. Ho, S.T. and D.W. Hutmacher, *A comparison of micro CT with other techniques used in the characterization of scaffolds.* Biomaterials, 2006. **27**(8): p. 1362-1376.

181. van Lenthe, G.H., et al., *Nondestructive micro-computed tomography for biological imaging and quantification of scaffold-bone interaction in vivo.* Biomaterials, 2007. **28**(15): p. 2479-2490.

182. Darling, A.L. and W. Sun, *3D microtomographic characterization of precision extruded poly-epsilon-caprolactone scaffolds.* Journal of Biomedical Materials Research Part B-Applied Biomaterials, 2004. **70B**(2): p. 311-317.

183. Lu, L.C., et al., *In vitro degradation of porous poly(L-lactic acid) foams.* Biomaterials, 2000. **21**(15): p. 1595-1605.

184. Alvarez-Barreto, J.F. and V.I. Sikavitsas, *Improved mesenchymal stem cell seeding on RGD-modified poly(L-lactic acid) scaffolds using flow perfusion.* Macromolecular Bioscience, 2007. **7**(5): p. 579-588.

185. Mikos, A.G., et al., *Wetting of poly(L-lactic acid) and poly(DL-lactic-co-glycolic acid) foams for tissue culture.* Biomaterials, 1994. **15**(1): p. 55-8.

186. de Rovere, A. and R.L. Shambaugh, *Melt-spun hollow fibers for use in nonwoven structures.* Industrial & Engineering Chemistry Research, 2001. **40**(1): p. 176-187.

187. Majumdar, B. and R.L. Shambaugh, *Air Drag on Filaments in the Melt Blowing Process.* Journal of Rheology, 1990. **34**(4): p. 591-601.

188. Zhang, D., et al., *Structure and properties of polypropylene filaments in a spunbonding process.* Journal of Thermal Analysis, 1997. **49**(1): p. 161-167.

189. Malkan, S.R., *An Overview of Spunbonding and Meltblowing Technologies.* Tappi Journal, 1995. **78**(6): p. 185-190.

190. Tandler, B., et al., *Melt processing of a new biodegradable synthetic polymer in high-speed spinning and underpressure spunbonding process.* Journal of Polymers and the Environment, 2001. **9**(4): p. 149-156.

191. Voronov, R., et al., *Computational modeling of flow-induced shear stresses within 3D salt-leached porous scaffolds imaged via micro-CT.* J Biomech, 2010.

192. Succi, S., *The lattice Boltzmann equation for fluid dynamics and beyond*. Numerical mathematics and scientific computation. 2001, Oxford, New York: Clarendon Press; Oxford University Press. xvi, 288 p.

193. Sukop, M.C., D.T. Thorne, and NetLibrary Inc., *Lattice Boltzmann modeling an introduction for geoscientists and engineers*. 2006, Springer: Berlin ; New York. p. ix, 172 p.^^

194. Chen, S. and G.D. Doolen, *Lattice Boltzmann method for fluid flows.* Annual Review of Fluid Mechanics, 1998. **30**: p. 329-364.

195. Wang, J.Y., et al., *Domain-decomposition method for parallel lattice Boltzmann simulation of incompressible flow in porous media.* Physical Review E, 2005. **72**(1): p. -.

196. Kandhai, D., et al., *Lattice-Boltzmann hydrodynamics on parallel systems.* Computer Physics Communications, 1998. **111**(1-3): p. 14-26.

197. Cosgrove, J.A., et al., *Application of the lattice Boltzmann method to transition in oscillatory channel flow.* Journal of Physics a-Mathematical and General, 2003. **36**(10): p. 2609-2620.

198. Boyd, J., J. Buick, and S. Green, *A second-order accurate lattice Boltzmann non-Newtonian flow model.* Journal of Physics a-Mathematical and General, 2006. **39**(46): p. 14241-14247.

199. Yoshino, A., et al., *A numerical method for incompressible non-Newtonian fluid flows based on the lattice Boltzmann method.* Journal of Non-Newtonian Fluid Mechanics, 2007. **147**(1-2): p. 69-78.

200. Gabbanelli, S., G. Drazer, and J. Koplik, *Lattice Boltzmann method for non-Newtonian (power-law) fluids.* Physical Review E, 2005. **72**(4): p. -.

201. Swift, M.R., et al., *Lattice Boltzmann simulations of liquid-gas and binary fluid systems.* Physical Review E, 1996. **54**(5): p. 5041-5052.

202. Qian, Y.H., D. Dhumieres, and P. Lallemand, *Lattice Bgk Models for Navier-Stokes Equation.* Europhysics Letters, 1992. **17**(6bis): p. 479-484.

203. Bhatnagar, P.L., E.P. Gross, and M. Krook, *A Model for Collision Processes in Gases .1. Small Amplitude Processes in Charged and Neutral One-Component Systems.* Physical Review, 1954. **94**(3): p. 511-525.

204. Lakhotia, S. and E.T. Papoutsakis, *Agitation Induced Cell Injury in Microcarrier Cultures - Protective Effect of Viscosity Is Agitation Intensity Dependent - Experiments and Modeling.* Biotechnology and Bioengineering, 1992. **39**(1): p. 95-107.

205. van den Dolder, J., et al., *Flow perfusion culture of marrow stromal osteoblasts in titanium fiber mesh.* Journal of Biomedical Materials Research Part A, 2003. **64**(2): p. 235-41.

206. Nabovati, A., E.W. Llewellin, and A.C.M. Sousa, *A general model for the permeability of fibrous porous media based on fluid flow simulations using the lattice Boltzmann method.* Composites Part a-Applied Science and Manufacturing, 2009. **40**(6-7): p. 860-869.

207. Stylianopoulos, T., et al., *Permeability calculations in three-dimensional isotropic and oriented fiber networks.* Physics of Fluids, 2008. **20**(12): p. -.

208. Skartsis, L., J.L. Kardos, and B. Khomami, *Resin Flow through Fiber Beds during Composite Manufacturing Processes .1. Review of Newtonian Flow through Fiber Beds.* Polymer Engineering and Science, 1992. **32**(4): p. 221-230.

209. Bird, R.B., *Transport phenomena*. 1960, New York,: Wiley. 780 p.

210. Sikavitsas, V.I., et al., *Flow perfusion enhances the calcified matrix deposition of marrow stromal cells in biodegradable nonwoven fiber mesh scaffolds.* Annals of Biomedical Engineering, 2005. **33**(1): p. 63-70.

211. Coelho, M.J. and M.H. Fernandes, *Human bone cell cultures in biocompatibility testing. Part II: effect of ascorbic acid, beta-glycerophosphate and dexamethasone on osteoblastic differentiation.* Biomaterials, 2000. **21**(11): p. 1095-102.

212. Pavalko, F.M., et al., *Fluid shear-induced mechanical signaling in MC3T3-E1 osteoblasts requires cytoskeleton-integrin interactions.* Am J Physiol, 1998. **275**(6 Pt 1): p. C1591-601.

213. Holtorf, H.L., J.A. Jansen, and A.G. Mikos, *Ectopic bone formation in rat marrow stromal cell/titanium fiber mesh scaffold constructs: effect of initial cell phenotype.* Biomaterials, 2005. **26**(31): p. 6208-16.

214. Voronov, R., et al., *Computational modeling of flow-induced shear stresses within 3D salt-leached porous scaffolds imaged via micro-CT.* J Biomech, 2010. **43**(7): p. 1279-86.

215. Guldberg, R.E., et al., *3D imaging of tissue integration with porous biomaterials.* Biomaterials, 2008. **29**(28): p. 3757-3761.

216. Brouwers, J.E.M., B. Van Rietbergen, and R. Huiskes, *No effects of in vivo micro-CT radiation on structural parameters and bone marrow cells in proximal tibia of Wistar rats detected after eight weekly scans.* Journal of Orthopaedic Research, 2007. **25**(10): p. 1325-1332.

217. Laperre, K., et al., *Development of micro-CT protocols for in vivo follow-up of mouse bone architecture without major radiation side effects.* Bone, 2011. **49**(4): p. 613-622.

218. Foster, W.K. and N.L. Ford, *Investigating the effect of longitudinal micro-CT imaging on tumour growth in mice.* Physics in Medicine and Biology, 2011. **56**(2): p. 315-326.

219. Zehbe Rolf, H.A., Schmidt Franziska, Riesemeier Heinrich, Kirkpatrick C. James, Schubert Helmut and Brochhausen Christoph, *High Resolution X-Ray Tomography - 3D Imaging for Tissue Engineering Applications*, in *Tissue Engineering*, D. Eberli, Editor. 2010, InTech.

220. Castano-Izquierdo, H., et al., *Pre-culture period of mesenchymal stem cells in osteogenic media influences their in vivo bone forming potential.* Journal of Biomedical Materials Research Part A, 2007. **82A**(1): p. 129-138.

221. Sikavitsas, V.I., et al., *Mineralized matrix deposition by marrow stromal osteoblasts in 3D perfusion culture increases with increasing fluid shear forces.* Proceedings of the National Academy of Sciences of the United States of America, 2003. **100**(25): p. 14683-14688.

222. VanGordon, S., et al., *Effects of Scaffold Architecture on Preosteoblastic Cultures under Continuous Fluid Shear.* Industrial & Engineering Chemistry Research, 2011. **50**(2): p. 620-629.